



**HAL**  
open science

# Synthesis of low density foam shells for inertial confinement fusion experiments

Cecile Lattaud

► **To cite this version:**

Cecile Lattaud. Synthesis of low density foam shells for inertial confinement fusion experiments. Other. Université de Bourgogne, 2011. English. NNT : 2011DIJOS033 . tel-00692058

**HAL Id: tel-00692058**

**<https://theses.hal.science/tel-00692058>**

Submitted on 27 Apr 2012

**HAL** is a multi-disciplinary open access archive for the deposit and dissemination of scientific research documents, whether they are published or not. The documents may come from teaching and research institutions in France or abroad, or from public or private research centers.

L'archive ouverte pluridisciplinaire **HAL**, est destinée au dépôt et à la diffusion de documents scientifiques de niveau recherche, publiés ou non, émanant des établissements d'enseignement et de recherche français ou étrangers, des laboratoires publics ou privés.

Université de Bourgogne - Faculté des Sciences et Techniques  
Institut de Chimie Moléculaire de l'Université de Bourgogne (ICMUB) – UMR CNRS 5260  
Equipe Systèmes Hybrides Multifonctionnels (SYMS)

## **Thèse**

*Pour obtenir le grade de*

**Docteur de l'Université de Bourgogne**

*Spécialité :* **Chimie et Physique**

*Présentée par :*

**Cécile LATTAUD**

le 27 Septembre 2011

# **Synthesis of low density foam shells for inertial confinement fusion experiments**

M <sup>f</sup> Etienne FLEURY	Professeur, INSA Lyon	<b>Rapporteur</b>
M <sup>f</sup> Keiji NAGAI	Professeur, Tokyo Institute of Technology	<b>Rapporteur</b>
M <sup>f</sup> Fabrice BUREL	Professeur, INSA Rouen	<b>Examineur</b>
M <sup>me</sup> Alexia BALLAND-LONGEAU	Docteur, CEA Ripault	<b>Examinatrice</b>
M <sup>f</sup> Nicolas BREMOND	Maître de conférences, ESPCI	<b>Examineur</b>
M <sup>f</sup> Lyonel GUILLOT	Docteur, CEA Valduc	<b>Examineur</b>
M <sup>me</sup> Claire-Hélène BRACHAIS	Maître de conférences, Université de Bourgogne	<b>Examinatrice</b>
M <sup>f</sup> Jean-Pierre COUVERCELLE	Professeur, Université de Bourgogne	<b>Directeur</b>

## **ACKNOWLEDGEMENTS**

This PhD would not have been possible without the guidance and the help of several individuals who in one way or another contributed and extended their valuable assistance in the preparation and completion of this study.

First, this PhD would not have been possible without the financial support of the CEA, the Burgundy Region and the ICMUB.

It is an honor for me that Etienne Fleury and Keiji Nagai willingly accepted to be the two chairmen of my PhD jury. I am especially grateful to Keiji Nagai to come from so far away for my viva voce.

I would like to thank Fabrice Burel, Nicolas Bremond, Alexia Balland-Longeau, Lyonel Guillot, Jean-Pierre Couvercelle and Claire-Hélène Brachais for being part of my PhD jury.

I would acknowledge Catherine Treimany, Jean-Marie Fontaine, Georges Genestier, Olivier Legaie, Emmanuel Fleury, Benoit Reneaume and Lyonel Guillot for giving me the opportunity to work on a very specific and interesting subject and for welcoming me at SMCI of Valduc CEA site. I thank them for making this work possible and for financing all the necessary equipments and materials.

I am grateful to Franck Denat for giving me the opportunity to work at the ICMUB and to Jean-Pierre Couvercelle for receiving me in his research team. I would like to appreciate deeply my supervisor Jean-Pierre Couvercelle for his guidance, understanding and valuable comments during this study. I am much indebted to him for his valuable advice in science discussion, supervision in my researches and furthermore, using his precious time to read this thesis and giving his critical comments about it.

I would like to express my deepest and warmest gratitude to my co-supervisor, Claire-Hélène Brachais not only for her guidance but also for her support, trust and encouragements throughout my PhD study. Her thoughtful advice, criticisms, suggestions and questions have been of great value along this thesis. I was also moved by her meticulously reading, promptly

## *Acknowledgements*

---

feeding back of my thesis drafts and stimulating suggestions. I am grateful for all she has done and for her kindness, availability and caring. I am indebted to her more than she knows. One simply could not wish for a better or friendlier supervisor.

I gratefully thank Nicolas Bremond for his interest on the subject, for all the time he spent answering and explaining all the questions of physics we wondered. It was nice and comforting to have someone like you looking at the subject from a physical point of view.

Many thanks are also due to Danielle Ballivet Tkatchenko who helped me and gave me tips when the gas chromatography did not work, to Sandrine Garrault for giving me the opportunity to work on her rheometer, to Catherine Labruère Chazal for her kind answer to my mathematical questions, to Gilles Boni who replied kindly to my questions about organic chemistry and to Marie-Laure Léonard who nicely helped me when I worked in her laboratories.

I am grateful to Vincent Eyraud and Patrice Antoine for their time and patience through the help they gave me with the ultra fast frame grabber camera.

I would like to thanks Cyril Hermerel for his help with the telecentric optical microscope and for always answering my questions in a mood for laughing.

It is also a pleasure to thank Laurence Hun and Aurélie Zentz for creating a pleasant and friendly working atmosphere in the laboratory at the CEA. It was nice chatting with you girls during these long days spent in the lab ! You have been a great help to dump the carcinogenic wastes. Thank you also Aurélie for letting me borrow your car so often.

I gratefully thank Remi Schlienger for the help and the moral support you gave me during these long hours spent on repairing the gas chromatography in the laboratory at the University.

I am thankful to Christophe Guerville who dealt kindly and patiently to all my computer issues.

## *Acknowledgements*

---

My special thanks go to Guilhem Allègre, Alexis Faivre, Etienne Brun, Richard Caland, Remi Bourdenet, Sielver Meux, Christophe Dauteil, for all the coffee breaks and lunches we had together and for so many other things. Thank you all for making me laugh so much with all your silly and funny stories. I will always remember my cute nickname ! It was nice having you there when I needed help or when I just wanted to talk with you guys.

In my daily work at the University, I have been blessed with a friendly and cheerful group of fellow students. I convey special acknowledgements to Faten Sadaka, Christelle Nguimjeu, Sebastien Narses, Mickael Lemoine, Souad Bennabi for the friendly and peaceful atmosphere at the office and in the lab. Thank you for all the fun I had with you, I will always remember the good times we shared together. I was glad to have you on my side and to have your warm support.

My warmest thanks go to Marie, Cyrielle, Colleen, Clémence and Clothilde. I have a great regard for your continued friendship, your support and your caring.

I owe my deepest gratitude and acknowledgements to my family. Thank you mum, dad, Claire and Sophie for your unconditional love, your endless encouragements and your loving support during my whole life. I would never have achieved all this without you in my life.

# **ABSTRACT**

This work deals with the fabrication process of low density foam shells and the sharp control of their shape (diameter, thickness, density, sphericity, non-concentricity). During this PhD we focused on the non-concentricity criterion which has to be lower than 1%. The shells are synthesized using a microencapsulation process leading to a double emulsion and followed by a thermal polymerization at 60°C. According to the literature, three major parameters, the density of the three phases, the deformations of the shells along the process and the kinetics of the polymerization have a direct influence on the shells non-concentricity. The results obtained showed that when the density gap between the internal water phase and the organic phase increases, the TMPTMA shells non-concentricity improves. A density gap of 0.078 g.cm<sup>-3</sup> at 60°C, leads to an average non-concentricity of 2.4% with a yield of shells of 58%. It was also shown that the synthesis process can be considered as reproducible. While using the same internal water phase, equivalent non-concentricity results are obtained using either a straight tube, a tube with areas of constriction or a short wound tube. The time required to fix the shell's shape is at least 20 minutes with thermal polymerization. So, it seems that the time spent by the shells inside the rotating flask allows the centering of the internal water phase inside the organic phase, whatever the circulation process used. In order to get higher polymerization rates and to avoid destabilization phenomena, we then focused our study on photopolymerization. When the synthesis is performed using a UV lamp with an efficient light intensity, the shells have a slightly higher thickness than the shells synthesized by thermal polymerization. Moreover, a really higher yield, around 80%, is achieved with UV polymerization. However, the average non-concentricity of the shells synthesized lays around 20%, which is really high compared to the 2.4% average non-concentricity obtained with thermal polymerization. It would be interesting to expose the shells to UV light at different times after collection in order to study the influence of the agitation time on the shells non-concentricity.

Keywords: density, dispersion, double emulsion, microencapsulation, non-concentricity, photopolymerization, radical polymerization, shell, trimethylolpropane trimethacrylate.

# **RESUME**



Ce travail porte sur le processus de fabrication de microballons en mousse basse densité et le contrôle fin de leur forme (diamètre, épaisseur, densité, sphéricité, non-concentricité). Durant cette thèse nous nous sommes concentrés sur le critère de non-concentricité qui doit être inférieure à 1%. Les microballons sont synthétisés en utilisant un procédé de microencapsulation conduisant à une émulsion double, suivie d'une polymérisation thermique à 60°C. Selon la littérature, trois paramètres majeurs, la densité des trois phases, les déformations du microballon pendant le procédé et la cinétique de polymérisation ont une influence directe sur la non-concentricité des microballons. Les résultats obtenus ont montré que lorsque l'écart de densité entre la phase aqueuse interne et la phase organique augmente, la non-concentricité des microballons TMPTMA s'améliore. Un écart de densité de 0,078 g.cm<sup>-3</sup> à 60°C conduit à une non-concentricité moyenne de 2,4% avec un rendement en microballons de 58%. Il a également été montré que la synthèse peut être considérée comme reproductible. Pour une même phase aqueuse interne, les résultats de non-concentricité sont équivalents en utilisant soit un tube droit, un tube à étranglement ou un serpentin court. Le temps requis pour fixer la forme des microballons est d'au moins 20 minutes avec la polymérisation thermique. Ainsi, il semble que le temps passé par les microballons à l'intérieur des bouteilles de réception permet le centrage de la phase aqueuse interne à l'intérieur de la phase organique, quel que soit le processus de circulation précédemment utilisé. Afin d'obtenir des vitesses de polymérisation plus élevées et d'éviter les phénomènes de déstabilisation, nous avons alors concentré notre étude sur la photopolymérisation. Lorsque la synthèse est effectuée en utilisant une lampe UV avec une intensité lumineuse efficace, les microballons ont une épaisseur légèrement supérieure à celle des microballons synthétisés par voie thermique. Par ailleurs, un rendement plus élevé, environ 80%, est obtenu avec la polymérisation UV. Toutefois, la non-concentricité moyenne des microballons synthétisés est environ de 20%, ce qui est vraiment élevé par rapport à la non-concentricité moyenne de 2,4% obtenue par polymérisation thermique. Il serait intéressant d'exposer les microballons à la lumière UV, à différents moments après la collecte afin d'étudier l'influence du temps d'agitation sur la non-concentricité des microballons.

Mots-clés: densité, microencapsulation, dispersion, émulsion double, microballon, triméthylolpropane triméthacrylate, polymérisation radicalaire, photopolymérisation, non-concentricité

## **ENGLISH/FRENCH GLOSSARY**

- shell: ballon
- nuclear stockpile: réserve d'armements nucléaires
- nuclear weapon: arme nucléaire
- inertial confinement fusion: fusion par confinement inertiel
- droplet: goutte
- mismatch: écart
- foam: mousse
- droplet generator: générateur de goutte
- dryer: sécheur
- surfactant: tensio-actif
- network: réseau
- extractor hood: hotte
- density: masse volumique
- internal water phase: phase aqueuse interne
- external aqueous phase: phase aqueuse externe
- organic phase: phase organique
- collecting flask: bouteille de reception
- needle: capillaire
- brass: laiton
- straight tube: tube droit
- tube with areas of constriction: tube à étranglement
- wound tube: serpent
- scintillation vial: flacon à scintillation
- clean room: salle blanche
- wall: paroi
- thickness: épaisseur
- shape: forme
- bulk polymerization: polymérisation en masse
- stir rate: vitesse d'agitation
- buoyancy: flottaison
- pattern: tendance

# TABLE OF CONTENTS

<b>INTRODUCTION</b> .....	1
<b>CHAPTER I. EXPERIMENTAL</b> .....	5
<b>I.1. SYNTHESIS PROCESS</b> .....	6
I.1.1. Solution preparation.....	6
I.1.2. The injection system .....	9
I.1.3. Shell's cleaning .....	13
I.1.4. Solvent's exchange .....	14
I.1.5. Shell's drying .....	14
<b>I.2. CHARACTERIZATION TECHNIQUES</b> .....	15
I.2.1. Characterization of shells in alcohol.....	15
I.2.2. Dry shells characterizations .....	16
<b>I.3. TIME PROGRESS OF A COMPLETE SYNTHESIS</b> .....	16
I.3.1. First week.....	16
I.3.2. Second week .....	18
<b>I.4. CONCLUSION</b> .....	18
<b>CHAPTER II. LITERATURE REVIEW</b> .....	20
<b>II.1. BASIC PRINCIPLES OF DOUBLE EMULSIONS</b> .....	21
II.1.1. Simple emulsions.....	21
II.1.2. Double emulsions .....	24
<b>II.2. GENERAL CHARACTER OF THE POLYMERIZATION PROCESS</b> .....	27
II.2.1. Thermal free radical polymerization process .....	27

II.2.2. UV free radical polymerization process .....	32
II.3. PARAMETERS INFLUENCING THE AIMED CRITERIA.....	35
II.3.1. Parameters influencing the diameter .....	35
II.3.2. Parameters influencing the thickness .....	36
II.3.3. Parameters influencing the density .....	36
II.3.4. Parameters influencing the sphericity.....	37
II.3.5. Parameters influencing the non-concentricity .....	37
II.4. STATE OF THE ART IN THE USA, JAPAN AND FRANCE .....	41
II.4.1. American results .....	41
II.4.2. Japanese results.....	46
II.4.3. French results.....	50
II.5. CONCLUSION .....	52
<b>CHAPTER III. OPTIMIZATION OF THE SHELLS NON-CONCENTRICITY.....</b>	<b>58</b>
III.1. INFLUENCE OF DENSITY ON THE SHELLS NON-CONCENTRICITY .....	59
III.1.1. Evolution of W2, W1 and O1 densities with temperature .....	59
III.1.2. Shells syntheses with several density gaps .....	63
III.1.3. Yields of the synthesis.....	68
III.1.4. Comparison of NC results and sphericity results .....	69
III.2. REPRODUCIBILITY OF THE PROCESS .....	71
III.3. INFLUENCE OF THE CENTERING OF THE DROPLET INJECTOR ON THE SHELLS NON-CONCENTRICITY .....	74
III.4. INFLUENCE OF INTERFACIAL TENSION ON THE SHELLS NON-CONCENTRICITY.....	77
III.5. CONCLUSION .....	82

<b>CHAPTER IV. STUDY OF THE CIRCULATION AND POLYMERIZATION PROCESSES</b> .....	84
IV.1. INFLUENCE OF THE CIRCULATION PROCESS ON THE SHELLS NON-CONCENTRICITY.....	85
IV.1.1. Presentation of the three circulation systems.....	85
IV.1.2. Synthesis of shells with three circulation systems and three density gaps .....	87
IV.1.3. Hypothesis to explain the shell's motion in the circulation systems .....	89
IV.2. INFLUENCE OF THE POLYMERIZATION KINETICS ON THE SHELLS NON-CONCENTRICITY.....	93
IV.2.1. Polymerization process .....	93
IV.2.2. Study of the shells location versus their viscosity .....	100
IV.3. CONCLUSION.....	104
<b>CHAPTER V. STUDY OF THE INFLUENCE OF INCREASED POLYMERIZATION RATES ON THE SHELLS CHARACTERISTICS</b> .....	107
V.1. STUDY OF THE INFLUENCE OF INCREASED POLYMERIZATION TEMPERATURES ON THE SHELLS CHARACTERISTICS .....	108
V.1.1. Behavior of the system with higher temperature.....	108
V.1.2. Shells synthesized at higher polymerization temperature .....	112
V.2. STUDY OF THE INFLUENCE OF POLYMERIZATION BY UV LIGHT ON THE SHELLS CHARACTERISTICS .....	116
V.2.1. Choice of the UV lamp and the photoinitiator .....	117
V.2.2. Characteristics of shells synthesized using UV polymerization .....	121
V.3. CONCLUSION .....	130
<b>CONCLUSION</b> .....	133

<b>APPENDIX</b> .....	137
A.1. Gas chromatography.....	138
A.2. Rheology .....	138
A.3. Density.....	139
A.4. Viscosity.....	140
A.5. Interfacial tension .....	141
A.6. Infrared spectroscopy .....	141
A.7. UV-visible spectroscopy .....	142
A.8. Telecentric optical microscope.....	142
A.9. Scanning electron microscope.....	145

## LIST OF FIGURES

Figure I.1: Polyvinyl alcohol partially hydrolyzed .....	6
Figure I.2: Dissolving and degassing system .....	7
Figure I.3: Filtration system .....	7
Figure I.4: Trimethylolpropane trimethacrylate .....	7
Figure I.5: 2,2'-azo-bis-isobutyronitrile .....	8
Figure I.6: Sorbitane monooleate .....	8
Figure I.7: Densitometer .....	8
Figure I.8: Injection system using a tube with areas of constriction .....	9
Figure I.9: Injection system .....	10
Figure I.10: Image of the TV screen linked to the camera in front of the injector .....	11
Figure I.11: Different tube systems through which the shell can go through after the tube 3. 12	
Figure I.12: The collecting flask .....	13
Figure I.13: Extractor hood with four bottles already collected placed into a heated water bath at 60°C under a nitrogen flow of 60 mL.min <sup>-1</sup> and rotated at 40 rpm .....	13
Figure I.14: The supercritical dryer and the ceramic support with alveoli .....	14
Figure I.15: Silica characterization plate with shells inside the alveoli and a shell seen with a telecentric optical microscope .....	15
Figure I.16: Definition of the non-concentricity .....	16
Figure II.1: Schematic representation of simple emulsion .....	21
Figure II.2: Schematic representation of the various breakdown processes in emulsions as proposed by Tadros [3] .....	23
Figure II.3: Schematic representation of double emulsions .....	24
Figure II.4: Bulk monomer conversion as a function of time [30] .....	30
Figure II.5: Autoacceleration in benzoyl peroxide-initiated polymerization of methyl methacrylate in benzene at 50°C. The different plots represent various concentrations of monomer in solvent. [29] .....	31
Figure II.6: Network formation [32] .....	31
Figure II.7: Definition of the three phases .....	35
Figure II.8: External diameter of the shell .....	35



Figure II.9: Illustration of the external phase which strips off the shell formed at the tip of the generator (IP: internal phase, SP: surrounding phase, EP: external phase) .....	36
Figure II.10: Thickness of the shell.....	36
Figure II.11: Definition of the non-concentricity.....	38
Figure II.12: The two graphics present the NC of SDRF and HDRF shells fabricated with the standard process (no SBS) and with the addition of SBS in the external phase (Mod 4). (SDRF: RF shells of low density, HDRF: RF shells of high density, SBS: styrene-butadiene-styrene block copolymer) [46] .....	40
Figure II.13: Illustration of a two-stage emulsification process to produce polymer shell [57] .....	43
Figure II.14: Evolution of the yield (%) of DVB foam shells as a function of their non-concentricity (%) [62] .....	45
Figure II.15: Schematic diagram of a dual-nozzle-in-orifice droplet generator [51].....	48
Figure II.16: Distribution of diameter and wall thickness for foam shells made by the two step emulsification process (hand-shake) and the dual-nozzle-in-orifice droplet generator [51]....	48
Figure II.17: Illustration of the optimized vigorous agitation conditions (The drum was rotated and its speed increased to 95 rpm within 15 minutes. 5 minutes later the rotation speed was then increased to 120 rpm. The maximum rotation speed was maintained for 1 minute, and then reduced to 95 rpm, which was maintained for 39 min.) [53] .....	49
Figure III.1: Density evolution of the internal water phase (W1), the organic phase (O1) and the external water phase (W2) as a function of temperature .....	60
Figure III.2: Evolution of density with temperature of the 14 internal water phases (W1) compared to the organic phase (O1) and the external water phase (W2). Results are presented in the order of the growing density with W1 (1) at the bottom and W1 (14) at the top.....	62
Figure III.3: Representation of the repartition of shells NC for six internal aqueous phases. Each graph represents the frequency of shells in percent versus the shells NC.....	64
Figure III.4: Average shells NC as a function of the density gap between the internal water phase and the organic phase at 60°C for the 38 bottles collected. ....	65
Figure III.5: Percentage of shells with NC < 4% as a function of the density gap between the internal water phase and the organic phase at 60°C for the 38 bottles collected. ....	66
Figure III.6: Plots of the percentage of shells as a function of the shells non-concentricity for the 14 different internal water phases .....	67

Figure III.7: Pictures of the final products obtained within two different bottles with different experimental parameters. On the left picture you can see a descent amount of shells with few beads (the beads are the white spheres of low diameter). On the right picture you can see just a few shells with a lot of beads. ....	68
Figure III.8: Yield of shells obtained as a function of the density gap between the internal water phase and the organic phase at 60°C. ....	69
Figure III.9: Average shells sphericity as a function of the density gap between the internal water phase and the organic phase at 60°C for the 38 bottles collected. ....	71
Figure III.10: Plots of the percentage of shells as a function of the shells non-concentricity for the 11 bottles collected while using W1(12) as the internal water phase.....	73
Figure III.11: Plots of the percentage of shells as a function of the shells non-concentricity for the 11 bottles collected while using W1(12) as the internal water phase (curves in color) and for the 14 different internal water phases (black dotted curves) .....	73
Figure III.12: Image of the droplet injector when the needle 1 is centered as best as it is possible (scale: 7 mm on the picture represents 200 $\mu\text{m}$ ) .....	74
Figure III.13: Image of the droplet injector when by purpose the needle 1 is not centered (scale: 7 mm on the picture represents 200 $\mu\text{m}$ ) .....	75
Figure III.14: Plots of the percentage of shells as a function of the shells non-concentricity for the four bottles collected (B1 and B2 are the bottles collected with the needle 1 centered and B3 and B4 with the one not centered). In addition, the results obtained with the 11 bottles collected for the reproducibility process are presented in the graphic by the doted black lines. ....	76
Figure III.15: Evolution of the density of the four internal water phases (W1(3), W1(7), W1(11) and W1(12)) and the organic phase (O1) with the temperature from 20 to 80°C .....	79
Figure III.16: Evolution of the interfacial tension between the organic phase O1 and the four internal water phases (W1(3), W1(7), W1(11) and W1(12)) with the temperature from 20 to 70°C.....	80
Figure IV.1: Illustration of the three different circulation systems available to synthesize foam shells.....	86
Figure IV.2: Plots of the percentage of shells as a function of the shells non-concentricity for the three different circulation systems while using three different internal water phases. The black doted lines represent the results obtained for the 11 bottles collected while using	

W1(12) as the internal water phase with the tube with areas of constriction as presented in Chapter III. ....	89
Figure IV.3: Shape of the shell at first and at the end of the whole synthesis process .....	90
Figure IV.4: Illustration of a shell going down the tube with areas of constriction and turning round on itself. The pictures come from the movie made with an ultra fast frame grabber camera. ....	91
Figure IV.5: Plots of the percentage of shells as a function of the shells non-concentricity for the straight tube (colored curves: green, red and blue) and for the tube with areas of constriction (black dotted curves) while using W1(12) as the internal water phase .....	92
Figure IV.6: Evolution of the percentage of residual monomer as a function of time for the organic phase during the synthesis process.....	96
Figure IV.7: Schematization of the successive steps of a crosslinking reaction: (a) mixture of monomers, (b), (c) and (d): intermediary steps, (e) final network [13] .....	97
Figure IV.8: Evolution of shear loss modulus $G''$ , and of shear storage modulus $G'$ , as a function of reaction time, for the organic phase at 60°C .....	97
Figure IV.9: Evolution of the kinematic viscosity of the organic phase along the synthesis at 60°C.....	99
Figure IV.10: Plots of the percentage of shells as a function of the shells non-concentricity for the long wound tube (colored curves: red, orange and blue) and for the tube with areas of constriction (black dotted curves) while using W1(12) as the internal water phase.....	101
Figure IV.11: Optimized rotation speed versus rotation time .....	103
Figure IV.12: Plots of the percentage of shells as a function of the shells non-concentricity for the tube with areas of constriction while using W1(12) as the internal water phase with collecting flasks empty (black dotted curves) and with 2 flasks filled before collection.....	104
Figure V.1: Evolution of shear loss modulus $G''$ , and of shear storage modulus $G'$ , as a function of reaction time, for the organic phase at 60, 70, 80 and 90°C.....	109
Figure V.2: Plot of $\ln(t)$ as a function of $1/T$ for the polymerization reaction of the organic phase.....	112
Figure V.3: Contents of a bottle collected with the tube with areas of constrictions followed by the flask heated at 90°C.....	113
Figure V.4: Bottles collected with the wound tube heated at 90°C .....	113
Figure V.5: IR spectrum of a mixture of Span 80 and oleic acid.....	115

Figure V.6: Spectra of pure Span 80 (blue spectrum) and of Span 80 mix with water at 90°C during 30 minutes (red spectrum) .....	116
Figure V.7: Absorbance spectrum in the UV domain for the organic phase O1 and the external water phase W2 .....	118
Figure V.8: Two kinds of UV lamp with a black neon UV lamp on the left and a UV spot on the right .....	118
Figure V.9: Absorption spectra of the four selected photoinitiators (Irgacure 184 = 1-hydroxycyclohexylphenylketone, Darocur 1173 = 2-hydroxy-2-methyl-1-phenyl-propan-1-one, DMPA = 2,2-dimethoxy-2-phenylacetophenone, BEE = benzoin ethyl ether).....	119
Figure V.10: Evolution of shear loss modulus $G''$ , and of shear storage modulus $G'$ , as a function of reaction time for the organic phase and each of the four photoinitiators .....	120
Figure V.11: Organic phases with the four photoinitiators exposed to a UV light intensity of 3 $mW.cm^{-2}$ during 1 min (samples on the left) or 5 min (samples on the right).....	121
Figure V.12: On the left, picture of the extractor wood with the UV black neon lamp placed on top of the rotating flasks. On the right, illustration of the distance between the UV lamp and the flask filled with shells.....	122
Figure V.13: Picture of a shell, on the left, and pictures of shells agglomerates, obtained during the synthesis of shells with 1% DMPA .....	123
Figure V.14: Pictures of shells synthesized by thermal polymerization .....	124
Figure V.15: Pictures of three shells obtained with 5% of DMPA .....	124
Figure V.16: Pictures of shells obtained with 10 and 15% of DMPA .....	125
Figure V.17: SEM images of the internal wall surface of dry shells synthesized with either 1, 5, 10 or 15% of DMPA. The magnification for the four SEM images is 10000. ....	125
Figure V.18: SEM images of the external wall surface of dry shells synthesized with 15% of DMPA. The magnification for the SEM image is 10000.....	126
Figure V.19: On the left, picture of the UV spot placed on top of the rotating flask. On the right, illustration of the distance between the UV spot and the flask filled with shells.....	127
Figure V.20: Pictures of shells obtained with the UV spot with either 1, 5, 10 or 15 % of DMPA .....	128
Figure V.21: SEM images of the internal wall surface (picture on the left) and of external wall surface (picture on the right) of dry shells synthesized with 10% of DMPA. The magnification for the SEM images is 10000. ....	128

Figure V.22: SEM images of the internal wall surface (picture on the left) and of external wall surface (picture on the right) of dry shells synthesized by thermal polymerization. The magnification for the SEM images is 10000. ....	129
Figure A.1: Gas chromatography GC 9000 series from Fisons Instruments .....	138
Figure A.2: ARES rheometer from Rheometric Scientific .....	139
Figure A.3: Densitometer DMA 5000.....	139
Figure A.4: Capillary viscometry with a micro-Ubbelohde viscometer .....	140
Figure A.5: pendant drop apparatus from GBX.....	141
Figure A.6: Illustration of the software used to analyze a shell.....	142
Figure A.7: Curves of the thickness variation of the real points (white dots) and of the fitted points (blue curve).....	143
Figure A.8: Curves of the sphericity deviation for the internal wall (pink dots) and for the external wall (green curve).....	144

## LIST OF TABLES

Table I.1: Composition of the organic phase .....	8
Table II.1: Results obtained by the United States from 1984 to 2011 on the foam shell syntheses (PS: polystyrene, PAN: polyacrylonitrile, PVAc: polyvinyl acetate, TMPTMA: trimethylolpropane trimethacrylate, RF: resorcinol formaldehyde, DVB: divinyl benzene)...	42
Table II.2: Results obtained by Japan from 1986 to 2006 on the foam shell syntheses (PS: polystyrene, MMA: methyl methacrylate, TMPTMA: trimethylolpropane trimethacrylate, RF: resorcinol formaldehyde) .....	46
Table II.3: Results obtained by France from 2002 to 2008 on the foam shell syntheses (TMPTMA: trimethylolpropane trimethacrylate, DVB: divinyl benzene) .....	50
Table III.1: Composition of the 14 internal water phases prepared .....	61
Table III.2 : Calculated density of the shell at 20 and 60°C for each internal water phase used .....	62
Table III.3: Density gaps between W1 and O1 at 20°C and 60°C for the 14 internal water phases used to synthesize foam shells.....	63
Table III.4: Percentage of shells fulfilling the NC criteria for the experiments realized before this PhD while using W1(3) as the internal water phase.....	70
Table III.5: Average non-concentricity (NC) of the 11 bottles collected while using W1(12) as the internal water phase.....	72
Table III.6: Average non-concentricity obtained for the two bottles collected with the needle 1 centered and the two bottles collected with the needle 1 not centered .....	75
Table III.7: Density differences between the internal water phase and the organic phase at specific temperatures .....	81

Table IV.1: Results of the average non-concentricity (NC) obtained for the three different circulation systems while using three different internal water phases .....	88
Table IV.2: Diameter of the shell at the exit of the droplet generator as a function of the flow of the external water phase W2, the organic phase O1 and the internal water phase W1.....	103
Table V.1: Times to reach a tridimensional network for the organic phase at various temperatures .....	110
Table V.2: Results of shells synthesis realized at 70 and 80°C .....	114
Table V.3: Yield, thickness and average non-concentricity results obtained for the synthesis of shells with 1, 5, 10 and 15% of DMPA and UV black neon lamp.....	123
Table V.4: Yield, thickness and average non-concentricity results obtained for the synthesis of shells with 1, 5, 10 and 15% of DMPA and the UV spot.....	127
Table A.1: Measurements and device constants for the micro-Ubbelohde viscometers .....	140

# **INTRODUCTION**



For about forty years the CEA have worked on plasma physics, particularly thanks to high power lasers like Phebus (8 kJ) in the beginning of the 80's. Then, in 1994, France started the Simulation program in order to ensure the safety and reliability of the French's nuclear stockpile. In this context, the French high power laser (LMJ: Megajoule laser) is a key element of the Simulation program. In fact, this kind of laser enables to reach very high temperatures and matter's densities. Different kinds of applications are possible such as laboratory astrophysics experiments or equation of state studies for materials under high solicitations. But one of the major interests of these high power lasers is that they enable nuclear fusion studies.

So, for the Simulation program, the Megajoule laser will be used to achieve inertial confinement fusion experiments. The inertial confinement fusion is a process where nuclear fusion is initiated by heating and compressing a fuel target, typically a plastic shell filled with a mixture of deuterium and tritium (DT).

In order to achieve ignition, different target designs are being developed, among which the gain targets and the targets for fusion preparation. The gain targets are basically composed of a cryogenic DT layer covered with a high density polymer ablator. Some specific targets are also designed for fusion preparation experiments. Some of them are composed of a low density organic foam shell covered with a high density polymer ablator. The low density organic foam can be used as a surrogate of the gain target's DT layer. The geometric characteristics of the target will have a really important influence on the quality of the implosion obtained. Thus, the targets must be made with extremely high precision and sphericity, with aberrations of no more than one micrometer over their surface. This PhD focused on the fabrication process and the sharp control of the shape of these low density organic foam shells.

The low density organic foam shells have to meet severe specifications listed below by priority order:

1. composition: C, H, O or C, H
2. diameter range: 1700-2100  $\mu\text{m}$
3. wall thickness: 100  $\mu\text{m}$
4. density: 250 and 100  $\text{mg}\cdot\text{cm}^{-3}$
5. sphericity > 99.9%

6. non-concentricity < 1%
7. porosity < 1  $\mu\text{m}$
8. roughness < 50 nm

At the beginning of this PhD, the CEA had already worked for six years on the synthesis of foam shells. The CEA chose to develop four systems of different composition and density:

- DVB shells of  $100 \text{ mg.cm}^{-3}$
- DVB shells of  $250 \text{ mg.cm}^{-3}$
- TMPTMA shells of  $100 \text{ mg.cm}^{-3}$
- TMPTMA shells of  $250 \text{ mg.cm}^{-3}$

DVB shells are made of divinyl benzene and styrene monomers and are only composed of C and H. TMPTMA shells are made of trimethylolpropane trimethacrylate monomer and are only composed of C, H and O. The shell's synthesis appears as a long and complicated process. Besides, the CEA also tested different circulation systems (tube with areas of constriction or wound tube) to synthesize the various kinds of shells.

After six years, the CEA was able to satisfy the first four restrictions (composition, diameter, thickness and density). However, the sphericity and non-concentricity requirements, which are the most difficult to meet, were far from being fulfilled. Furthermore, the non-concentricity results varied with the polymeric nature of the shells and their density.

At this point, the CEA needed to understand which major parameters of the process were influencing the sphericity and the non-concentricity. It was also necessary to know where and when the shell had an optimum non-concentricity during the synthesis process in order to set the shell's shape fast once it is perfect.

At the beginning of this PhD, it was decided to focus this work on a unique system, the TMPTMA foam shells of  $250 \text{ mg.cm}^{-3}$ . According to the literature, the three major parameters influencing the shells non-concentricity are the density, the deformations of the shells along the synthesis and the kinetics of polymerization. In this PhD work, which comprises five chapters, the effect of each of these major parameters has been studied.

Thus, the first chapter presents the shells synthesis and characterization processes and all the specific apparatus used in this aim.

In a second chapter, the literature review deals with the double emulsions, the radical polymerization, the parameters influencing the aimed specifications and the state of the art of shells synthesis in other nations involved in inertial confinement fusion experiments.

The influence of density and interfacial tension on the shells non-concentricity is discussed in Chapter III, as well as the reproducibility of the process.

Then, the Chapter IV focuses on the influence of the circulation process and the polymerization kinetics on the shells non-concentricity.

Finally, the effect of increased polymerization rates on the shells characteristics and more specifically the effect of UV polymerization are developed in Chapter V.

## **CHAPTER II. LITERATURE REVIEW**

This chapter is divided in four parts. The first part presents the basic principles of double emulsion which is the chosen process to generate shells. The following second part concerns the basic principles of radical polymerization. The third part presents the different parameters influencing diameter, thickness, density, sphericity and non-concentricity. Then, the last part describes the state of the art of shells design in the United States, Japan and France.

From the polymerization reaction point of view, the system used to synthesize foam shells can be considered as a suspension, whereas from a physical point of view the system used is considered as an emulsion. The initiator used is organosoluble as in a suspension reaction. The size of the objects synthesized by suspension mechanism is 10 to 500  $\mu\text{m}$ , whereas in emulsion process the diameter range between 0.05 and 5  $\mu\text{m}$ . The shells synthesized during this PhD are 2 mm in diameter and 100  $\mu\text{m}$  thickness, so the shell size fits to a suspension. However, the concentration of surfactant is high in our system as in an emulsion process (1 to 5 wt %), whereas in a suspension there is only around 0.1wt % of surfactant.

## II.1. BASIC PRINCIPLES OF DOUBLE EMULSIONS

### II.1.1. Simple emulsions

#### II.1.1.1. Definition of emulsions

An emulsion is a dispersion of two immiscible liquids, one being dispersed (the disperse phase) in the other (the continuous phase). There are two different kinds of simple emulsion: the oil-in-water (O/W) emulsions (direct emulsions), in which the oil droplets are dispersed within the water medium, and the water-in-oil (W/O) emulsions (inverse emulsions), which are the opposite (Figure II.1).

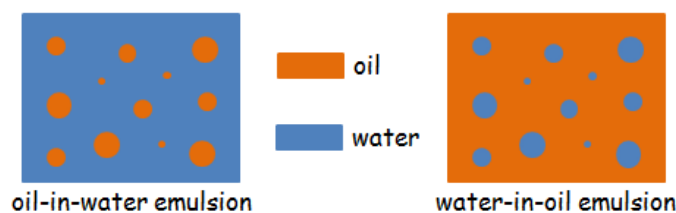


Figure II.1: Schematic representation of simple emulsion

The emulsions are highly unstable thermodynamic systems because the mixing of the two phases is not spontaneous. Indeed, an emulsifier is required to disperse two immiscible liquids and obtain a more stable system. The choice of the emulsifier is crucial for both the formation of the emulsion and its stability. Depending on their preferential solubility in either water or oil, surfactants will rather initiate an inverse or a direct emulsion. Griffin [1] developed a semi-empirical scale, the hydrophilic-lipophilic balance (HLB) number, to quantify the surfactant affinity for each phase. The scale is based on the relative percentage of hydrophilic to lipophilic groups in the surfactant molecule. The scale goes from 0 to 20 and the HLB value increases when the percentage of hydrophilic groups increases. According to the Bancroft's rule [2], stabilization of direct emulsions requires a surfactant with a high HLB number whereas inverse emulsion requires the use of a low HLB surfactant.

#### II.1.1.2. Destabilization pathways for simple emulsions

The breakdown of simple emulsions can occur according to different pathways as illustrated in Figure II.2. The breakdown is either reversible (creaming, sedimentation and flocculation) or irreversible (phase inversion, coalescence and Ostwald ripening). A summary of each of the instability pathways is given below as Tadros [3] and Binks [4] explained it in their work.

##### ✓ Creaming and sedimentation

These processes result from external forces such as gravitational or centrifugal forces. If the external forces exceed the thermal motion of the droplets (Brownian motion), a concentration gradient appears in the system such that the larger droplets move more quickly either to the top or bottom of the container. The creaming is the motion of the droplets up to the top of the container. This phenomenon occurs when the density of the droplets is less than that of the medium. The sedimentation is the motion of the droplets down to the bottom of the container which occurs when the density of the droplets is higher than that of the medium.

##### ✓ Flocculation

This process results from the Van der Waals attractions between droplets. Flocculation consists of the aggregation of the droplets (without any change in primary droplet size) into larger units, without rupture of the stabilizing layer at the interface. Flocculation may be either weak (reversible) or strong (not easily reversible), depending on the magnitude of the attractive energy involved between droplets.

✓ Phase inversion

Phase inversion consists of the exchange between the disperse phase and the continuous phase. There are two types of phase inversion, namely the transitional inversion and the catastrophic inversion. The transitional inversion is induced by changing external parameters (temperature, electrolyte concentration...) which affect the HLB of the system. The catastrophic inversion is induced by increasing the fraction of the dispersed phase.

✓ Coalescence

This process results from the thinning and disruption of the liquid film between the droplets. Coalescence consists of the fusion of two or more droplets to form a larger one. When coalescence is brought to its end, a complete separation of the emulsion into two distinct liquid phases is observed.

✓ Ostwald ripening

This process results from the solubility difference of the dispersed phase between the small and the big droplets of the emulsion. The Ostwald ripening consists of the molecule diffusion from the smaller droplets to the larger droplets through the continuous phase. The Ostwald ripening occurs without any contact between droplets.

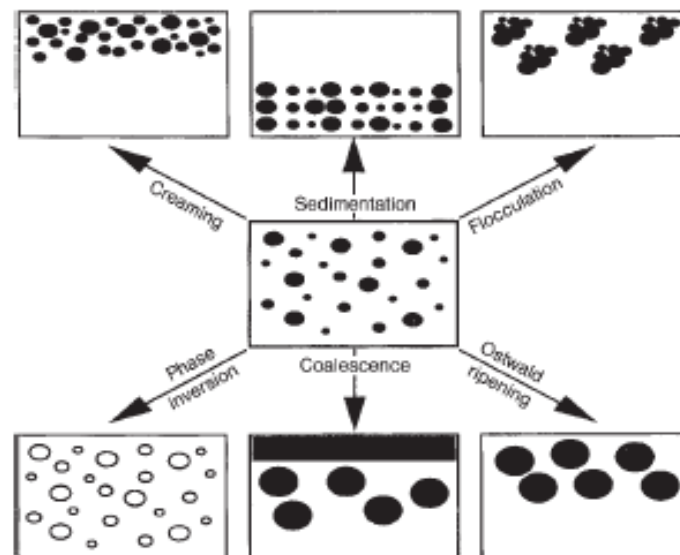


Figure II.2: Schematic representation of the various breakdown processes in emulsions as proposed by Tadros [3]

## II.1.2. Double emulsions

### II.1.2.1. Definition of double emulsions

Double emulsions are complex systems, also known as “emulsion of emulsion”, where a first emulsion of two liquids is further dispersed in another liquid. There are two kinds of double emulsions: water-in-oil-in-water (W/O/W) and oil-in-water-in-oil (O/W/O) (Figure II.3). The W/O/W double emulsion consists of one or several water droplets entrapped within a larger oil droplet that in turn is dispersed in a continuous water phase. The oil droplet is also called the globule. In this work, the double emulsion obtained consists of only one water droplet entrapped within an oil droplet.

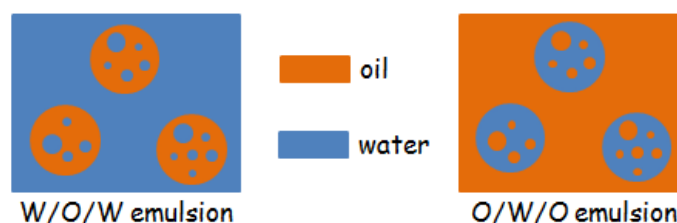


Figure II.3: Schematic representation of double emulsions

These emulsions find many applications in industries such as pharmaceuticals [5], [6], [7], cosmetics [8], [9], [10], and food [11], where they act as a reservoir of encapsulated substances that can be released by an external stimulus (pH, ionic strength, temperature...).

### II.1.2.2. Processes leading to double emulsions

Since most physical properties of these materials are size dependent, controlling their mono-dispersity as well as their uniformity in shapes and composition is a necessity. Two-stage emulsification [12] is the classical process leading to double emulsions. Highly uniform emulsion droplets can also be generated by membrane-emulsification techniques [13] and these have been applied to the production of double emulsions [14]. In recent years, there have been intensive studies of microfluidic techniques to produce droplets of highly uniform size [15], [16], [17]. For this specific application, double emulsions can be produced using either a two steps drop break-up method with a mere succession of two T junctions [18], [19], or a single step process with parallel co-flowing streams [20], [21]. In this PhD work, a droplet generator with parallel co-flowing streams is used to obtain a W/O/W double emulsion. This droplet generator is described in the first chapter.



### II.1.2.3. Destabilization pathways for double emulsions

Double emulsions are highly metastable systems with the presence of two thermodynamically unstable interfaces. In general, two different surfactants of opposite solubility are used for their stabilization. One low HLB surfactant stabilizes the internal interface (W/O) and one high HLB surfactant stabilizes the external interface (W/O). Compared with simple emulsions, double emulsions present much more destabilization processes to take into consideration, such as the release of encapsulated internal phase from the internal droplet to the continuous phase. The several destabilization pathways which can happen with double emulsions are listed below as Schmidts *et al.* [22], Florence *et al.* [23], and Leal-Calderon *et al.* [24] explained it:

- coalescence of the internal droplets
- coalescence of the globules
- coalescence of the thin liquid film separating the internal droplets and the globule surface, leading to the loss of the internal droplets with film rupturing
- “compositional ripening” leading to the loss of the internal droplets without film rupturing

Compositional ripening occurs either by diffusion or by permeation of the encapsulated molecules through the globule. Besides, diffusion of the active material can take place either by a solubility process or an inverse micelle process.

### II.1.2.4. Stabilization improvements for double emulsions

#### II.1.2.4.1. Polymeric stabilizers

Since short surfactants are not able to ensure long-term stability of double emulsions, experiments have been carried out to incorporate polymeric stabilizers [25]. Polymeric stabilizers improve the stability of double emulsions and also delay the release of molecules through interfaces since they form thick films and cannot form inverse micelles [26]. Michaut *et al.* [27] have shown that using Span 80 (short surfactant) for the internal interface (O/W) and an amphiphilic polymer for the external interface (W/O), let the interfaces asymmetric without migration of the polymer through the oil phase. In addition “slow release rates and remarkably long shelf life were obtained compared to typical double emulsions stabilized by two commonly used surfactants” [28].

#### II.1.2.4.2. Polymerization of the oily or aqueous phases of the emulsion

Another way to stabilize double emulsions is to gel or polymerize the oily or aqueous phases of the emulsion, as proposed by Florence *et al.* [23]. In our case, once the double emulsion is formed, the organic phase of the globule is polymerized.

## II.2. GENERAL CHARACTER OF THE POLYMERIZATION PROCESS

In order to polymerize the globule which contains the organic phase, a free radical polymerization process is used. Even if the polymerization process takes place within a double emulsion, the radical polymerization of the globule can be considered as a solution polymerization and not as an emulsion polymerization. Indeed, the polymerization occurs inside the organic phase layer containing the solvent, the organosoluble initiator and the monomer.

### II.2.1. Thermal free radical polymerization process

The radical polymerization is the most used industrial polymerization process since more than 50% of the polymeric materials are obtained by this process. Among the polymer of everyday use obtained by radical polymerization are: polyvinyl chloride (PVC), polyethylene (PE), polystyrene (PS), polytetrafluoroethylene (PTFE) and poly(methyl methacrylate) (PMMA). Radical polymerization reactions occur either in bulk, solution, dispersion, suspension or emulsion, at moderate temperature, between 40 and 150°C in general. However, it is necessary to work without molecular oxygen during radical polymerization reactions since it is known to cause transfer reaction or even to inhibit polymerization reactions.

Free radical polymerization consists of a sequence of three kinetics steps named initiation, propagation and termination [29], [30], [31].

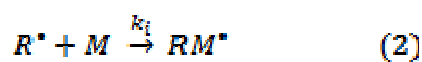
#### II.2.1.1. Initiation Step

The initiation step is composed of two reactions:

- the decomposition of the initiator  $I$  which yields to a pair of radicals  $R^\bullet$

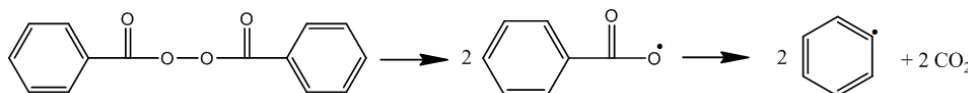


- the initiation of the polymerization which consists of the addition of the radical  $R^\bullet$  to a monomer unit  $M$

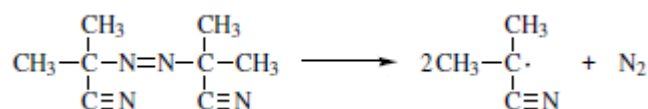


$k_d$  is the decomposition rate constant of the initiator and  $k_i$  is the initiation rate constant of the primary radical. The most popular initiators are peroxide and aliphatic azo compounds. For example, the thermal decomposition of benzoyl peroxide and azobisisobutyronitrile are presented below:

Benzoyl peroxide:



Azobisisobutyronitrile:

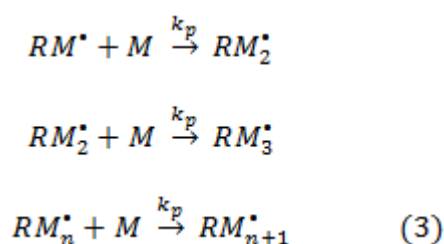


Thermal initiators are used within a specific temperature interval which depends on their kinetics of decomposition. In fact, only a part of the radicals will initiate a polymeric chain. Some of the radicals are lost in side reactions, such as, for example, a recombination of the azo compounds. The fraction of radicals which actually initiate a polymeric chain is called the efficiency factor  $f$ . In most polymerization processes, the initiation reaction is much faster than the decomposition reaction. The decomposition of the initiator is rate-determining in the initiation step. The initiation step rate is then:  $R_d = \frac{d[\text{RM}^*]}{dt} = 2 f k_d [I]$

In this polymerization process, the three steps, initiation, propagation and termination, occur as soon as the polymerization reaction begins. This means that since the polymerization reaction starts, growing polymeric chains, dead chains and monomers coexist in the solution.

### II.2.1.2. Propagation step

The propagation consists of successive additions of monomer units to the active extremity of the growing polymeric chain:

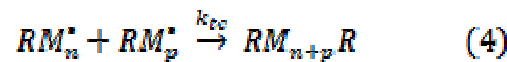


The macro-radicals created by the successive additions of monomer have the same reactivity even if their number of monomer units increases. Thus, it is assumed that the rate constants  $k_p$  for all the propagation reactions are the same. The rate of propagation is the sum of many individual propagation reactions and is expressed by:  $R_p = -\frac{d[M]}{dt} = k_p [M][M^*]$  where  $[M^*]$  represents the concentration of radicals.

### II.2.1.3. Termination step

The termination step consists in annihilating the radical center of the growing polymeric chain. The termination step can occur via two types of bimolecular free radical reactions:

- by combination (coupling) of two growing chains leading to one dead chain with combined length of the two growing chains



- by disproportionation of two growing chains leading to two dead chains, one with a saturated extremity and one with an unsaturated extremity



$k_{tc}$  and  $k_{td}$  are the termination rate constants for combination and disproportionation, respectively. The termination rate can be expressed as:  $R_t = 2 k_t [M^*]^2$  with  $k_t$  as the termination rate constant. Because of these two different termination processes which are random, the polydispersity index of radical polymerization is largely superior to one.

### II.2.1.4. Free radical polymerization kinetics

In order to determine the rate of polymerization, the amount of consumed monomer has to be measured. The initiation and the propagation steps are the two reactions consuming monomers. For a polymerization process leading to high molecular weight chains, far more monomer molecules react during the propagation reactions than during the initiation reaction. Thus, the rate of initiation can be neglected and the polymerization rate is equivalent to the rate of propagation:

$$R_{pol} = R_p = k_p [M][M^*] \quad (6)$$

Since the concentration of free radicals  $[M^*]$  is very low, this value cannot be measured easily and needs to be eliminated from equation (6). In order to simplify equation (6), the steady-state assumption is made that the concentration of radicals remains constant during the course of the polymerization. This implies that the rate of initiation  $R_i$  and termination  $R_t$  are equal:

$$2 f k_d [I] = 2 k_t [M^*]^2 \quad (7)$$

The rate of polymerization can then be deduced from equations (6) and (7):

$$R_p = k_p [M] \sqrt{\frac{f k_d [I]}{k_t}} \quad (8)$$

### II.2.1.5. Gel effect

Figure II.4 plots the bulk monomer conversion as a function of time for an ideal kinetics and when a gel effect appears in the medium. The polymerization rate is normally expected to fall with time since the monomer and initiator concentrations decrease with time. However, after a certain conversion, the viscosity of the bulk system increases as conversion increases. The increase viscosity has a slight impact on the diffusion rate of the small monomer molecule, so the polymerization rate does not drop, but the growing chains (which are big molecules) cannot diffuse fast enough and the termination rate constant decreases faster and faster, thereby leading to the auto-acceleration of the polymerization rate (“gel effect” in Figure II.4). As a consequence, many free radical polymerizations are characterized by a sudden increase of the polymerization rate when a certain conversion is reached. This phenomenon is called the gel effect or Trommsdorff effect. In diluted solution the effect of viscosity is weak, therefore the gel effect does not occur as illustrated in Figure II.5. In this PhD work, the monomer concentration is around 10% so no gel effect has to be considered.

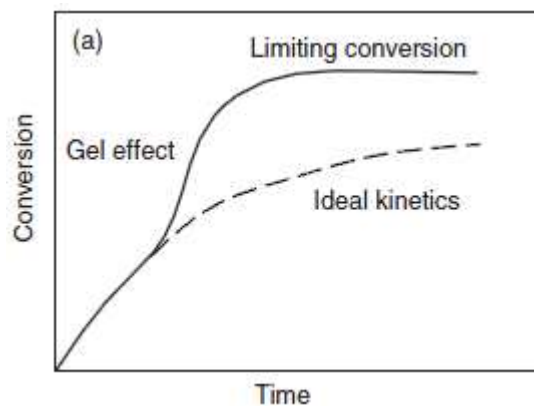


Figure II.4: Bulk monomer conversion as a function of time [30]

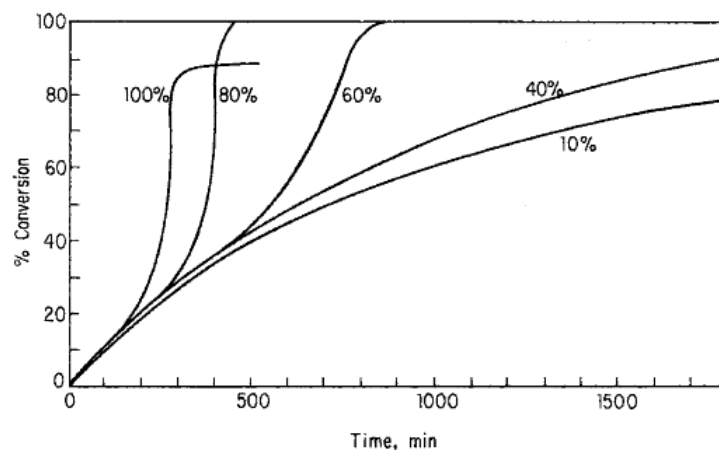


Figure II.5: Autoacceleration in benzoyl peroxide-initiated polymerization of methyl methacrylate in benzene at 50°C. The different plots represent various concentrations of monomer in solvent. [29]

### II.2.1.6. Crosslinking

Mono-functional monomers lead to linear polymers whereas multifunctional monomers as TMPTMA used in this work lead to quite different polymers concerning their structure. As explained by Andrzejewska [32], multifunctional monomers are first incorporated within polymer chains as units containing pendant bonds. Then, further propagation follows different pathways as illustrated in Figure II.6:

- path (a): addition of the next monomer unit
- path (b): intramolecular attack of the radical on the pendant double bond
- path (c): intermolecular attack of the radical on the pendant double bond

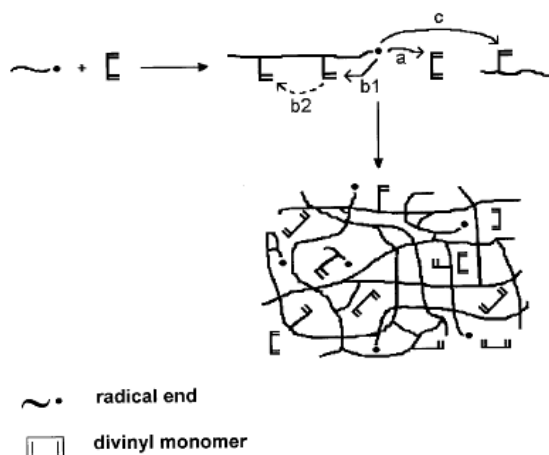


Figure II.6: Network formation [32]

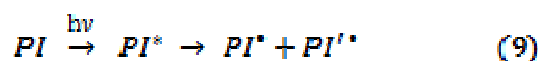
Once the number of intermolecular crosslinking reaction is high enough, a three-dimensional network is obtained. The formation of a network is noticed by the apparition of a gel inside the solution. The “gel point” is the point at which an infinite polymer network first appears. Beyond the gel point, the reaction mixture is a polymer network of infinite viscosity. Moreover, if the functionality of the monomer increases, the crosslink density and the polymerization rate increase whereas the final conversion decreases. For monomers with functionality higher than three it is difficult to reach high conversion and the gel point cannot be predicted.

The consequences of crosslinking reactions on the physic-chemical properties of the polymers are very important. Crosslinking reactions lead to a loss of crystallinity, a loss of the thermoplastic behavior and a loss of solubility of the material which becomes mechanically rigid and fragile.

### II.2.2. UV free radical polymerization process

Photoinitiation of the polymerization offers several advantages. The polymerization can be spatially directed and be turned on and off simply by turning the UV light source on and off. The process is solvent-free so the toxicity is limited and the process is classified as environmental-friendly. The reaction time and the drying step are so fast that the fabrication time and the energetic consumption are drastically lowered compared to other thermal polymerization process. These are the reasons why photopolymerization is a low-cost process. However, the main drawback to photopolymerization is the low penetration through thick or charged materials, limiting uses to the surface-type applications. The main applications of photopolymerization are the protective or decorative surface treatments of materials (wood, metal, paper, plastics, glass...), the photolithography to produce integrated and printed circuits, the anti-adhesive supports and the dental materials.

Photoinduced polymerization occurs when radicals are generated by a UV or visible light source irradiating a reactive monomer. The difference between a thermal and a photoinduced polymerization process is the initiation step. For the photopolymerization process, the initiation step is a photochemical reaction with a photoinitiator *PI*:





The initiation rate ( $R_i$ ) is given by:  $R_i = \Phi_i I_0 (1 - e^{-2.3A})$  (10)

with: -  $\Phi_i$ : quantum yield of initiation

-  $I_0$ : incident light intensity

-  $I_t$ : transmitted light intensity

-  $A$ : absorbance, defined as  $A = \log \frac{I_0}{I_t}$

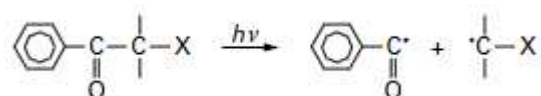
The absorbance depends on the concentration of the photoinitiator  $[PI]$  and the path length  $l$ :

$$A = \epsilon l [PI] \text{ with } \epsilon \text{ as the molar absorption coefficient}$$

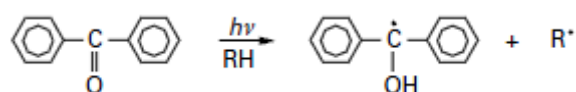
The initiation rate is controlled by the nature of the photoinitiator. To be efficient, a photoinitiator has to satisfy the following criteria [33]:

- the photoinitiator should have a high absorption within the emission spectrum of the light source used
- the singlet and triplet excited states should have a short life time to avoid their quenching by  $O_2$  or the monomer
- the radicals coming from the excited states should be produced with a quantum yield as high as possible and be active towards the monomer molecules

There are two types of processes to explain the homolysis of radical photoinitiators, called type I and type II. In the type I process, the photoinitiators, such as aromatic ketones, undergo a homolysis by cleavage into two free radicals under a UV exposition (Norrish type I reaction):



In the type II process, the mechanism requires the presence of a photosensitizer in the medium. The photoinitiator undergoes homolysis by an intermolecular hydrogen abstraction in the presence of a hydrogen donor molecule (photosensitizer) under a UV exposition:



The rate of UV polymerization can then be deduced from equations (7) and (10):

$$R_p = \frac{k_p}{\sqrt{2k_t}} [M] \sqrt{\Phi_i I_0 (1 - e^{-2.3 \epsilon_l [PI]})} \quad (11)$$

In addition, as in thermal free radical polymerization, a particular care has to be taken with oxygen. The free radical polymerizations are slowed down when operated under oxygen. To lessen the impact of oxygen, the dissolved oxygen has to be removed from the solution by degasification of the system and by polymerizing under inert atmosphere.

## II.3. PARAMETERS INFLUENCING THE AIMED CRITERIA

The following part presents the various parameters of the process influencing the diameter, thickness, density, sphericity and non-concentricity of the foam shells. For a better understanding, the three different phases used to synthesize a shell, either with a W/O/W emulsion or an O/W/O emulsion, are named internal phase (IP), surrounding phase (SP) and external phase (EP) as mentioned in Figure II.7.

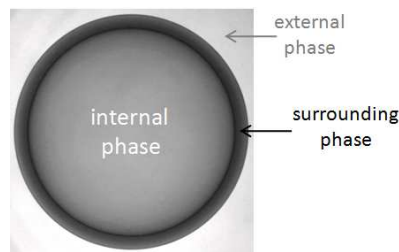


Figure II.7: Definition of the three phases

### II.3.1. Parameters influencing the diameter

The diameter is, to be more precise, the external diameter of the shell (Figure II.8). The diameter is mainly controlled by the use of a triple orifice droplet generator to synthesize shells. In fact, the diameter is controlled by the flow of the external phase which strips off the shell from the generator ([34], [35], [36], [37], [38], [39]) as illustrated in Figure II.9. The use of a droplet generator allows the synthesis of foam shells with a controlled diameter and within a narrow range of distribution. Once the shell is synthesized, the diameter of the shell varies along the polymerization and drying steps. These steps induce a shrinkage of about 10% depending especially on the quality of the drying step. The diameter of the shell, in humid and dry states, is measured with a telecentric optical microscope as exposed in Chapter I.

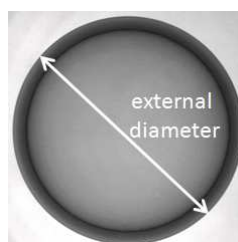


Figure II.8: External diameter of the shell

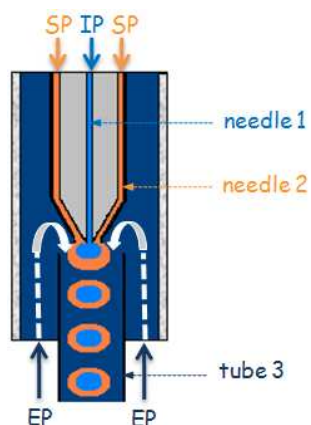


Figure II.9: Illustration of the external phase which strips off the shell formed at the tip of the generator (IP: internal phase, SP: surrounding phase, EP: external phase)

### II.3.2. Parameters influencing the thickness

The thickness of the shell is illustrated in Figure II.10. The shell thickness is determined by the ratio of the internal phase and the surrounding phase flow rates ([34], [35], [36], [37], [39]). Once the shell is synthesized, the thickness of the shell varies along the polymerization and drying steps as observed previously for the diameter. The thickness of a humid shell is deduced from the measures of the inner and outer diameters of the shell obtained with a telecentric optical microscope. The thickness of a dry shell is measured from the X-rays images of the shell.



Figure II.10: Thickness of the shell

### II.3.3. Parameters influencing the density

During the fabrication process, the density of the shell is controlled by the monomer concentration in the surrounding phase ([37], [40]). However, as for the diameter and thickness, the density varies along the polymerization and drying steps. Once again, the influence of the drying step is predominant. Indeed, a bad control of the drying process is able

to increase dramatically the density of the shell. The density of the dry shell is calculated from the measure of the diameter, thickness and weight of the dry shell.

### II.3.4. Parameters influencing the sphericity

The sphericity is a measure of the roundness of a three-dimensional object. According to the literature, several parameters influence the shells sphericity:

- the interfacial tension between the surrounding phase and the external phase
- the density of the different phases
- the viscosity of the external phase
- the stir rate

McQuillan *et al.* [41], [42], determined that for poly( $\alpha$ -methylstyrene) (PAMS) shells the density mismatch between the surrounding phase and the external phase had to be minimized to obtain higher shells sphericity. In addition, the stirring rate also has to be optimized to get better shells sphericity [41].

Cook *et al.* [43] and Takagi *et al.* [44] demonstrated that an increase of the interfacial tension between the surrounding phase and the external phase lead to higher PAMS shells sphericity. Moreover, they showed that the sphericity was sensitive to the density match of the external phase to the compound droplet (internal phase plus surrounding phase).

Paguio *et al.* [45] established that both an increased interfacial tension and a density matching between the three phases lead to higher PAMS shells sphericity.

One year later, Paguio *et al.* [46] showed that an increase of the interfacial tension between the surrounding phase and the external phase as well as an increase of the external phase viscosity lead to higher RF shells sphericity. However, the effects of interfacial tension and viscosity on shells sphericity could not be distinguished separately.

### II.3.5. Parameters influencing the non-concentricity

The non-concentricity (NC) value has to be minimized in order to get shells with a uniform wall thickness. Figure II.11 illustrates the difference between a shell with a low NC and one with a high NC. The non-concentricity is the hardest specification to meet. The wall non-uniformity adversely effects the implosions, so the foam shells are required to have a non-

concentricity lower than 1%. As explained in Chapter I, the non-concentricity of a humid shell is measured with a telecentric optical microscope, and the non-concentricity of a dry shell is measured from the X-rays images of the shell.

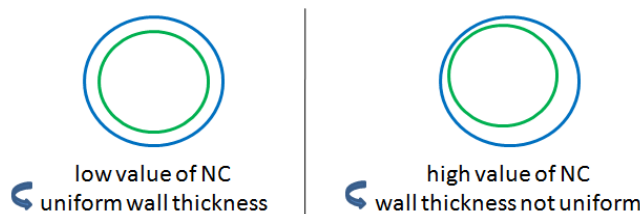


Figure II.11: Definition of the non-concentricity

The numerous parameters of the process having an influence on the NC are listed below.

### II.3.5.1. Influence of the density on the shells NC

From 1991 to 2003, [35], [47], [36], [48], the following concepts can be found in the literature: the density of the internal phase has to be equal to the density of the surrounding phase in order to obtain more concentric shells, and the density matching temperature is the polymerization temperature at which the shell's shape is set. Moreover, in order to eliminate shell sagging caused by gravity and to keep the shells suspended in solution during polymerization, the density of the external phase must be equal or slightly less than the density of the compound drop (internal phase plus surrounding phase), [36], [47], [44], [48].

In 2003, Streit *et al.* [37] studied the effect of density matching on the non-concentricity (NC) of divinyl benzene foam shells (DVB). It appeared that “the percent of NC would be minimized with a room temperature density difference between 0.008 and 0.009 g.cm<sup>-3</sup>”. They also emphasize that “other production process variables scatter the data in this range, making it difficult to determine the effect of the density difference”. Thus, in 2005, Streit *et al.* [49] concluded that “matching density beyond a rough match has not had a clear effect on NC”. However, in 2005 and 2006, [50], [38], Paguio *et al.* explained that a slight density mismatch between the internal phase and the surrounding phase (0.01 g.cm<sup>-3</sup> at 70°C for low density RF shells and 0.005 g.cm<sup>-3</sup> for high density RF shells) was one of the two factors that helped to produce resorcinol-formaldehyde (RF) shells with good wall uniformity.

Finally, the influence of density on the shell NC seems to be a largely discussed criterion in the literature. So, it seems interesting to study the influence of this criterion in the continuation of this work.

#### **II.3.5.1. Influence of the deformations on the shells NC**

When a stress is applied, a W/O emulsion distorts from its originally spherical shape and a core-centering force is generated and the water droplet moves towards the center of the oil droplet [51]. In 1999, Norimatsu *et al.* [52] showed that “non-uniform emulsion turns to be uniform by repeating instantaneous deformations followed with continuous rotation around the horizontal axis”. Shells produced with flow disruptions lead to shells with improved NC [49]. In addition, according to Ito *et al.* [53], there is an optimized rotation speed which gives shells with uniform thickness without breaking the emulsion.

#### **II.3.5.2. Influence of the polymerization kinetics on the shells NC**

This parameter is directly linked to the evolution of viscosity of the surrounding phase. The gelation time has to be long enough to let the internal phase center into the shell. Thus, it is admitted that slowing down the gelation time improves the shells NC [54], [39], [49], [50]. However, the rate of gelation has to be relatively fast due to the intrinsic instability of the double emulsion. Indeed, if the gelation time is too long the shells tend to agglomerate by flocculation and to lose their internal phase by diffusion [37], [47].

#### **II.3.5.1. Influence of the viscosity on the shells NC**

According to Norimatsu *et al.* [52], the internal phase drop moves toward the center of the emulsion depending on the viscosity of the surrounding phase. The viscosity of the surrounding phase is clearly a parameter which affects the rate of centering of the internal drop. If the centering of the internal drop is too slow compare to the increase of viscosity in the surrounding phase, non-concentric shell will be obtained. Paguio *et al.* [46], showed that the viscosity changes of the external phase cannot be completely ruled out from having an effect on the RF shells NC.

### II.3.5.2. Influence of the interfacial tension on the shells NC

Cook *et al.* [43], Takagi *et al.* [44] and Paguio *et al.* [46], [45], [55], demonstrated that increasing the interfacial tension between the surrounding phase and the external phase improves both the shells NC and the shells sphericity as stated before. Figure II.12 shows the improvement of the yield of shells that meet the NC specification by the addition of SBS block copolymer to the external phase of the emulsion. The addition of SBS to the external phase increases the interfacial tension between the surrounding phase and the external phase and also increases the viscosity of the external phase.

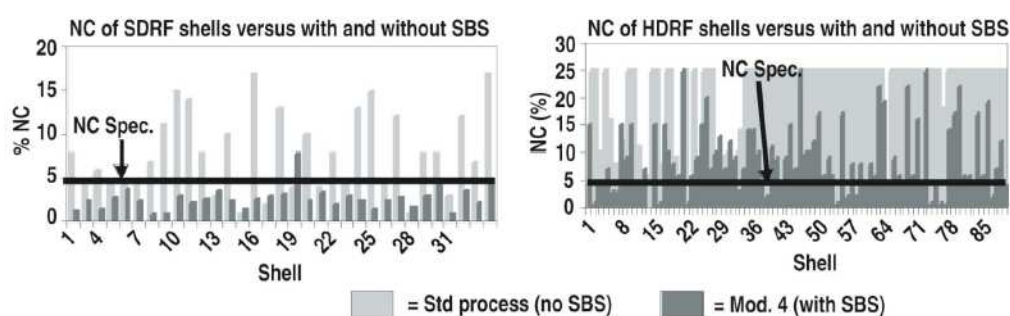


Figure II.12: The two graphics present the NC of SDRF and HDRF shells fabricated with the standard process (no SBS) and with the addition of SBS in the external phase (Mod 4). (SDRF: RF shells of low density, HDRF: RF shells of high density, SBS: styrene-butadiene-styrene block copolymer) [46]

To conclude, three of the aimed criteria, the diameter, thickness and density, are relatively easy to fulfill. The non-concentricity is the most difficult criteria to meet. According to the literature, five principal parameters are influencing the non-concentricity. However, the viscosity and the interfacial tension do not seem to have a direct impact on the non-concentricity. Indeed, papers always study the influence of these two parameters on the sphericity and show that there is also an impact on the shells non-concentricity, but no straightforward study of their influence on the non-concentricity have been realized.



## **II.4. STATE OF THE ART IN THE USA, JAPAN AND FRANCE**

The aim of this part is to compare the progress reports and the technologic choices, about the foam shell fabrication process, of major countries involved in fusion experiments until now, i.e. the United States, Japan and France. The results found and summarized below come from publications, internal progress reports and workshop presentations.

### **II.4.1. American results**

The results obtained by the United States on the foam shell synthesis from 1984 to 2011 are summarized in Table II.1. Before discussing about the results obtained by the American researchers it seems important to detail the way the non-concentricity results are presented in the literature. There are in fact two different ways to express the NC results. The American Laboratories either give the average NC of a batch of shells or the percentage of shells which have a non-concentricity below the 5% specification.

Table II.1: Results obtained by the United States from 1984 to 2011 on the foam shell syntheses (PS: polystyrene, PAN: polyacrylonitrile, PVAc: polyvinyl acetate, TMPTMA: trimethylolpropane trimethacrylate, RF: resorcinol formaldehyde, DVB: divinyl benzene)

Year	Composition	Diameter ( $\mu\text{m}$ )	Wall thickness ( $\mu\text{m}$ )	Density ( $\text{mg}\cdot\text{cm}^{-3}$ )	Accessible data on the non-concentricity (NC)	Ref
1984	PS - PAN - PVAc	50-400	5-25	-	the NC was typically less than 5%	[56]
1990	PS	100-700	2-7	-	-	[57]
1993	TMPTMA	500-1500	10-120	50	NC better than 2%	[58]
1994	TMPTMA	-	-	-	non-uniform wall thickness	[34]
1995	TMPTMA	1000-2000	100	-	lowest average batch NC = 5% lowest individual shell NC = 1%	[35]
1995	RF	2000	100	60	bad wall uniformity	[47] [36]
2003	DVB	4000	300	100	lowest average batch NC = 7% lowest individual shell NC = 3%	[37]
2004	RF	800-900	50-100	100	average NC of 5-6%	[54]
2004	DVB	4000	300	100	lowest average batch NC = 3% lowest individual shell NC = 2%	[59]
2006	RF	800-900	50-100	100	30-50% of the shells have NC < 5%	[38]
2006	RF	800-900	80-120	180-250	10-20% of the shells have NC < 5%	[38]
2006	DVB	800-3500	80-350	-	75% of the shells with NC < 5%	[60]
2007	RF	800-900	50-100	100	90% of the shells have NC < 5%	[46]
2007	RF	800-900	80-120	180-250	5% of the shells have NC < 5%	[46]
2007	DVB	4600	176	100	90% of the shells have NC < 5% 60% of the shells have NC < 3%	[61]
2011	RF	1500-5000	100-200	100	50% of the shells have NC < 5%	[55]

### II.4.1.1. Type of process

Until 1984, the USA used glass microballoons as targets. Then, in 1984, they started development of low-atomic-number foam shells. From 1984 to 1993 the foam shells were synthesized using a two-stage emulsification process developed by Kubo *et al.* [62] in Japan, which gave a W/O/W double emulsion as illustrated in Figure II.13.

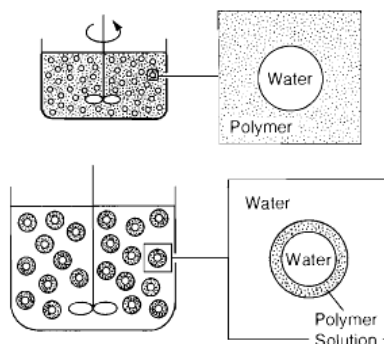


Figure II.13: Illustration of a two-stage emulsification process to produce polymer shells [56]

In the period between 1984 [56] and 1990 [57], a polymer was solubilized in the organic phase which encapsulated a water droplet and the solvent was driven off to produce the shell. Since 1993 [58], the shells were produced by thermal polymerization of a monomer in the organic phase. The major issue of the two-stage emulsification process was the broad distribution of diameter and thickness in the shell population. So, in 1994 Overturf *et al.* [34] started using a triple orifice droplet generator, similar to the one design by the Osaka University, which gave a W/O/W double emulsion. The TMPTMA globules coming out of the generator were delivered into a PVA solution inside a flask heated by a water bath and attached to a rotary evaporator set-up. The foam shells produced by this new system had a narrow size distribution but had often non-uniform wall thickness. Since 1994, the triple orifice droplet generator has been systematically used to synthesize foam shells.

### II.4.1.2. Nature of the foam

Until 1995, only TMPTMA foam shells were developed. However, studies at the Lawrence Livermore National Laboratory (LLNL) [35], showed that TMPTMA foams were “too opaque to allow optical characterization of the fuel fill at the required level of accuracy in capsules with 100  $\mu\text{m}$  thick foam walls”. “This opacity is largely due to excessive scattering of light by the relatively large, 1 to 3  $\mu\text{m}$ , cell structure which is characteristic of methacrylate

foams". So, in 1995, the LLNL started developments on RF foam shells. RF aerogel has a cell size on the order of 0.1  $\mu\text{m}$  and is significantly more transparent than the methacrylate foams. RF foam shells were then synthesized using a triple orifice generator with a reverse O/W/O double emulsion [47], [36].

TMPTMA and RF foam shells were produced for future Inertial Confinement Fusion (ICF) targets at the University of Rochester Laboratory on the Omega Upgrade facility and for the planned National Ignition Facility (NIF). In 2003, new target designs for the Inertial Fusion Energy (IFE) needed foam shells only composed of carbon and hydrogen. The RF and TMPTMA foam shells were not suitable anymore since they both contain oxygen in their chemical structure. Thus, new foam shells made of divinylbenzene (DVB) were developed by Streit *et al.* [37].

#### II.4.1.3. Studies on the NC control

In 1995, Schroen *et al.* [35] improved NC results of TMPTMA foam shells by matching the densities of the organic phase and the internal water phase at polymerization temperature (90°C). This led to TMPTMA foam shells with an average non-concentricity as low as 5% for shell batches and less than 1% for some individual shells.

Concerning the DVB foam shells, Streit *et al.* [59], in 2004, obtained better NC results by upgrading the agitation system and by matching the densities. By using a half full cylindrical horizontal flask instead of a full or two-third full angled pear shaped flask, the lowest average batch non-concentricity was 3% and some individual shells non-concentricity was less than 2%.

In addition, Cook presented in Moscow [61] the latest DVB shells results obtained with the optimization of the rotobreaker "curing" (Figure II.14). The rotobreaker "curing" process was not detailed in this presentation. 90% of the shells had a non-concentricity lower than 5%, and 60% of the shells had a non-concentricity lower than 3%.

Concerning the RF foam shells, Nikroo *et al.* [54], in 2004, discovered that two main factors improved the yield of shells: a gentle agitation and an optimum gelation time. With these optimized parameters, high yield (without further quantification) of 100  $\text{mg}\cdot\text{cm}^{-3}$  RF foam shells were synthesized with an average non-concentricity of 5%-6%.

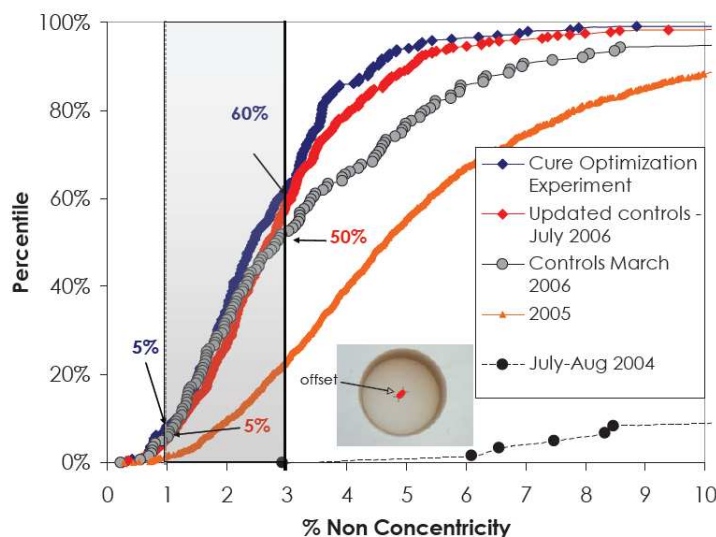


Figure II.14: Evolution of the yield (%) of DVB foam shells as a function of their non-concentricity (%) [61]

In 2006, Paguio *et al.* [38] produced shells with good wall uniformity by introducing a slight density mismatch between the organic phase and the RF precursor. For the  $100 \text{ mg.cm}^{-3}$  RF foam shells, approximately 30-50% of the shells met the non-concentricity specification of less than 5%. For the  $180\text{-}250 \text{ mg.cm}^{-3}$  RF foam shells, it was only around 10-20% of the shells.

Modifying the components of the external organic phase (which modify the interfacial tension and the viscosity) led to higher yield of shells with non-concentricity below the 5% specification as explained by Paguio *et al.* [46] in 2007. With this modification, 90% of the  $100 \text{ mg.cm}^{-3}$  RF foam shells, and 25% of the  $180\text{-}200 \text{ mg.cm}^{-3}$  RF foam shells had a non-concentricity lower than 5%.

In 2011, Paguio *et al.* [55], synthesized  $100 \text{ mg.cm}^{-3}$  RF foam shells with higher dimensions. Increasing the interfacial tension resulted in shells with better wall uniformity, leading to 50% of the RF shells which had a non-concentricity lower than 5%.

The density of the various phases appears to be a key factor over the control of non-concentricity, however it is not sufficient. In addition, it can be noted that the non-concentricity of RF foam shells is more difficult to control than for DVB and TMPTMA foam shells.

## II.4.2. Japanese results

The results obtained by Japan on the foam shell syntheses from 1986 to 2006 are summarized in Table II.2.

Table II.2: Results obtained by Japan from 1986 to 2006 on the foam shell syntheses (PS: polystyrene, MMA: methyl methacrylate, TMPTMA: trimethylolpropane trimethacrylate, RF: resorcinol formaldehyde)

Year	Composition	Diameter ( $\mu\text{m}$ )	Wall thickness ( $\mu\text{m}$ )	Density ( $\text{mg}\cdot\text{cm}^{-3}$ )	Accessible data on the non-concentricity (NC)	Ref
1986	deuterated PS	130	10	-	-	[63]
1986	polymer	110-120	3-5	-	-	[64]
1991	PS	500-1000	30-100	40	10% of the shells have NC < 5%	[65]
1991	MMA + TMPTMA	100-1500	10-120	90-130	NC better than 3%	[40]
1994	TMPTMA	300-1500	10-50	45	NC better than 2%	[51]
1994	TMPTMA	1500-1550	10-15	-	-	[51]
1998	PS	2000	-	-	50% of the shells have NC < 2%	[66]
2006	RF	1400	-	-	average NC of 12% lowest shell NC is 2%	[53]

### II.4.2.1. Two-step emulsification process

In 1986, Japan started development of low-atomic-number polymer shells. From 1986 to 1994, foam shells were synthesized using a two-step emulsification process (Figure II.13) developed by Kubo *et al.* [67].

In 1986, Kubo *et al.* [63], solubilized deuterated polystyrene in the organic phase which encapsulated a water droplet and the organic solvent was driven off to produce the shell.

Then, Takagi *et al.* [40] in 1991 used a two-step emulsification process combined with the cross-linked copolymerization of methyl methacrylate with trimethylpropane trimethacrylate in the oil phase of the emulsion. In addition, the density of the organic phase was adjusted to be equal to the density of the internal water phase in order to obtain a uniform wall. The non-concentricity of the foam shells obtained was better than 3%.

In 1994, Norimatsu *et al.* [51] used a density matched emulsion method with trimethylolpropane trimethacrylate as the only monomer in the oil phase. The shells were produced by thermal polymerization of the monomer in the organic phase. Foam shells, 300-1500  $\mu\text{m}$  diameter, 10-50  $\mu\text{m}$  wall thickness, 45  $\text{mg}\cdot\text{cm}^{-3}$  density, were fabricated with sphericity better than 98% and non-concentricity better than 2%.

#### II.4.2.2. Droplet generator

In 1986, R. Crawley [64] produced polymer foam shells (without any further information) using a specific double nozzle technique in the atmosphere. This double nozzle technique lays on the use of a gas as the internal phase and do not lead to the formation of an emulsion. This system is described by the author as follow: “the inner orifice injects bubbles of a desired gas into the polymer solution droplet stream” and “the stream is agitated using a piezoelectric diaphragm and produces uniformly sized hollow droplets”. In 1991, Chen *et al.* [65] used this dual-nozzle droplet generator and a freeze-dry technique to synthesize PS foam shells. 10% of the foam shells had a non-concentricity lower than 5%.

In 1994, Norimatsu *et al.* [51] at the Osaka University, produced shells using a dual-nozzle-in-orifice droplet generator in liquid phase as illustrated in Figure II.15. The W/O/W emulsion produced by this droplet generator was then stirred with a propeller and heated to 70°C to polymerize the TMPTMA monomer in the organic phase. 80% of the foam shells obtained had a diameter ranging from 1500 to 1550  $\mu\text{m}$  and a wall thickness ranging from 10 to 15  $\mu\text{m}$ . Thus, the droplet generator allow the synthesis of foam shells with controlled diameter and wall thickness in a narrow range as it can be illustrated in Figure II.16.

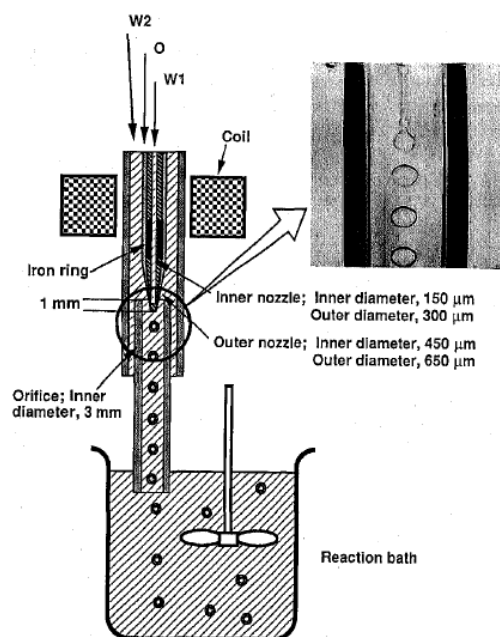


Figure II.15: Schematic diagram of a dual-nozzle-in-orifice droplet generator [51]

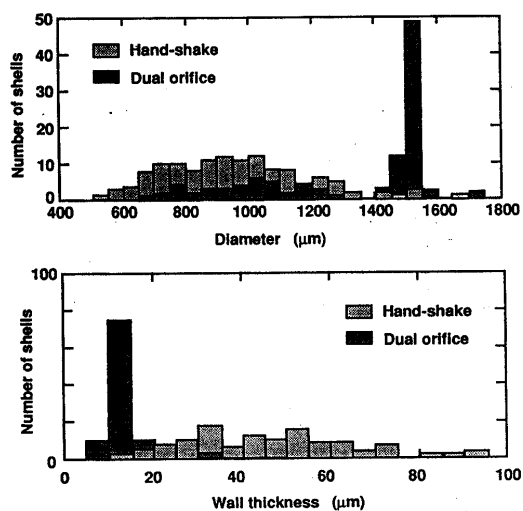


Figure II.16: Distribution of diameter and wall thickness for foam shells made by the two step emulsification process (hand-shake) and the dual-nozzle-in-orifice droplet generator [51]

In 1998, Norimatsu *et al.* [66] synthesized polystyrene shells with a triple orifice droplet generator. The W/O/W emulsion was then stirred with an inverse pitch propeller and heated at 65°C to completely remove the solvent from the oil phase. Within the 2 mm diameter shells produced, 50% had a non-concentricity lower than 2%.

Ito *et al.* [53] studied the influence of vigorous agitation conditions on the wall thickness variation in 2006. They synthesized resorcinol-formaldehyde foam shells of 1.4 mm diameter using a droplet generator. The optimized vigorous agitation conditions, illustrated in Figure



II.17, gave shells with an average non-concentricity of 12%. The best non-concentricity reached was 2%.

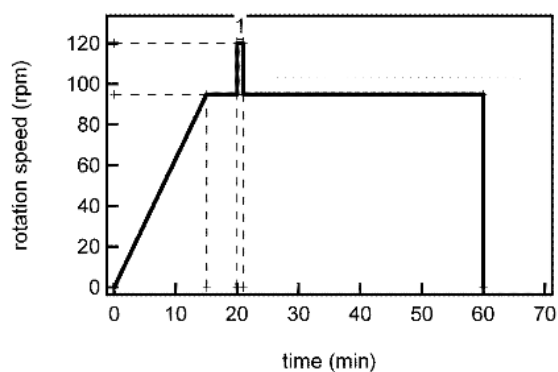


Figure II.17: Illustration of the optimized vigorous agitation conditions (The drum was rotated and its speed increased to 95 rpm within 15 minutes. 5 minutes later the rotation speed was then increased to 120 rpm. The maximum rotation speed was maintained for 1 minute, and then reduced to 95 rpm, which was maintained for 39 min.) [53]

Finally, the use of a droplet generator gives shells with narrower diameter and wall thickness distributions than with a two-step emulsification process. The agitation conditions seem to be also an important parameter over the control of non-concentricity.

### II.4.3. French results

Experiments at the CEA have started for about ten years. Until now, efforts have been focused on TMPTMA and DVB foam shells. Detailed results have not been published by the CEA during the past years. The results obtained by France on the foam shell syntheses from 2002 to 2008 are summarized in Table II.3.

Table II.3: Results obtained by France from 2002 to 2008 on the foam shell syntheses (TMPTMA: trimethylolpropane trimethacrylate, DVB: divinyl benzene)

Year	Composition	Diameter ( $\mu\text{m}$ )	Wall thickness ( $\mu\text{m}$ )	Density ( $\text{mg.cm}^{-3}$ )	Accessible data on the non-concentricity (NC)
2002	TMPTMA	1330	40-70	-	NC higher than 50%
2002	TMPTMA	1500 or 2500	-	-	NC higher than 50%
2003	TMPTMA	2300	100	250	average NC of 10% lowest shell NC is 3%
2005	TMPTMA	2000-2300	105-175	200-250	29% of the shells have NC < 4% 4% of the shells have NC < 2%
2006	TMPTMA	-	100	100	24% of the shells have NC < 4%
2007	DVB	1700 or 2000	150	110	30% of the shells have NC < 4% 10% of the shells have NC < 2%
2008	DVB	2000	130	240	30% of the shells have NC < 4% 6% of the shells have NC < 2%

The first foam shells were synthesized in 2002 using trimethylolpropane trimethacrylate as a monomer. The first process was based on a two-step emulsification process which was quickly dropped to use a triple orifice droplet generator known to give a narrower distribution of the shells diameter and thickness. In addition to the droplet generator, a fully original circulation process, a wound tube of 17 meters long, was developed to avoid flocculation and inversion phase phenomena during the synthesis.

In 2003, the process was improved with the degassing of the external water phase which led to a better yield of shells. Another improvement was the density matching of the internal

water phase with the organic phase which led to better shells NC. TMPTMA foam shells, 2300  $\mu\text{m}$  diameter, 100  $\mu\text{m}$  thickness, 250  $\text{mg}\cdot\text{cm}^{-3}$  density, with an average NC of 10%, were thus synthesized.

In 2004, a wound tube of 10 meters long was patented [68]. In 2005, with this patented wound tube heated at 90°C, 200-250  $\text{mg}\cdot\text{cm}^{-3}$  TMPTMA foam shells were produced with 29% of the shells having a non-concentricity lower than 4% and 4% of the shells having a non-concentricity lower than 2%.

In 2006, with a wound tube twice longer (20 m) and the use of a co-initiator, 100  $\text{mg}\cdot\text{cm}^{-3}$  TMPTMA foam shells were produced with 24% of the shells having a non-concentricity lower than 4%.

Since 2006, the process used for TMPTMA foam shells synthesis has been transposed to DVB foam shells synthesis with poor results. Then, a new process was developed using a droplet generator followed by a tube with areas of constriction and the organic phase was pre-heated before injection. In 2007, 110  $\text{mg}\cdot\text{cm}^{-3}$  DVB foam shells were synthesized: 30% of the shells had a non-concentricity lower than 4%, and 10% of the shells had a non-concentricity lower than 2%.

In 2008, the same process was used to synthesize 240  $\text{mg}\cdot\text{cm}^{-3}$  DVB foam shells. After some adjustment of the parameters, 30% of the shells had a non-concentricity lower than 4% and 6% of the shells had a non-concentricity lower than 2%.

## II.5. CONCLUSION

Shells are synthesized via a W/O/W double emulsion. Emulsions can undergo several destabilization pathways such as creaming, sedimentation, flocculation, phase inversion, coalescence and Ostwald ripening. In addition to all these breakdown phenomena, the double emulsions can also release the encapsulated internal droplets, with or without film rupturing. All these destabilization phenomena lead to beads instead of shells. To avoid these destabilization phenomena, a polymeric stabilizer can be used and/or one of the phases of the emulsion can be polymerized. In our case, the emulsion is stabilized by a polymeric stabilizer, the polyvinyl alcohol, and the organic phase is also polymerized.

Indeed, a free radical polymerization process in solution is used to polymerize the organic phase. The free radical polymerization is a three steps process namely initiation, propagation and termination steps, which all three occur as soon as the polymerization reaction begins. The polymerization reaction can be initiated either by thermal decomposition of the initiator or by photochemical reaction of a photoinitiator. Besides, with a multifunctional monomer as trimethylolpropane trimethacrylate with a functionality of six, intermolecular crosslinking reactions occur leading to a three-dimensional network. The time at which an infinite polymer network appears is the gel point. For monomers with functionality higher than three, the gel point cannot be theoretically predicted which means that experimental studies are necessary.

The aimed criteria for the shells, i.e. diameter, thickness, density, sphericity and non-concentricity, are influenced by several parameters during the synthesis process. During this PhD, we focused on the non-concentricity which is the most difficult specification to meet. The non-concentricity is influenced by many parameters such as the density of the three phases, the deformations of the shells along the process, the kinetics of the polymerization, the interfacial tensions and the viscosity of the phases. According to the literature, only the first three parameters have a direct influence on the shells non-concentricity. However, the parameter the most studied in the literature seems to be the density gap between the internal and surrounding phases. Thus, we decided to first study the influence of the densities on the non-concentricity of the shells synthesized with our specific process. The influence of the deformations and the kinetics were studied afterwards.

To finish, until now, three nations, the United States, Japan and France have been involved in the fabrication process of foam shells. The US and Japan have been precursors in this field. The US teams have worked on several kinds of monomers but nowadays they focused their researches on DVB and RF foam shells. The Japanese teams focused more on PS and RF foam shells. Unlike the US and Japan, France decided to carry on with TMPTMA and DVB foam shells. However, in all cases, a droplet generator is used to synthesize shells since it gives shells with narrower diameter and wall thickness distributions than with a two-step emulsification process. The density of the various phases appears to be a key factor over the control of non-concentricity, however it is not sufficient. The deformations applied to the shells before gelation seem to be also an important parameter over the control of non-concentricity. Moreover, in the literature, the reproducibility of the synthesis process is poorly described.

Since 2009, Chinese researchers have started to synthesize DVB and trimethylpropane triacrylate (TMPTA) foam shells. Today, little information is available in English language (only abstracts). It seems that they synthesize TMPTA foam shells (1.5-4 mm diameter) using a triple orifice droplet generator and UV polymerization. They synthesize DVB foam shells using either a triple orifice droplet generator (1-4 mm diameter and 90-360  $\mu\text{m}$  thickness) or a T-microchannel droplet generator (0.7-1.2 mm diameter, 60-100  $\mu\text{m}$  thickness, 90-120  $\text{mg}\cdot\text{cm}^{-3}$  density).

**Bibliographic references**

1. Griffin, W.C., *Classification of surface-active agents by HLB*. Journal of the Society of Cosmetics Chemists, 1949. **1**: p. 311-326.
2. Bancroft, W., *The theory of emulsification*. Journal of Physical Chemistry, 1913. **17**(6): p. 501.
3. Tadros, T.F., *Emulsion Science and Technology: A General Introduction*, in *Emulsion Science and Technology*, T.F. Tadros, Editor. 2009, WILEY-VCH. p. 1-56.
4. Binks, B.P., *Emulsions - Recent advances in understanding*, in *Modern aspects of emulsion science*, B.P. Binks, Editor. 1998, Royal Society of Chemistry. p. 1-55.
5. Fukushima, S., M. Nishida, and M. Nakano, *Preparation of and drug release from W/O/W type double emulsions containing anticancer agents using an oily lymphographic agent as an oil phase*. Chemical and Pharmaceutical Bulletin, 1987. **35**: p. 3375-3381.
6. Ferreira, L.A.M., et al., *Vehicle influence on in vitro release of metronidazole: role of W/O/W multiple emulsion*. International Journal of Pharmaceutics, 1994. **109**: p. 251-259.
7. Khopade, A.J. and N.K. Jain, *Multiple emulsions containing rifampicin*. Pharmazie, 1999. **54**: p. 915-919.
8. Vasudevan, T.V. and M.S. Naser, *Some aspects of stability of multiple emulsions in personal cleaning systems*. Journal of Colloid and Interface Science, 2002. **256**: p. 208-215.
9. Yoshida, K., et al., *Stability of vitamin A in oil-in-water-in-oil-type multiple emulsion*. Journal of the American Oil Chemists' Society, 1999(76): p. 195-200.
10. Yanaki, T., *Preparation of O/W/O type emulsions and its application to cosmetics*. Studies in Surface Science and Catalysis, 2001. **132**: p. 1009-1014.
11. Lobato-Calleros, C., et al., *Reduced-fat white fresh cheese-like products obtained from W1/O/W2 multiple emulsions: Viscoelastic and high-resolution image analyses*. Food Research International 2006. **39**(6): p. 678-685.
12. Matsumoto, S., Y. Kita, and D. Yonewaza, *An attempt at preparing water-in-oil-in-water multiple-phase emulsions*. Journal of Colloid and Interface Science, 1976. **57**: p. 353-361.
13. Nakashima, T., M. Shimizu, and M. Kukizaki, *Particle control of emulsion by membrane emulsification and its application*. Advanced Drug Delivery Rev, 2000. **45**: p. 47-56.
14. Graaf, S.v., C.G.P.H. Schroen, and R.M. Boom, *Preparation of double emulsions by membrane emulsification – a review*. Journal of Membrane Science, 2005. **251**: p. 7-15.
15. Umbanhowar, P.B., V. Prasad, and D. Weitz, *Monodisperse emulsion generation via drop break off in a coflowing stream*. Langmuir, 2000. **16**: p. 347-351.
16. Anna, S., N. Bontoux, and H. Stone, *Formation of dispersions using flow focusing in microchannels*. Applied Physics Letters, 2003. **82**: p. 364-366.
17. Xu, S., et al., *Generation of monodisperse particles by using microfluidics: control over size, shape, and composition*. Angewandte Chemie International Edition, 2005. **44**: p. 724-728.
18. Okushima, S., et al., *Controlled production of monodisperse double emulsions by two-step droplet breakup in microfluidic devices*. Langmuir, 2004. **20**(9905-9908).
19. Panizza, P., et al., *Controlled production of hierarchically organized large emulsions and particles assemblies on line of co-axial flow devices*. Colloids Surfaces A: Physicochemical and Engineering Aspects, 2008. **312**: p. 24-31.

20. Utada, A.S., et al., *Monodisperse double emulsions generated from a microcapillary device*. Science, 2005. **308**: p. 537-541.
21. Nie, Z., et al., *Polymer particles with various shapes and morphologies produced in continuous microfluidic reactors*. Journal of the American Chemical Society, 2005. **127**: p. 8058-8063.
22. Schmidts, T., et al., *Influence of hydrophilic surfactants on the properties of multiple W/O/W emulsions*. Journal of Colloid and Interface Science, 2009. **338**(1): p. 184-192.
23. Florence, A.T. and D. Whitehill, *Stability and stabilization of water-in-oil-in-water multiple emulsion*, in *Macro- and Microemulsions*, D.O. Shah, Editor. 1985, American Chemical Society. p. 359-380.
24. Leal-Calderon, F., V. Schmitt, and J. Bibette, *Double emulsions*, in *Emulsion Science - Basic Principles*. 2007, Springer. p. 173-199.
25. Sela, Y., S. Magdassi, and N. Garti, *Polymeric surfactants based on polysiloxanes-graft-poly(oxyethylene) for stabilization of multiple emulsions*. Colloids and Surfaces A: Physicochemical and Engineering Aspects, 1994. **83**: p. 143-150.
26. Garti, N. and R. Lutz, *Recent progress in double emulsions*, in *Emulsion: Structure Stability and Interactions*, D.N. Petsev, Editor. 2004, Elsevier. p. 557-605.
27. Michaut, F., P. Perrin, and P. Hébraud, *Interface composition of multiple emulsions: rheology as a probe*. Langmuir, 2004. **20**: p. 8576-8581.
28. Michaut, F., P. Hebraud, and P. Perrin, *Amphiphilic polyelectrolyte for stabilization of multiple emulsions*. Polymer International, 2003. **52**: p. 594-601.
29. Odian, G., *Radical chain polymerization*, in *Principles of Polymerization*. 2004, John Wiley & Sons, Inc. p. 198-349.
30. Chern, C.-S., *Introduction*, in *Principles and Applications of Emulsion Polymerization*. 2008, John Wiley & Sons, Inc. p. 1-22.
31. Herk, A.v., *Introduction to Radical (co)Polymerisation*, in *Chemistry and Technology of Emulsion Polymerisation*, A.v. Herk, Editor. 2005, Blackwell Publishing. p. 25-45.
32. Andrzejewska, E., *Photopolymerization kinetics of multifunctional monomers*. Progress in Polymer Science, 2001. **26**: p. 605-665.
33. Decker, C., *Polymerisation sous rayonnement UV*. Techniques de l'ingénieur: p. 1-14.
34. Overturf, G.E., et al., *Progress report of foam shell project*. 1994, Lawrence Livermore National Laboratory. p. 1-18.
35. Schroen-Carey, D., et al., *Hollow foam microshells for liquid-layered cryogenic inertial confinement fusion targets*. Journal of Vacuum Science and Technology A, 1995. **13**(5): p. 2564-2568.
36. Lambert, S.M., et al., *Fabrication of low-density foam shells from resorcinol-formaldehyde aerogel*. Journal of Applied Polymer Science, 1997. **65**: p. 2111-2122.
37. Streit, J. and D. Schroen, *Development of divinylbenzene foam shells for use as inertial fusion energy reactor targets*. Fusion Science and Technology, 2003. **43**: p. 321-326.
38. Paguio, R.R., et al., *Fabrication of modified density and tin doped RF foam shells and beads for direct drive experiments*. Polymeric Materials: Science & Engineering, 2006. **95**: p. 872-874.
39. Vermillon, B.A., et al., *Mass Production Methods for IFE Targets*. General Atomic Report, 2004.
40. Takagi, M., et al., *A novel technique to make foam shells with high sphericity and wall uniformity for cryogenic laser fusion targets*. Journal of Vacuum Science and Technology A, 1991. **9**(3): p. 820-823.
41. McQuillan, B.W. and A. Greenwood, *Microencapsulation process factors which influence the sphericity of 1 mm o.d. PAMS shells for ICF*. Fusion Science and Technology, 1999. **35**: p. 194-197.

42. McQuillan, B.W., et al., *The use of CaCl<sub>2</sub> and other salts to improve surface finish and eliminate vacuoles in ICF microencapsulated shells*. Fusion Science and Technology, 1999. **35**: p. 198-201.
43. Cook, R., et al., *The development of plastic mandrels for NIF targets*. 2000, Lawrence Livermore National Laboratory. p. 1-12.
44. Takagi, M., et al., *Decreasing out-of-round in poly( $\alpha$ -methylstyrene) mandrels by increasing interfacial tension*. Fusion Science and Technology, 2000. **38**: p. 46-49.
45. Paguio, R.R., et al., *Improving the yield of target quality omega size PAMS mandrels by modifying emulsion components*. Fusion Science and Technology, 2006. **49**: p. 743-749.
46. Paguio, R.R., et al., *Improving the wall uniformity of resorcinol formaldehyde foam shells by modifying emulsion components*. Fusion Science and Technology, 2007. **51**: p. 682-687.
47. Overturf, G.E., et al., *Resorcinol/formaldehyde foam shell targets for ICF*. Fusion Science and Technology, 1995. **28**: p. 1803-1808.
48. Czechowicz, D., et al. *Foam shell fabrication R&D at general atomics*. in *2nd US-Japan Workshop*. 2003. San Diego, CA.
49. Streit, J. and D. Schroen. *Foam shells: overcoating progress*. in *High Average Power Laser Program Workshop*. 2005. Lawrence Livermore National Laboratory.
50. Paguio, R.R., et al., *Fabrication capabilities for spherical foam targets used in ICF experiments*. 2005, General Atomics.
51. Norimatsu, T., et al., *Cryogenic Targets and Related Technologies at ILE Osaka University*. Journal of Vacuum Science and Technology A, 1994. **12**(4): p. 1293-1295.
52. Norimatsu, T., et al., *Modeling of the centering force in a compound emulsion to make uniform plastic shells for laser fusion targets*. Fusion Science and Technology, 1999. **35**: p. 147-156.
53. Ito, F., et al., *Optimization of gelation to prepare hollow foam shell of resorcinol-formalin using a phase transfer catalyst*. Fusion Science and Technology, 2006. **49**: p. 663-668.
54. Nikroo, A., et al., *Fabrication and properties of overcoated R/F shells for Omega experiments*. Fusion Science and Technology, 2004. **45**: p. 84-89.
55. Paguio, R.R., et al., *Development and fabrication of NIF-scale resorcinol formaldehyde foam shells for ICF experiments*. Fusion Science and Technology, 2011. **59**: p. 199-204.
56. *Polymer Microballoon Development*. LLE Review - Quarterly Report, 1984. **20**: p. 155-159.
57. *Fabrication of plastic shells*. LLE Review - Quarterly Report, 1990. **42**: p. 70-75.
58. *Fabrication of foam shells overcoated with plastic layers*. LLE Review - Quarterly Report, 1993. **56**: p. 216-221.
59. Streit, J., et al., *Divinylbenzene (DVB) Shells*, in *High Average Power Laser Program Workshop*. 2004: Princeton, NJ.
60. Paguio, R.R., et al., *Fabrication and overcoating of divinylbenzene foam shells using dual initiators*. Journal of Applied Polymer Science, 2006. **101**: p. 2523-2529.
61. Cook, R.C., et al., *Mass Production targets for inertial fusion energy*, in *Third Moscow Workshop on Targets and Applications*. 2007: Moscow.
62. Kubo, U., M. Nakatsuka, and M. Tsubakihara, *Annual progress report*. 1979, ILE, Osaka University. p. 177.
63. Kubo, U. and H. Tsubakihara, *Development of a coating technique for inertial confinement fusion plastic targets*. Journal of Vacuum Science and Technology A, 1986. **4**(3): p. 1134-1137.



64. Crawley, R., *A hollow droplet generator for polymer shell production*. Journal of Vacuum Science and Technology A, 1986. **4**(3): p. 1138-1141.
65. Chen, C., et al., *Development of foam shells for cryogenic laser fusion target*. Journal of Vacuum Science and Technology A, 1991. **9**(2): p. 340-344.
66. Norimatsu, T., et al., *Fabrication of vacuole-free polystyrene shells over a wide diameter range using W/O/W emulsion method*. Journal of the Moscow Physical Society, 1998. **8**: p. 71-78.
67. Tsubakihara, H., M. Nakatsuka, and U. Kubo, *Review of Laser Engineering (Japanese)*, 1979. **7**: p. 172.
68. Guillot, L., P. Vedrenne, and J. Etheve, *Procédé et dispositif de fabrication de billes ou de ballons en mousse polymère*. 2004.

## **CHAPTER III. OPTIMIZATION OF THE SHELLS NON-CONCENTRICITY**

The density of the three phases of the double emulsion seems to be one of the parameters the most studied over the years within the literature. So the influence of density gaps between the internal water phase W1 and the organic phase O1 on the shells NC was carefully studied during this PhD. However, despite several attempts by various authors [1], [2], [3], there is no complete theory of the physics affecting non-concentricity in the complicated synthesis process used to make shells. In this chapter, the influence of density gaps between W1 and O1 on the shells non-concentricity was studied first. Since the reproducibility of the synthesis process is an unexplored criterion, we decided to investigate it. Then the influence of the centering of the droplet injector on the shells non-concentricity was also discussed. Finally, the role of the interfacial tensions of the system has also been studied briefly.

## III.1. INFLUENCE OF DENSITY ON THE SHELLS NON-CONCENTRICITY

### III.1.1. Evolution of W2, W1 and O1 densities with temperature

TMPTMA foam shells are synthesized using an internal water phase (W1), an organic phase (O1) and an external water phase (W2). Their compositions are described in Chapter I. Previously to this PhD work, the ratio water/deuterated water in the internal water phase used for CEA experiments was calculated to obtain:  $d_{W1} = d_{O1} - 0.02 \text{ g.cm}^{-3}$  at room temperature. The density evolutions of these three phases were measured with a DMA 5000 densitometer presented in Chapter I. The evolution of the organic phase density with temperature is measured without the initiator in order to avoid polymerization reactions inside the densitometer tube. The density evolutions of W1, O1 and W2 from 20 to 80°C are presented in Figure III.1.

As expected, when temperature increases, the density of the organic phase decreases with a linear pattern whereas the densities of the water phases decrease with a slight curve pattern. The graphic in Figure III.1 shows that at polymerization temperature (60°C) the density of W1 is almost equal to the density of O1 (density gap around  $0.001 \text{ g.cm}^{-3}$ ) and the density of W2 is also close to the density of O1 (difference of  $0.0023 \text{ g.cm}^{-3}$ ). In this configuration, the density of the shell at 60°C is slightly less than the density of W2. It is the opposite of what is suggested in the literature, as explained in Chapter II.

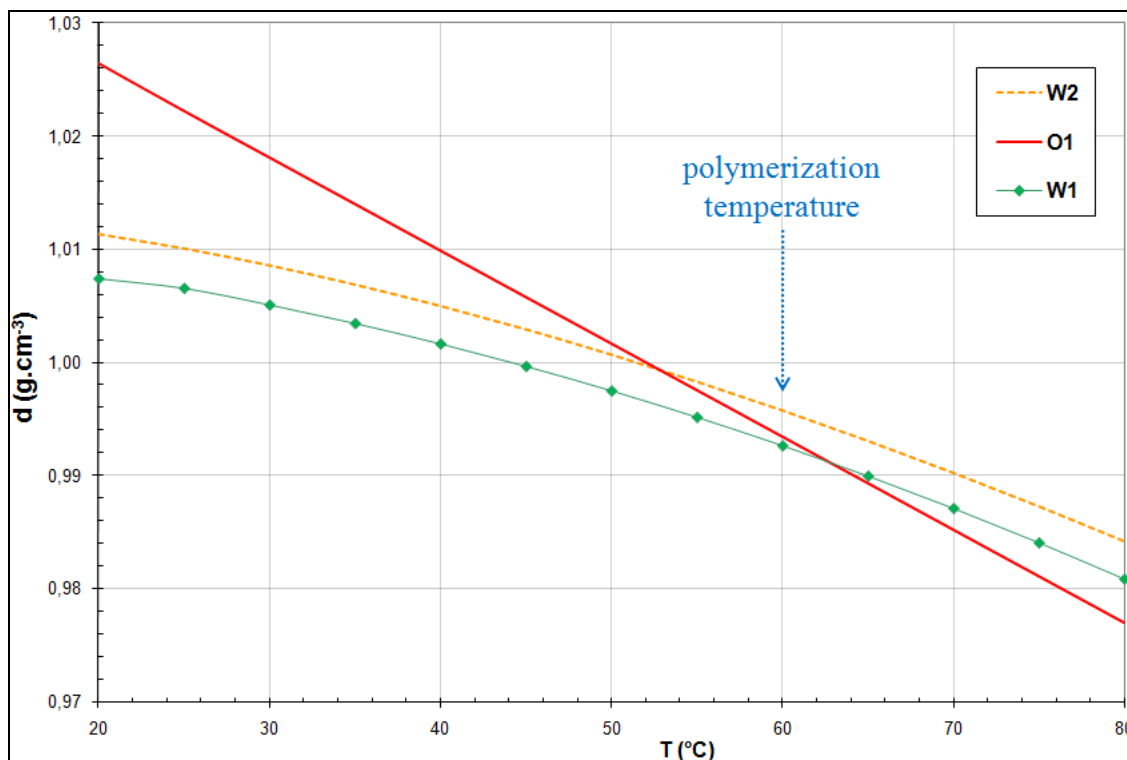


Figure III.1: Density evolution of the internal water phase (W1), the organic phase (O1) and the external water phase (W2) as a function of temperature

To study the influence of density on NC, TMPTMA foam shells were synthesized with varying density mismatch between the W1 and O1 phases. The compositions of O1 and W2 are always the same to hold their density constant. Therefore, several internal water phases (W1) (mixture of water and deuterated water) are used with different densities to find out which density gap will lead to the lowest non-concentricity. Moreover, the density of W1 will be either higher or lower than the density of O1, at polymerization temperature, in order to study the effect of a density mismatch between W2 and the shell (O1/W1). The density of the internal water phase can vary from the density of pure water (W1 (1)) to the density of pure deuterated water (W1 (14)). Thus, the density of the internal water phase can be up to 10% of the density of the organic phase.

Fourteen internal water phases have been prepared, their composition are given in Table III.1. W1(1) is pure water, then, for higher numbers, the amount of deuterated water increases and the amount of water decreases, until W1(14) which is pure deuterated water. The internal water phase used to make TMPTMA foam shells previously to this study is now called W1(3).

Table III.1: Composition of the 14 internal water phases prepared

	Concentration (wt %)	
	H <sub>2</sub> O	D <sub>2</sub> O
W1 (14)	0	100
W1 (13)	6.6	93.4
W1 (12)	16.2	83.8
W1 (11)	27.5	72.5
W1 (10)	35.8	64.2
W1 (9)	44.6	55.4
W1 (8)	53.8	46.2
W1 (7)	61	39
W1 (6)	67.5	32.5
W1 (5)	75.6	24.4
W1 (4)	83.1	16.9
W1 (3)	90.6	9.4
W1 (2)	98.2	1.8
W1 (1)	100	0

The results of the evolution of density with temperature, for O1, W1 and W2 are illustrated in Figure III.2. The density of W1 (1), pure water, is lower than the density of O1 at 60°C. If the amount of deuterated water in the internal water phase increases, the density of W1 increases and becomes eventually higher than the density of the organic phase (W1 (4) to W1 (14)).

In addition, there is, as expected, a linear relationship between the amount of deuterated water added to the internal water phase and its density at a specific temperature. The plot of the weight percent of deuterated water inside the internal water phase as a function of its density at 60°C gave a straight line with the following equation:  $y = 0.0011 x + 0.9819$  and a linear regression coefficient  $R^2$  equal to 0.9992.

The density difference between the aqueous bath (W2) and the average density of the shell formed (O1/W1) can also be interpreted from Figure III.2. Considering a shell with a 2 mm diameter and a 100  $\mu\text{m}$  thickness, the respective volume of O1 and W1 can be easily calculated. From this, it may be deduced that the density of the shell is made of 27.12% of the organic phase density plus 72.88% of the internal water phase density. Thus, the calculated shells densities at 20 and 60°C for each internal water phase are presented in Table III.2.

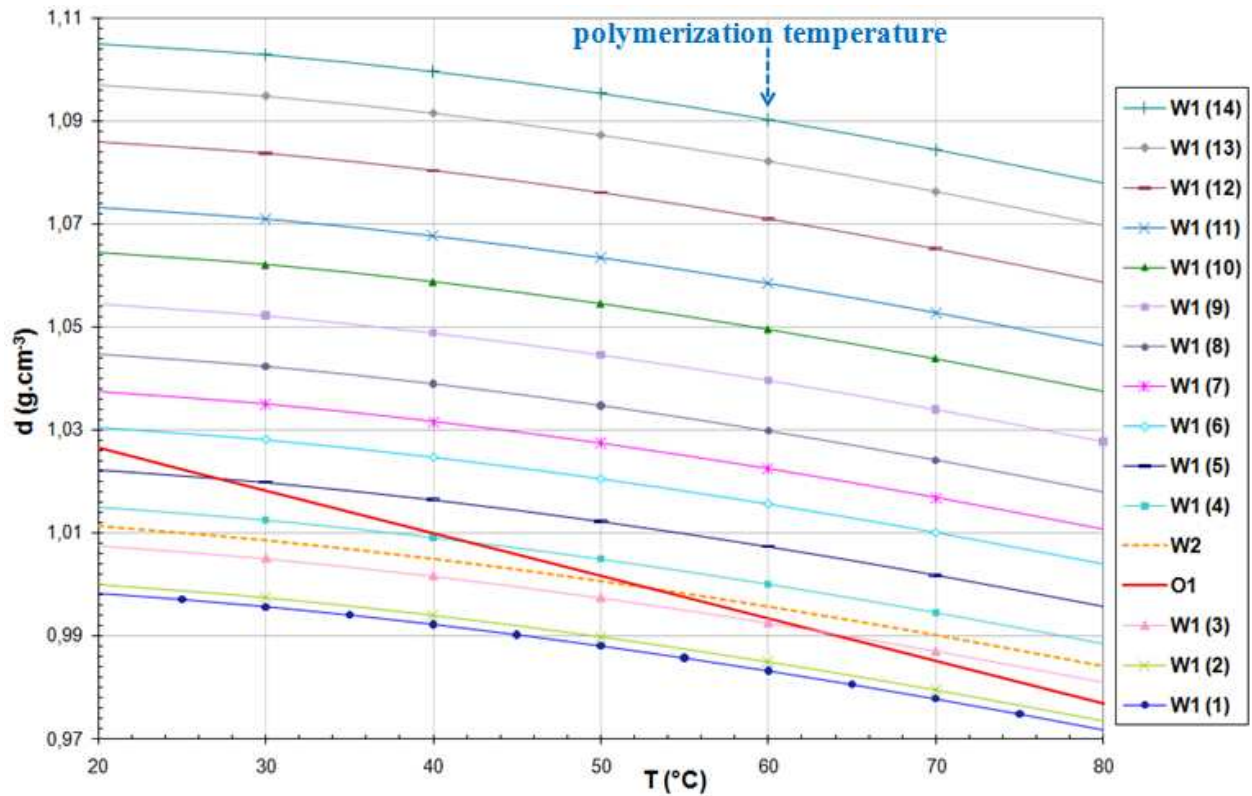


Figure III.2: Evolution of density with temperature of the 14 internal water phases (W1) compared to the organic phase (O1) and the external water phase (W2). Results are presented in the order of the growing density with W1 (1) at the bottom and W1 (14) at the top.

Table III.2 : Calculated density of the shell at 20 and 60°C for each internal water phase used

	calculated density of the shell at 20°C (g.cm <sup>-3</sup> )	calculated density of the shell at 60°C (g.cm <sup>-3</sup> )
W1 (14)	1.084	1.064
W1 (13)	1.078	1.058
W1 (12)	1.070	1.050
W1 (11)	1.061	1.041
W1 (10)	1.054	1.034
W1 (9)	1.047	1.027
W1 (8)	1.040	1.020
W1 (7)	1.034	1.015
W1 (6)	1.029	1.010
W1 (5)	1.023	1.004
W1 (4)	1.018	0.998
W1 (3)	1.013	0.993
W1 (2)	1.007	0.987
W1 (1)	1.006	0.986

The density of the external water phase W2 is equal to 1.011273 g.cm<sup>-3</sup> at 20°C and 0.995671 g.cm<sup>-3</sup> at 60°C. It is easy to see that the internal water phases W1 (1) and W1 (2) lead to an average shell density lower than the density of the external water phase. The

internal water phases, from W1 (4) to W1 (14), lead to an average shell density higher than the external water phase. The W1 (3) phase leads to an average shell density slightly less than the density of the aqueous bath as shown before.

### III.1.2. Shells syntheses with several density gaps

Fourteen internal water phases of different density have been used to synthesize TMPTMA foam shells. The compositions of the 14 internal water phases are described in Table III.1. The compositions of the external water phase and the organic phase are described in Chapter I. Table III.3 gives the density differences between W1 and O1 at 20°C and 60°C for each internal water phase. The syntheses were realized using the tube with areas of constriction described in Chapter I. During one experiment, a maximum of six bottles of shells are collected. For each bottle collected only one internal water phase can be used, from W1 (1) to W1 (14).

Table III.3: Density gaps between W1 and O1 at 20°C and 60°C for the 14 internal water phases used to synthesize foam shells.

	density difference at 20°C: dW1 - dO1 (g.cm <sup>-3</sup> )	density difference at 60°C: dW1 - dO1 (g.cm <sup>-3</sup> )
W1 (14)	0.078	0.097
W1 (13)	0.070	0.089
W1 (12)	0.059	0.078
W1 (11)	0.047	0.065
W1 (10)	0.038	0.056
W1 (9)	0.028	0.046
W1 (8)	0.018	0.036
W1 (7)	0.011	0.029
W1 (6)	0.004	0.022
W1 (5)	-0.004	0.014
W1 (4)	-0.011	0.007
W1 (3)	-0.019	-0.001
W1 (2)	-0.027	-0.008
W1 (1)	-0.028	-0.01

In order to study different density gaps between W1 and O1, 38 bottles of shells were collected from several sets of experiment. First, shells were collected with density gaps close to the equality of density (dW1 – dO1 at 60°C between -0.01 and 0.029 g.cm<sup>-3</sup>), since the literature showed that better NC results were obtained with density matching. Then, as better

NC results were obtained with higher density gaps than with density matching, shells were synthesized using higher and higher density gaps (dW1 – dO1 at 60°C between 0.029 and 0.097 g.cm<sup>-3</sup>).

Figure III.3, illustrates the repartition of shells NC as it is usually done in result reports at the CEA. As it can be seen, the repartition of shells NC is really wide for W1 (1) and W1 (3) and become narrower with W1 (7), (11), (12) and (14). The narrowest repartition is obtained with W1 (12), that is to say with a density difference between W1 and O1 equal to 0.078 at 60°C.

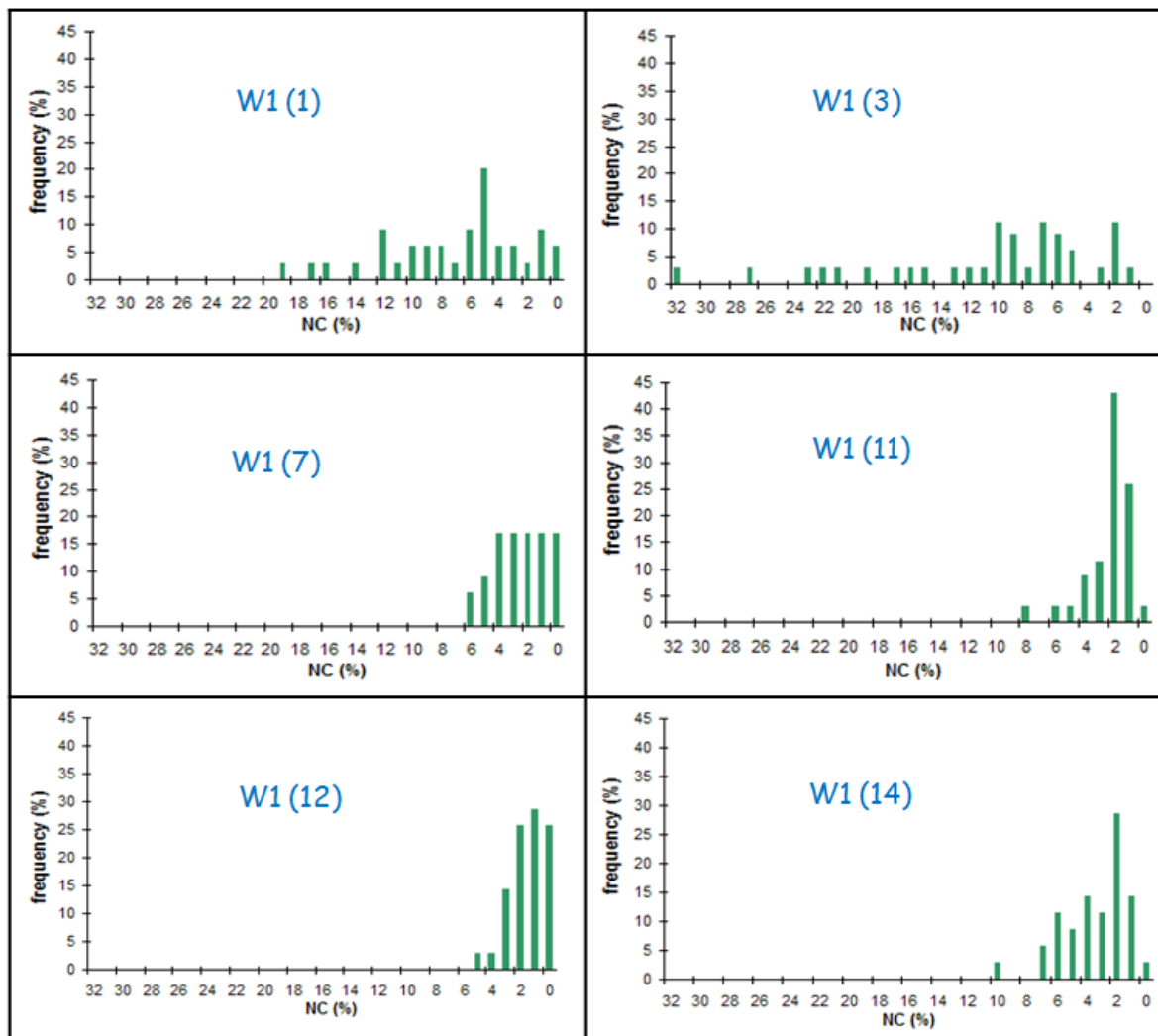


Figure III.3: Representation of the repartition of shells NC for six internal aqueous phases. Each graph represents the frequency of shells in percent versus the shells NC.

Figure III.4 illustrates the average NC of the shells as a function of the density gap between W1 and O1 at polymerization temperature for the 38 bottles collected. The results obtained do not show a straight line evolution of the average NC with the density mismatch between W1



and O1. At first, when the density gap increases from  $-0.01$  to  $-0.001 \text{ g.cm}^{-3}$ , the average NC increases from 7.5% to 11.3%. Second, when the density gap increases from  $-0.001$  to  $0.089 \text{ g.cm}^{-3}$ , the average NC decreases down to 2%. Then, a further increase of the density gap from  $0.089$  to  $0.097 \text{ g.cm}^{-3}$  increases the average NC value to 3.9%. Thus, the best NC results are obtained with both internal water phases W1(12) ( $dW1 - dO1 = 0.078 \text{ g.cm}^{-3}$  at  $60^\circ\text{C}$ ) and W1(13) ( $dW1 - dO1 = 0.089 \text{ g.cm}^{-3}$  at  $60^\circ\text{C}$ ) with an average NC of almost 2%. The dispersion of the measures is studied in part III.2 of this chapter through a reproducibility study.

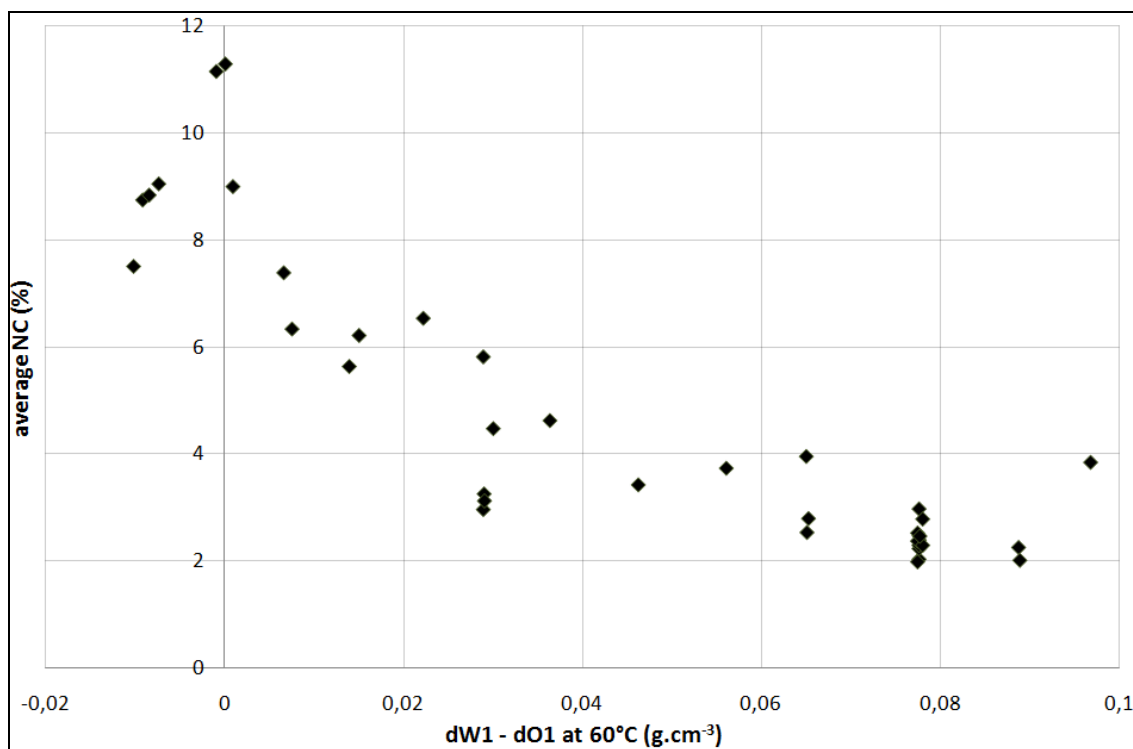


Figure III.4: Average shells NC as a function of the density gap between the internal water phase and the organic phase at  $60^\circ\text{C}$  for the 38 bottles collected.

In a second time, we focused on the amount of shells showing the best NC values with a criterion of NC lower than 4%. Classically, at the CEA, the criterion of NC lower than 4% was used before this PhD work started. The foam shells specifications stipulate that the shell non-concentricity has to be lower than 1%. However, it was specified that shells with non-concentricity as high as 4% could be used for first trial shots. The percentage of shells with  $\text{NC} < 4\%$  as a function of the density gap between the internal water phase and the organic phase at  $60^\circ\text{C}$  is illustrated on Figure III.5. The evolution of these results can be directly related to the one presented on Figure III.4. At first, when the density gap increases from

-0.01 to  $-0.001 \text{ g.cm}^{-3}$ , the percentage of shells with  $\text{NC} < 4\%$  decreases from 29% to 12%. Second, when the density gap increases from  $-0.001$  to  $0.089 \text{ g.cm}^{-3}$ , the percentage of shells with  $\text{NC} < 4\%$  increases up to 97%. Then, a further increase of the density gap from  $0.089$  to  $0.097 \text{ g.cm}^{-3}$  results in decreasing the percentage of shells with  $\text{NC} < 4\%$  to a final value of 57%. For the density gap of  $0.097 \text{ g.cm}^{-3}$ , there is only one data, so the result might be not significant.

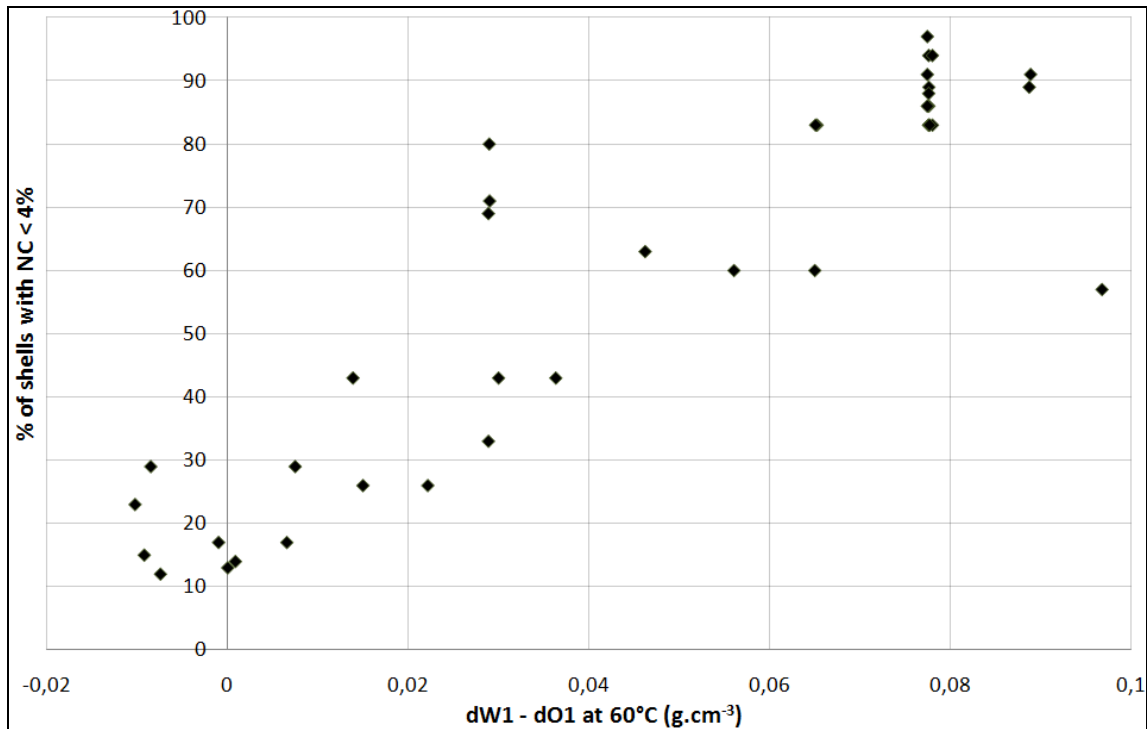


Figure III.5: Percentage of shells with  $\text{NC} < 4\%$  as a function of the density gap between the internal water phase and the organic phase at  $60^\circ\text{C}$  for the 38 bottles collected.

The results described in Figure III.4 and Figure III.5 show that widening the density gap up to  $0.089 \text{ g.cm}^{-3}$  (W1 (13)) will enhance the average NC and the percentage of shells with NC lower than 4%. With a further increase, from  $0.089$  to  $0.097 \text{ g.cm}^{-3}$ , lower results are obtained. As stated above, the result obtained at  $0.097 \text{ g.cm}^{-3}$  might be not significant since it is the only data for this density gap. All the results obtained also show that better NC results are obtained when the density of the shell is higher than the density of W2 at polymerization temperature.

Another way to present the results is to plot the percentage of shells as a function of the shells non-concentricity as illustrated in Figure III.6. This graphic shows the percentage of shells reaching certain NC values as a function of the density gaps between W1 and O1. Figure III.6 emphasizes the previous analyzes of the results showing that when the density gap increases,

from W1(4) to W1(12) and W1(13), the percentage of shells with a better non-concentricity value increases. In addition, it can be noticed from the graphic that even though the NC results are better with W1(12) and W1(13), the results obtained with W1(11) are very close to the best values. Furthermore, two different evolutions of the NC results can be noticed. For the internal water phases from W1(1) to W1(6) the evolutions of the NC results are more chaotic than for those obtained with the internal water phases from W1(7) to W1(14) which are more straightforward. A kind of gap in the values of the non-concentricity reached can be noticed between these two groups of internal water phases. This gap might be explained by the density difference between the external water phase W2 and the shell (Table III.3). When the shell's density is lower, equal or slightly higher than the density of W2, worse results of non-concentricity are obtained than when the shell's density is really higher than the density of W2.

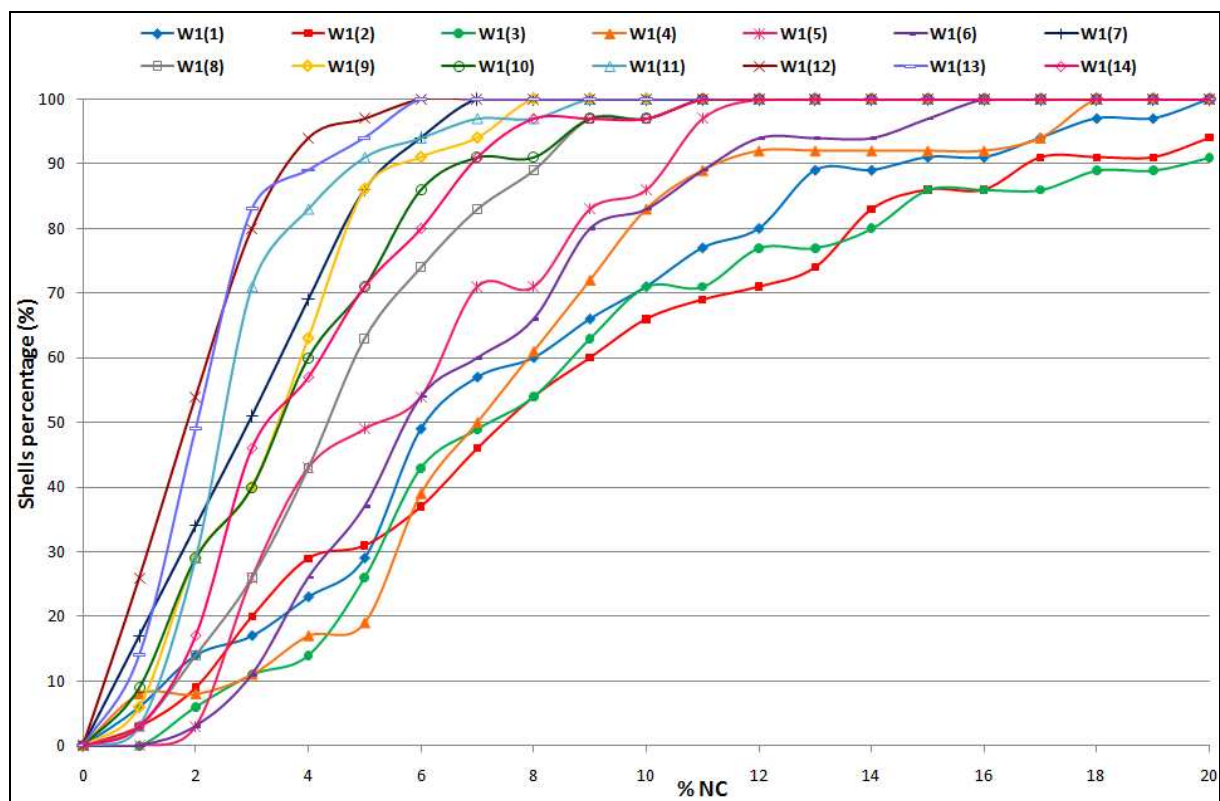


Figure III.6: Plots of the percentage of shells as a function of the shells non-concentricity for the 14 different internal water phases

### III.1.3. Yields of the synthesis

In addition to the NC study, the yields of the various syntheses were investigated. In each bottle of collected shells, reversible flocculation and irreversible phase inversion occur more or less, leading to the formation of beads instead of shells. The flocculation is a reversible phenomenon because the shells may flocculate during the water washes but they separate from each other in alcohol. Figure III.7 shows the difference between two collected bottles, one with a high yield of shells and one with a very low yield of shells.

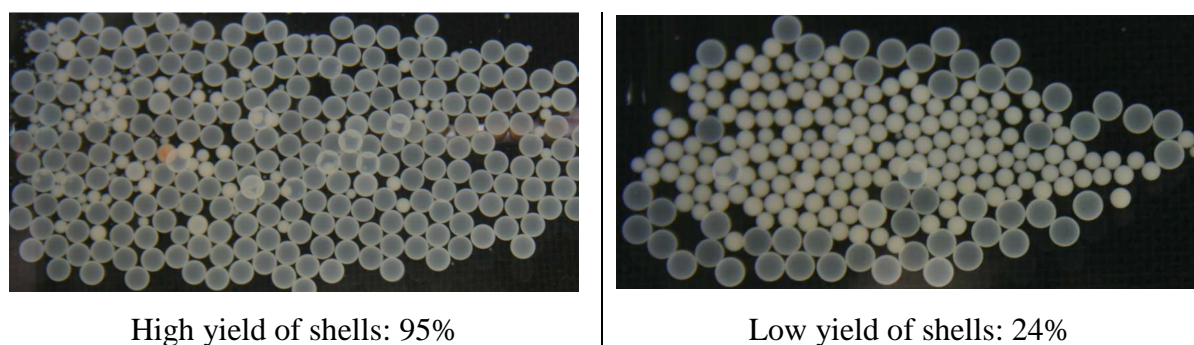


Figure III.7: Pictures of the final products obtained within two different bottles with different experimental parameters. On the left picture you can see a descent amount of shells with few beads (the beads are the white spheres of low diameter). On the right picture you can see just a few shells with a lot of beads.

The yield is calculated with the number of shells obtained in each bottle at the end of the syntheses, after the alcohol exchanges, compared to 250 shells (the maximum of shells that can be obtained with an untroubled experiment). It has to be emphasized that during the synthesis, the number of shells collected within one bottle can vary from one bottle to another. The bottle is filled horizontally until the neck of the bottle is reached by the external water phase, but the shells collected are not counted up. In addition, during the shell's cleaning and alcohol exchanges, few shells can be randomly lost. Moreover, shells are collected after five minutes of stabilization of the system and if a great disruption happens in the droplet injector, the collected shells are thrown away and new shells are collected again.

The yield of shells as a function of the density gap between W1 and O1 at polymerization temperature is presented in Figure III.8. For each density gap, the reported point is the average of the yields obtained for different bottles. Overall, the curve shows a bell-shaped profile with yield values higher than 50% for density gaps between  $-0.008$  and  $0.078 \text{ g.cm}^{-3}$  (from W1 (2) to W1 (12)). However, the yields are very low for extreme values of the density

gap:  $-0.01$ ,  $0.089$  and  $0.097$   $\text{g}\cdot\text{cm}^{-3}$  (W1 (1), (13) and (14)). As mentioned before, the best NC results are obtained for both a density gap of  $0.078$  and  $0.089$   $\text{g}\cdot\text{cm}^{-3}$ . However, the yield of shells for a density gap of  $0.078$   $\text{g}\cdot\text{cm}^{-3}$  is 58% whereas it falls to 26% for a density gap of  $0.089$   $\text{g}\cdot\text{cm}^{-3}$ . A hypothesis could be that heavy W1 phases (W1(13) and W1(14)), while moving inside the O1 globule, create film ruptures of the organic layer leading to beads instead of shells.

A compromise has thus to be made between good NC results and a high yield of shells. This is the reason why the internal water phase W1(12) ( $dW1 - dO1 = 0.078$   $\text{g}\cdot\text{cm}^{-3}$  at  $60^\circ\text{C}$ ) has been used for further experiments.

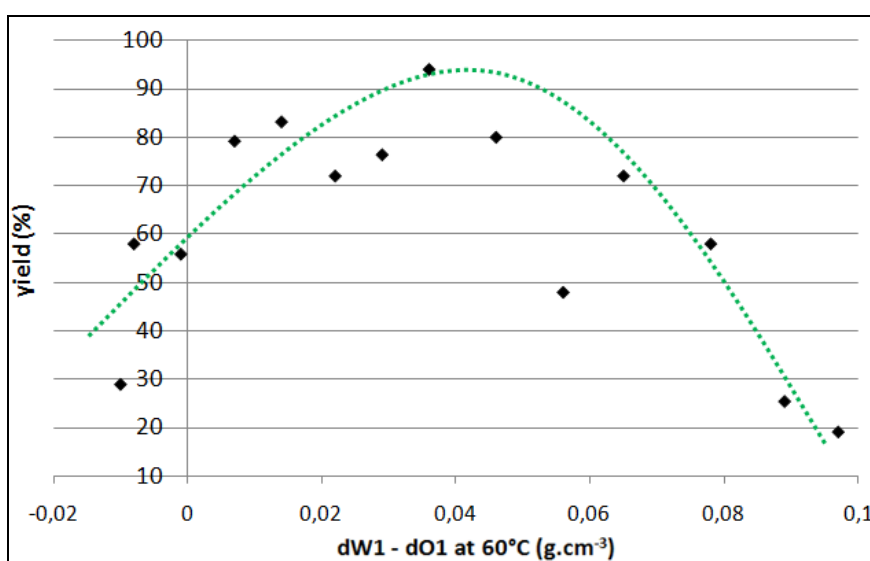


Figure III.8: Yield of shells obtained as a function of the density gap between the internal water phase and the organic phase at  $60^\circ\text{C}$ .

### III.1.4. Comparison of NC results and sphericity results

#### III.1.4.1. Comparison of previous and optimized NC results

Table III.4 presents the percentage of shells fulfilling the non-concentricity criteria (10, 8, 6, 4, and 2%) for the shells synthesized before this PhD started using W1(3) and the ones synthesized in this chapter using W1(12). Almost all the shells (99%) synthesized with W1(12) have a non-concentricity lower than 6%. In addition, 89% of the shells have a non-concentricity lower than 4% and 44% of the shells have a non-concentricity lower than 2%. A huge improvement on the shells non-concentricity has been made by increasing the density gap between the internal water phase and the organic phase.

However, major process parameters have changed between the shells synthesized before this PhD started and the ones synthesized in this chapter. Before, the shells were synthesized using a short wound tube heated at 90°C and the collecting flask was placed inside a water bath at ambient temperature. In this chapter, the shells are synthesized using a tube with areas of constriction at ambient temperature and the flask is placed inside a water bath at 60°C. Before this PhD started, DVB shells synthesized at 60°C with a tube with areas of constriction gave better results than TMPTMA shells synthesized at 90°C with a short wound tube. Then, since the beginning of this PhD, TMPTMA shells are synthesized using the DVB process. In addition, the ratio water/deuterated water in the internal water phase used before was calculated to obtain  $d_{W1} = d_{O1} - 0.02 \text{ g.cm}^{-3}$  at room temperature (W1(3)). In this chapter, W1(12) was used as the internal water phase ( $d_{W1} = d_{O1} + 0.059 \text{ g.cm}^{-3}$  at room temperature). The circulation process used may also have an influence on the improvement of the non-concentricity results. Thus, the influence of the circulation process on the shell non-concentricity will be studied in the following Chapter IV.

Table III.4: Percentage of shells fulfilling the NC criteria for the experiments realized before this PhD while using W1(3) as the internal water phase and for the experiments realized in this chapter while using W1(12)

	percentage of shells fulfilling the NC criteria	
	before with W1(3)	in this chapter with W1(12)
NC ≤ 10%	73%	100%
NC ≤ 8%	60%	99%
NC ≤ 6%	47%	99%
NC ≤ 4%	31%	89%
NC ≤ 2%	5%	44%

#### III.1.4.2. Sphericity results

It was important to check that a density gap between the internal water phase and the organic phase does not critically damage the sphericity of the shells while increasing their non-concentricity. Figure III.9 presents the average shells sphericity as a function of the density gap between the internal water phase and the organic phase at 60°C for the 38 bottles collected. No patterns emerge from the results in Figure III.9, so it can be concluded that the density mismatch between W1 and O1 has no influence on the shells sphericity.

The average sphericity obtained before this PhD started was 99.55%. The average sphericity for the 14 bottles collected in this chapter is 99.86%. So, the sphericity was not degraded and has even slightly improved between the two processes used before and during this PhD.

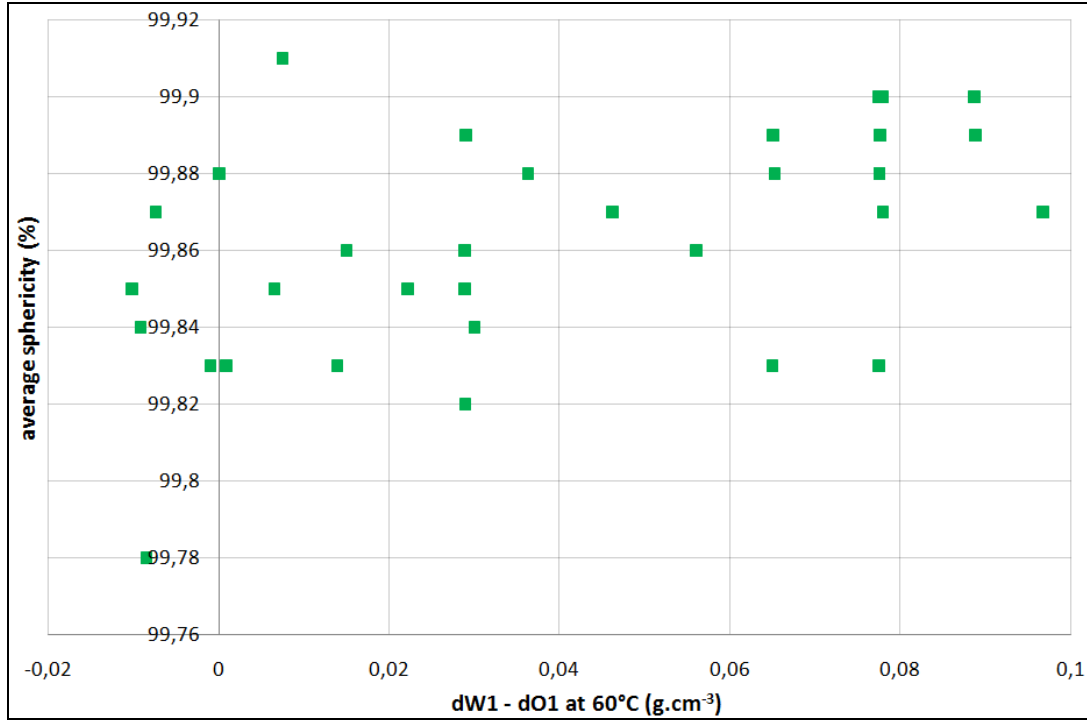


Figure III.9: Average shells sphericity as a function of the density gap between the internal water phase and the organic phase at 60°C for the 38 bottles collected.

## III.2. REPRODUCIBILITY OF THE PROCESS

The reproducibility of the process has been tested with 11 bottles collected while using W1(12) as the internal water phase. These 11 bottles have been collected in the same conditions during five different experiments realized between June 2010 and May 2011. Table III.5 presents the average non-concentricity obtained for the 11 bottles collected.

The average non-concentricity of these 11 bottles is equal to 2.40 %. The standard deviation is then equal to 0.29. The standard deviation  $\sigma$  is calculated with the formula below:

$$\sigma = \sqrt{\frac{1}{N} \sum_{i=1}^N (x_i - \mu)^2}, \quad \text{where } \mu = \frac{1}{N} \sum_{i=1}^N x_i$$

with  $\mu$  as the average,  $N$  as the number of samples and  $x_i$  as the value of the different samples.

Table III.5: Average non-concentricity (NC) of the 11 bottles collected while using W1(12) as the internal water phase

bottle	average NC (%)
1	2.04
2	2.40
3	2.48
4	2.24
5	2.30
6	2.98
7	2.53
8	2.38
9	1.99
10	2.79
11	2.30

With a standard deviation of 0.29, there is a variation of the NC values of 12% around the average NC of 2.4%.

Figure III.10 presents the percentage of shells as a function of the shells non-concentricity for the 11 bottles collected while using the same internal water phase W1(12). The evolution of the results show the same trend for each bottle with slight differences in the NC values obtained. Even so, the graphic in Figure III.10 shows that the results are homogeneous for these 11 collected bottles and taking into account the technological issues, the process can be considered as reproducible.

To emphasize this analyses the Figure III.11 plots the percentage of shells as a function of the shells non-concentricity for the 11 bottles collected while using W1(12) as the internal water phase (as in Figure III.10), and for the 14 different internal water phases used before (black dotted curves). The curves with the internal water phases from W1(1) to W1(10) are well separated from the 11 curves using W1(12) as internal water phase. The curves using W1(11) and W1(13) are mixed inside the 11 curves using W1(12), which is legitimate since their average NC results are really close (the density difference between W1(11), W1(12) and W1(13) is really slight).



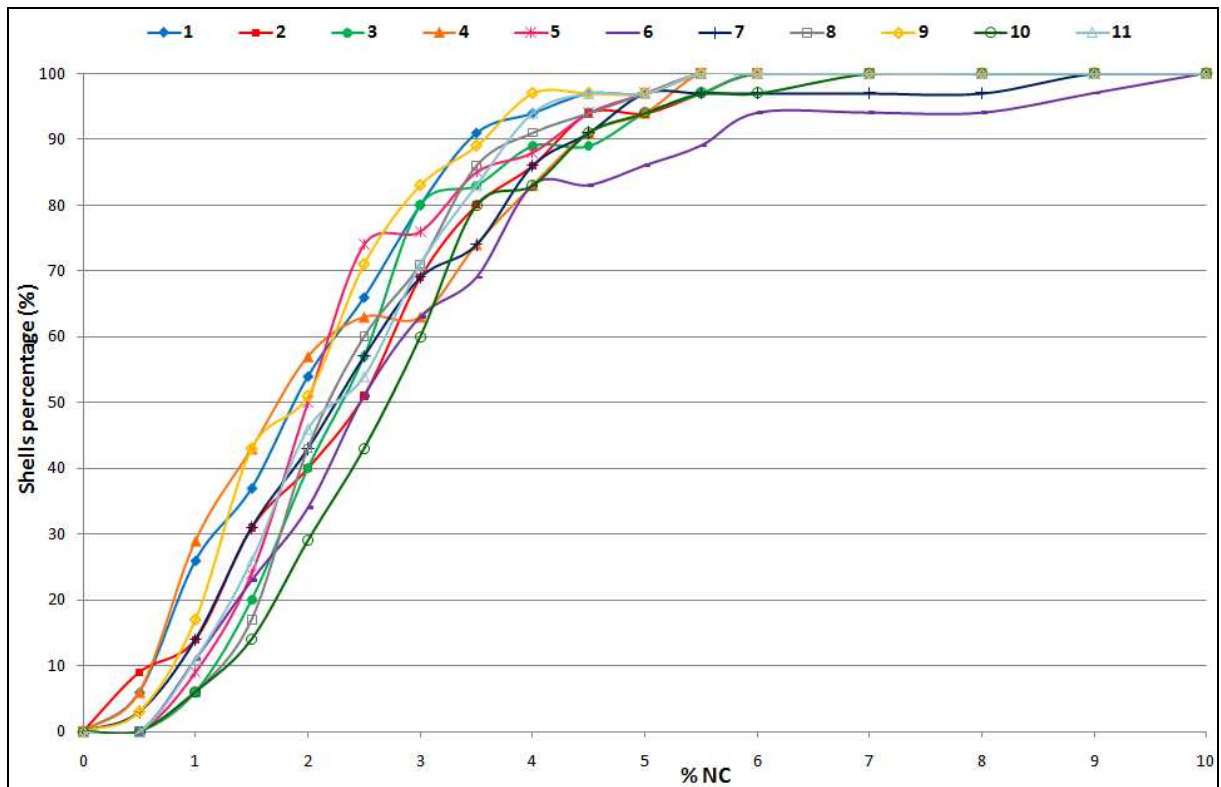


Figure III.10: Plots of the percentage of shells as a function of the shells non-concentricity for the 11 bottles collected while using W1(12) as the internal water phase

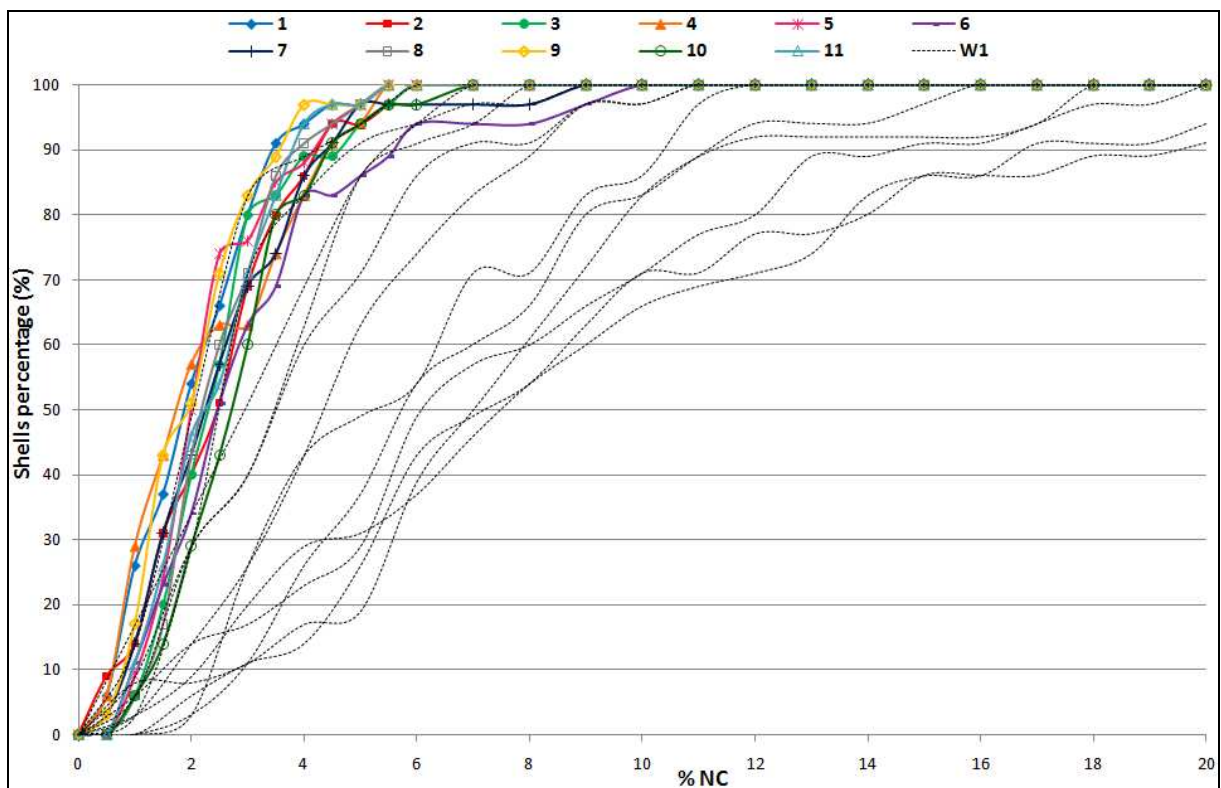


Figure III.11: Plots of the percentage of shells as a function of the shells non-concentricity for the 11 bottles collected while using W1(12) as the internal water phase (curves in color) and for the 14 different internal water phases (black dotted curves)

The slight variation in the results obtained may be due to the fact that this synthesis is a complicated and heavy process where the least little dust or air bubble can destabilize the whole injection process. Moreover, the only manually set parameter is the centering of the needle 1 inside the center of the needle 2. All the other parameters that are controllable are set automatically. So, at this point, we wonder if the centering of the droplet generator had an impact on the NC values obtained, which will be discussed in the following part.

### III.3. INFLUENCE OF THE CENTERING OF THE DROPLET INJECTOR ON THE SHELLS NON-CONCENTRICITY

As it is explained in Chapter I, the droplet generator is taken apart after each injection to clean every piece. When the droplet generator is reassembled, the centering of the needle 1 into the needle 2 is checked with a binocular. However, the centering is not measured and is only checked with the naked eye. Thus, a synthesis was planned with two different droplet injector configurations: one with the needle 1 centered as best as it is possible and one with the needle 1 intentionally moved off center. For this experiment, the centering of the needle 1 inside the needle 2 was measured precisely using a microscope.

The image obtained for the needle 1 centered at best is presented in Figure III.12. The moving off centre is measured on x and y axis. In Figure III.12, the moving off centre along x is equal to  $2.5 \mu\text{m}$  and the moving off centre along y is equal to  $1.2 \mu\text{m}$ . It can also be noticed from the picture that the needle 2 is more oval than circular and the needle 1 is not a perfect circle either.

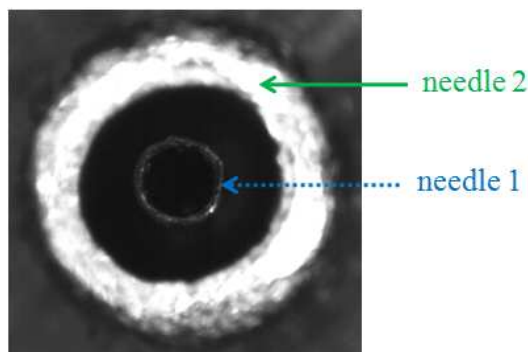


Figure III.12: Image of the droplet injector when the needle 1 is centered as best as it is possible (scale: 7 mm on the picture represents  $200 \mu\text{m}$ )

The needle 1 can be moved off center but not too much because there still need to be a space between the walls of the needles for the organic phase to flow through. Otherwise, if the needle is moved too much off centre, it won't be possible to form the shell (the internal water phase will run away from the organic phase and they will never mix) and only beads will be synthesized. The image obtained when the needle 1 is not centered is presented in Figure III.13. The moving off centre of the needle 1 is easily seen in the picture compared to the previous one. The moving off centre measured in Figure III.13 is in x equal to  $46.1\ \mu\text{m}$  and in y equal to  $8.7\ \mu\text{m}$ .

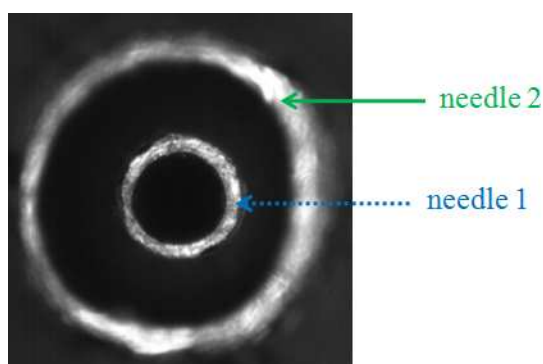


Figure III.13: Image of the droplet injector when by purpose the needle 1 is not centered (scale: 7 mm on the picture represents  $200\ \mu\text{m}$ )

Thus, two bottles were collected with the needle 1 centered and two other bottles were collected with the needle 1 not centered. For these syntheses the same process as earlier was used and the internal water phase used was W1(12). The four bottles were collected the same day and the only difference between both couple of bottles collected was the centering of the droplet injector.

The average non-concentricity obtained for the two couples of bottle collected are presented in Table III.6. Better values of the average non-concentricity are obtained when the needle 1 is not centered by comparison with the needle 1 centered. This observation means that the centering of the two needles in the droplet injector is not a key factor governing the shells NC.

Table III.6: Average non-concentricity obtained for the two bottles collected with the needle 1 centered and the two bottles collected with the needle 1 not centered

		average NC (%)
needle 1 centered	B1	2.8
	B2	2.3
needle 1 not centered	B3	2.2
	B4	1.9

However, we wondered if the moving off centre had an impact on the reproducibility of the results. Figure III.14 presents the percentage of shells as a function of the shells non-concentricity for the 4 bottles collected and also for the 11 bottles collected for the reproducibility process presented before. As for the results presented in Table III.6, the graphic shows that better results of non-concentricity are obtained with the needle 1 not centered. However, the evolutions of the NC results for the 4 bottles collected fit inside the curves of the 11 bottles collected with the same internal water phase W1(12). The 11 bottles were collected with the needle 1 more or less centered inside the needle 2. So the slight variation in the reproducibility results obtained may be partly explained by the centering of the needle 1 inside the needle 2.

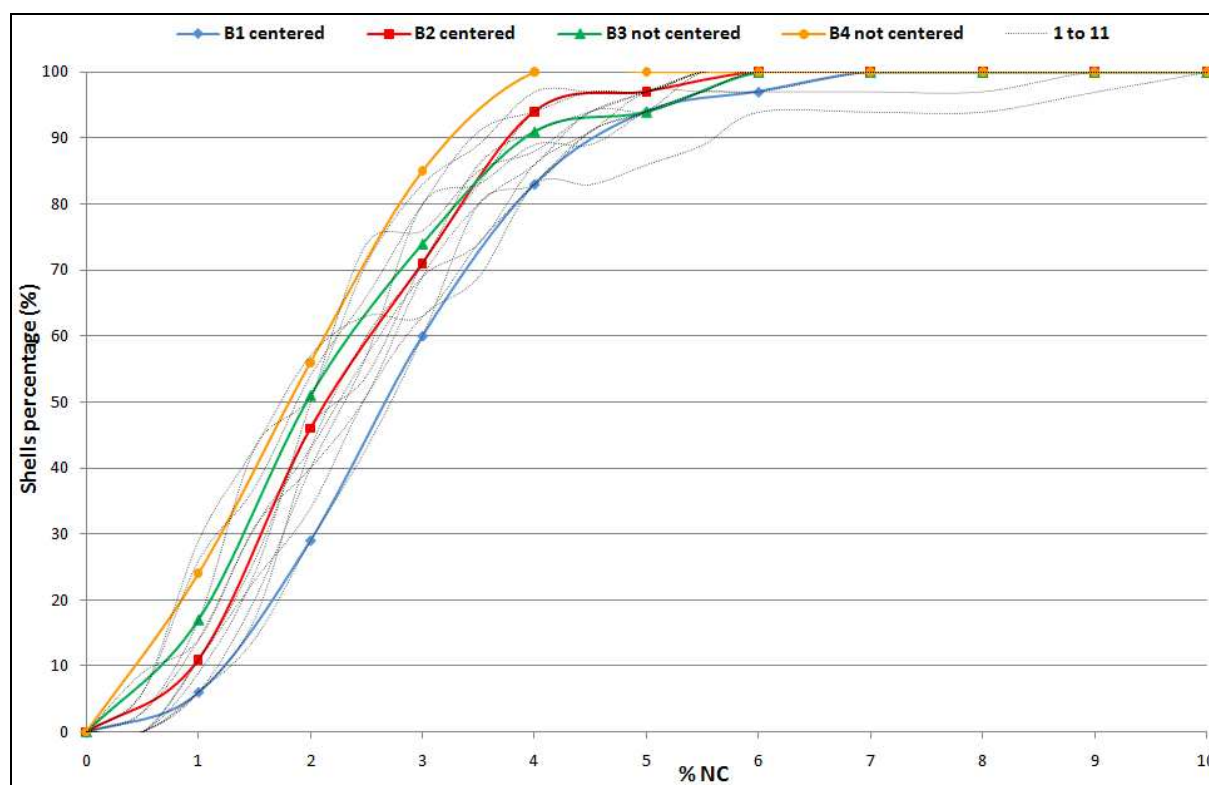


Figure III.14: Plots of the percentage of shells as a function of the shells non-concentricity for the four bottles collected (B1 and B2 are the bottles collected with the needle 1 centered and B3 and B4 with the one not centered). In addition, the results obtained with the 11 bottles collected for the reproducibility process are presented in the graphic by the dotted black lines.

When the centering of the needle 1 within the needle 2 is not perfect (which is impossible anyway), the internal water phase has to center itself within the organic phase to obtain shells with a good NC. Paguio *et al.* [4] explained that a slight density mismatch may be beneficial as it allows the internal water phase to move and center inside the organic phase. This could explain why better NC results are obtained with important density mismatch for TMPTMA

foam shells. The movements of the internal water phase inside the organic phase will be studied in Chapter IV.

### III.4. INFLUENCE OF INTERFACIAL TENSION ON THE SHELLS NON-CONCENTRICITY

The interfacial tension is the surface tension at the interface of two liquids. The surface tension is a measurement of the cohesive energy presents at an interface. The surface tension is the energy required to increase the surface area of a liquid by a unit of area. The unit of the surface tension or interfacial tension is Newton per meter ( $\text{N.m}^{-1}$ ) in SI units or dyne per centimeter ( $\text{dyn.cm}^{-1}$ ). It can also be considered in terms of work per unit area, the SI unit in that case is joule per square meter ( $\text{J.m}^{-2}$ ).

In a liquid, the molecules attract each other. The interactions between molecules in a liquid bulk are balanced by an equal attractive force in all directions. Molecules on the surface of a liquid experience an imbalance of forces. This creates some internal pressure and forces liquid surfaces to contract to the minimal area. The surface tension is responsible for the shape of liquid droplets. Although easily deformed, droplets of all liquids tend to be pulled into a spherical shape by the cohesive forces of the surface layer. In the absence of other forces, including gravity, drops of all liquids would be perfectly spherical.

Therefore, the surface tension tries to minimize the surface area, resulting in liquids forming spherical droplets. So, the shell's sphericity is linked to the interfacial tension between the organic phase O1 and the surrounding phase W2. As explained in Chapter II, Cook *et al.* [5], Takagi *et al.* [6] and Paguio *et al.* [7], [8], demonstrated that increasing the interfacial tension between the surrounding phase and the external phase improves both the shells NC and the shells sphericity. The interfacial tension between the organic phase and the external water phase is fixed by both their composition that we intentionally kept constant. However, none of the paper talks about the influence of the interfacial tension between the internal water phase and the organic phase on the shell non-concentricity. Thus, at the sight of the NC results obtained with the various density gaps, we wondered if while using internal water phases of different density the interfacial tension also changed. So, the idea was to measure the interfacial tension between the internal water phase and the organic phase at polymerization temperature  $60^{\circ}\text{C}$ .

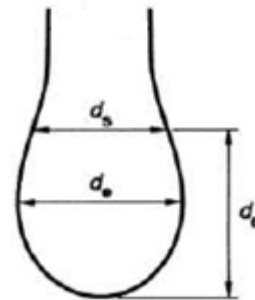
The interfacial tension between the two phases was measured using a pendant drop apparatus. The pendant drop method is based on the study of the shape of a drop of a first liquid hanging from a capillary tip inside a glass container filled with a second liquid. In that configuration, the first liquid shows a higher density than the second liquid. The pendant drop is symmetric about a central vertical axis. The balance between the interfacial tension and the buoyancy forces (Archimedes' principle) controls the drop shape. The interfacial tension tends to make the drop spherical whereas the gravity tends to elongate it.

The interfacial tension  $\sigma$  is determined by the method of Andreas, Hauser and Tucker [9] using the equation (1). The equations are based on the balance between gravitational and buoyancy forces between the liquid drop and the suspending medium. The interfacial tension is determined from the equilibrium shape of the drop profile and the density difference between the two components at relevant temperature. The shape of the drop can be described as the ratio in equation (2). Tables of  $S$  values as a function of  $H$  values had been empirically evaluated from water pendant drops [9].

$$\sigma = \frac{(\rho_1 - \rho_2)g d_s^2}{H} \quad (1)$$

$$S = \frac{d_s}{d_e} \quad (2)$$

$$H = \frac{\Delta \rho g d_s^2}{\sigma} \quad (3)$$



with  $\sigma$ : interfacial tension  
 $g$ : acceleration of gravity  
 $\rho_1$  and  $\rho_2$ : density of the drop and the medium  
 $d_e$ : diameter at the equator of the drop  
 $d_s$ : diameter at a distance  $d_s$  from the bottom of the drop  
 $H$ : shape factor

The evolutions of the interfacial tension between the internal water phase and the organic phase were measured between 20 and 70°C, each 10°C, with four different internal water phases: W1(3), W1(7), W1(11) and W1(12). During the experiments, the organic phase did not contain initiator to avoid polymerization. The densities of the phases used for the measures have to be known precisely for each measurement temperature. The evolutions of

density with temperature of the four internal water phases and the organic phase used are illustrated in Figure III.15. The graphic showed that the measurements with W1(7), W1(11) and W1(12) are made with the internal water phase as the drop and the organic phase as the suspending medium, whereas the measurements with W1(3) are made with the opposite configuration. These two systems are necessary because with the pendant drop configuration, the drop must always show a higher density than the suspending medium. The results that could be obtained before the apparatus was out of order are presented in Figure III.16.

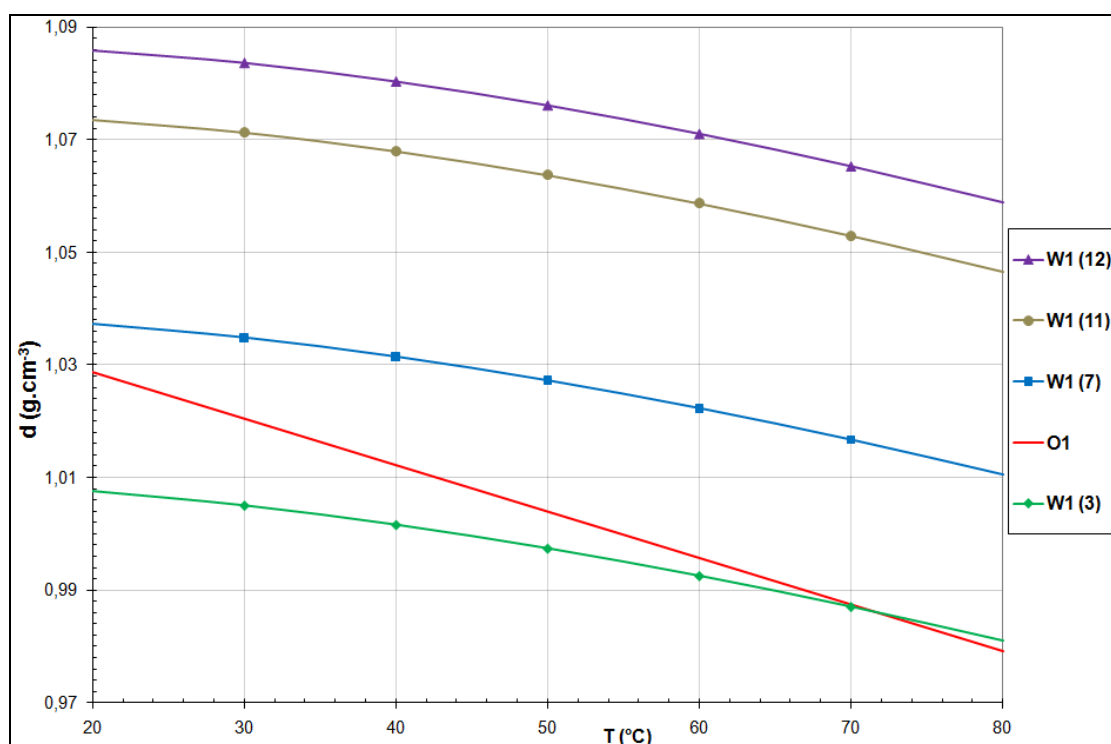


Figure III.15: Evolution of the density of the four internal water phases (W1(3), W1(7), W1(11) and W1(12)) and the organic phase (O1) with the temperature from 20 to 80°C

A major issue appeared during the measures while using W1(3), the drops obtained at 40 and 50°C were so big that they almost did not fit anymore inside the camera field. At 60 and 70°C there were too huge to allow any measurement. This can be attributed to a density difference between the two phases that is almost equal to zero. In fact, Xing *et al.* [10], maintain that the density difference between two polymer blends should be larger than 4 to 5% for the drop to reach equilibrium and determine the interfacial tension. In addition, Ravera *et al.* [11] said that the only limitation of the drop shape method for the study of liquid-liquid interface is set by very low density contrast couples of liquids. Flock *et al.* [12] measured the interfacial tension between heavy crude oil and water. The authors stated that “the pendent drop technique cannot be used to measure interfacial tensions when the density difference between

the two fluids is less than  $0.01 \text{ g.cm}^{-3}$ . However, the lowest density gap that the authors used to measure the interfacial tension was  $0.04 \text{ g.cm}^{-3}$ . The internal water phase and the organic phase used in our case have really low viscosities compared to polymer blends, so the time to reach equilibrium for the drop is much faster. However, we can wonder until which minimal value of the density difference we will obtain reliable results. Table III.7 gives the density differences between the internal water phase and the organic phase at the measurement temperatures. The density differences between O1 and W1(3) or W1(7) lie respectively between 0 and 2% or between 1 and 3%. The density difference between O1 and W1(11) or W1(12) are markedly higher since they lie between 4 and 8%. The interfacial tension results obtained at the interface between O1 and W1(3) (Figure III.16) should certainly not be taken into consideration particularly since these results do not seem interpretable.

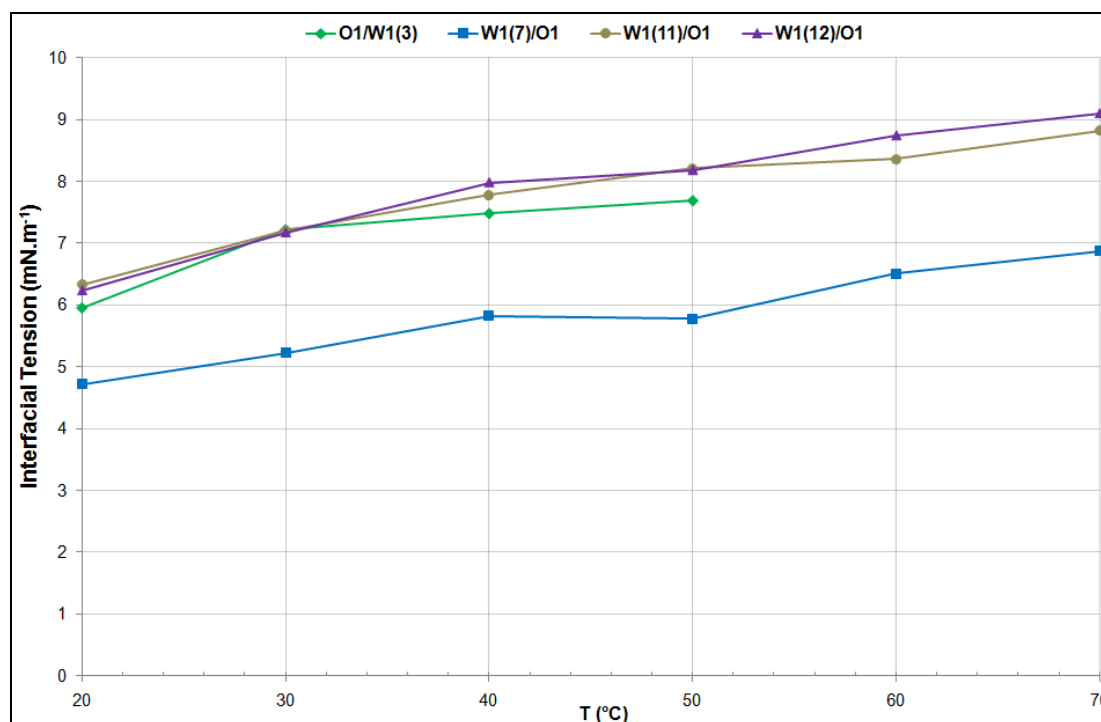


Figure III.16: Evolution of the interfacial tension between the organic phase O1 and the four internal water phases (W1(3), W1(7), W1(11) and W1(12)) with the temperature from 20 to 70°C

Figure III.16 illustrates the evolution of the interfacial tension as a function of the temperature. In an astonishing way, the interfacial tension increases when the temperature increases whereas classically the interfacial tension decreases with temperature. This unexpected behavior is not the only example in the literature. Indeed, in the field of petroleum extraction, Flock *et al.* [12] also mention that for one heavy oil the interfacial tension increased with



temperature and for two heavy oils the interfacial tension initially decreased then increased with temperature. The authors stated that “no just explanation for the increasing interfacial tension was established”.

The results on Figure III.16 show that the evolution of the interfacial tension with temperature for W1(11) and W1(12) are the same with almost identical values of interfacial tension. The internal water phase W1(7) shows also the same trend in the interfacial tension evolution with temperature. However, the values of interfacial tension for W1(7) are lower than the one for W1(11) and W1(12). At 60°C, the polymerization temperature process, the interfacial tension at the interface W1(7)/O1 is equal to 6.5 mN.m<sup>-1</sup> and for the interfaces W1(11)/O1 and W1(12)/O1 the interfacial tension is equal to 8.4 and 8.7 mN.m<sup>-1</sup> respectively. So, the higher values of interfacial tension obtained with W1(11) and W1(12), could explain the better NC results obtained with these internal water phases than with W1(7).

Table III.7: Density differences between the internal water phase and the organic phase at specific temperatures

Temperature (°C)	dW1(3) - dO1 (g.cm <sup>-3</sup> )	dW1(7) - dO1 (g.cm <sup>-3</sup> )	dW1(11) - dO1 (g.cm <sup>-3</sup> )	dW1(12) - dO1 (g.cm <sup>-3</sup> )
20	-0.021	0.009	0.045	0.057
30	-0.015	0.014	0.051	0.063
40	-0.011	0.019	0.056	0.068
50	-0.007	0.023	0.060	0.072
60	-0.003	0.027	0.063	0.075
70	-0.0004	0.029	0.065	0.078

In addition to these measurements, the interfacial tension between the organic phase O1 and the external water phase W2 was measured at 20°C. The density difference between the organic phase and the external water phase is equal to 0.017 g.cm<sup>-3</sup> which is very low. The interfacial tension at this interface was then equal to 2.4 mN.m<sup>-1</sup>. According to Paguio *et al.* [13] (RF shells with a O1/W1/O2 system) a high value of the interfacial tension between the aqueous phase W1 and the external organic phase O2 ( $\sigma = 13$  mN.m<sup>-1</sup>) leads to shells with better wall uniformity. The interfacial tension value at the external interface O1/W2 of our shell is very low compared to Paguio’s one. Therefore, the influence of the interfacial tension of the external interface on shells NC could be studied later on by varying the nature and concentration of the surfactant dissolved in the external water phase.

### III.5. CONCLUSION

When the density gap between the internal water phase W1 and the organic phase O1 increases, the TMPTMA shells non-concentricity improves. The curve of the yield of shells as a function of the density gap shows a bell-shaped profile, with yield values higher than 50% for density gaps between  $-0.008$  and  $0.078 \text{ g.cm}^{-3}$  at  $60^\circ\text{C}$ . A density gap of  $0.078 \text{ g.cm}^{-3}$  at  $60^\circ\text{C}$  (using W1(12)), leads to an average non-concentricity of 2.4% with a yield of 58%. Besides, a density gap of  $0.089 \text{ g.cm}^{-3}$  at  $60^\circ\text{C}$  (using W1(13)), leads to an average non-concentricity even better of 2.1%. However, while using W1(13), the yield falls down to 26%. A compromise has thus to be made between good non-concentricity results and a high yield of shells. This is the reason why the internal water phase W1(12) ( $dW1 - dO1 = 0.078 \text{ g.cm}^{-3}$  at  $60^\circ\text{C}$ ) has been used for further experiments.

An experiment of reproducibility realized with 11 bottles collected in the same conditions, at different times over a year, shows that the process can be considered as reproducible. The slight variation in the reproducibility results obtained may be partly explained by the centering of the needle 1 inside the needle 2. Better values of the average non-concentricity are obtained when the needle 1 is not centered which means that the centering of the two needles is not a key factor governing the shells non-concentricity.

The better non-concentricity results obtained with an important density mismatch for TMPTMA foam shells could be explained by the movements of the internal water phase inside the organic phase which will be studied in the next Chapter IV. Besides, the higher values of interfacial tension obtained at the interface W1(11)/O1 and W1(12)/O1 than at the interface W1(7)/O1 may also be linked to the better NC results obtained, even if the results obtained are not entirely trustworthy.

**Bibliographic references**

1. Lee, C.P. and T.G. Wang, *The centring dynamics of a thin liquid shell in capillary oscillations*. Journal of Fluid Mechanics, 1988. **188**: p. 411-435.
2. Norimatsu, T., et al., *Modeling of the centering force in a compound emulsion to make uniform plastic shells for laser fusion targets*. Fusion Science and Technology, 1999. **35**: p. 147-156.
3. Lee, C.P., A.V. Anilkumar, and T.G. Wang, *A theoretical model for centering of a thin viscous liquid shell in free and forced capillary oscillations*. Physics of Fluids, 1996. **8**(10): p. 2580-2589.
4. Paguio, R.R., et al., *Fabrication of modified density and tin doped RF foam shells and beads for direct drive experiments*. Polymeric Materials: Science & Engineering, 2006. **95**: p. 872-874.
5. Cook, R., et al., *The development of plastic mandrels for NIF targets*. 2000, Lawrence Livermore National Laboratory. p. 1-12.
6. Takagi, M., et al., *Decreasing out-of-round in poly( $\alpha$ -methylstyrene) mandrels by increasing interfacial tension*. Fusion Science and Technology, 2000. **38**: p. 46-49.
7. Paguio, R.R., et al., *Improving the wall uniformity of resorcinol formaldehyde foam shells by modifying emulsion components*. Fusion Science and Technology, 2007. **51**: p. 682-687.
8. Paguio, R.R., et al., *Improving the yield of target quality omega size PAMS mandrels by modifying emulsion components*. Fusion Science and Technology, 2006. **49**: p. 743-749.
9. Andreas, J.M., E.A. Hauser, and W.B. Tucker, *Boundary tension by pendant drops*. The Journal of Physical Chemistry, 1938. **42**(8): p. 1001-1019.
10. Xing, P., et al., *Critical experiment comparison between five techniques for the determination of IT in polymer blends*. Macromolecules, 2000. **33**: p. 8020-8034.
11. Ravera, F., M. Ferrari, and L. Liggieri, *Adsorption and partitioning of surfactants in liquid-liquid systems*. Advances in Colloid and Interfaces Science, 2000. **88**: p. 155-158.
12. Flock, D.L., T.H. Le, and J.P. Gibeau, *The Effect Of Temperature On The Interfacial Tension Of Heavy Crude Oils Using The Pendant Drop Apparatus*. Journal of Canadian Petroleum Technology, 1986. **25**(2): p. 72-77.
13. Paguio, R.R., et al., *Development and fabrication of NIF-scale resorcinol formaldehyde foam shells for ICF experiments*. Fusion Science and Technology, 2011. **59**: p. 199-204.

## **CHAPTER IV. STUDY OF THE CIRCULATION AND POLYMERIZATION PROCESSES**

As explained in the previous Chapter III, better non-concentricity results are obtained when the density gap between the internal water phase W1 and the organic phase O1 is high, which means equal to  $0.078 \text{ g.cm}^{-3}$  at  $60^\circ\text{C}$  (W1(12)). However, the density gap alone cannot explain why better non-concentricity results are obtained. The results presented in Chapter III were obtained with a circulation of the shells in a tube with areas of constriction. Two other circulation systems are available at the CEA and we wondered if differences or similarities could be found between these three systems. In this chapter we focused our attention on the influence of the deformations applied to the shells when circulating in the system, on the non-concentricity. These deformations may be responsible for the centering of W1 inside O1 and thus govern the final non-concentricity. This means that we studied the circulation process with the different tube systems available and the polymerization process to know when and where the shells polymerize during the synthesis process.

## **IV.1. INFLUENCE OF THE CIRCULATION PROCESS ON THE SHELLS NON-CONCENTRICITY**

### **IV.1.1. Presentation of the three circulation systems**

Three different circulation systems at the CEA can be used to synthesize foam shells, as illustrated in Figure IV.1. These circulation systems are placed between the droplet injector and the collecting flask. The first system uses a straight tube, the second one a tube with areas of constriction and the third one a short wound tube [1]. These circulation systems are described in details in Chapter I. In this part we described shortly all the phenomena occurring in these three circulation systems and which are visible to the naked eye.

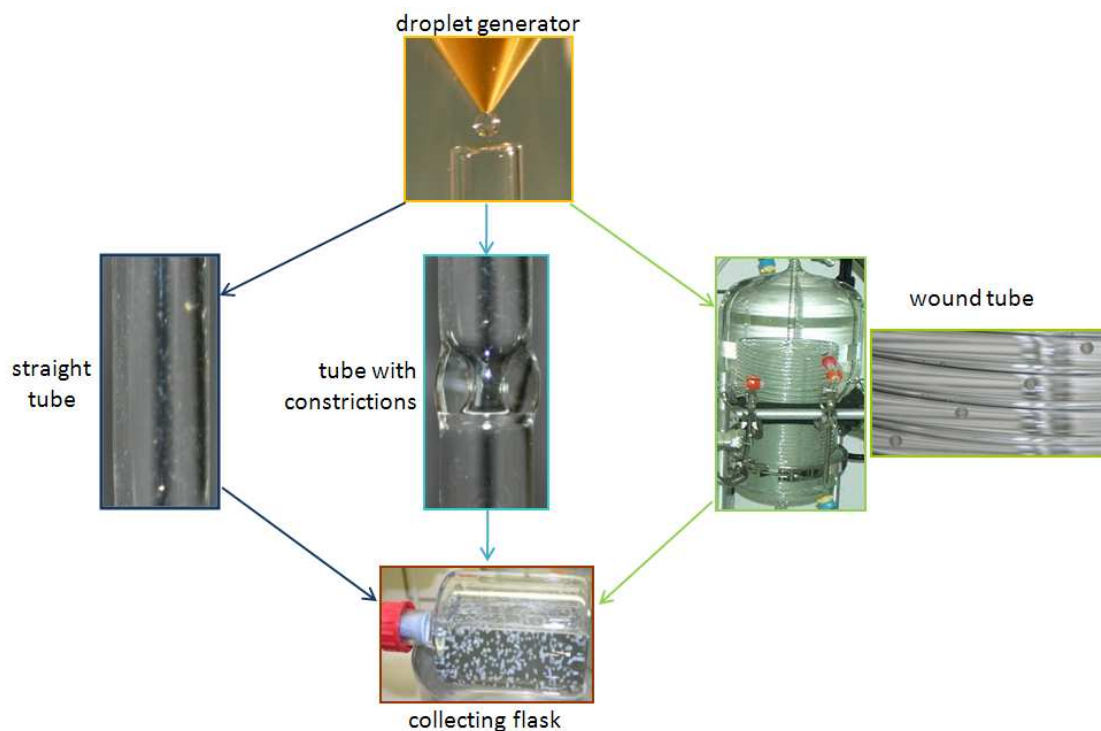


Figure IV.1: Illustration of the three different circulation systems available to synthesize foam shells

#### IV.1.1.1. Circulation of the shells in a straight tube

The straight tube is a short circulation system (length = 50 cm) whose function is only to lead the shells from the extremity of the droplet generator to the collecting flask. In this kind of system, the gravity and the velocity gradient are responsible for the stress applied to the shell during its circulation. Moreover, an experiment realized with shells marked with a black dot revealed that the shells turn round on themselves while going down along the tube.

#### IV.1.1.2. Circulation of the shells in a tube with areas of constriction

Different tubes are available with constrictions more or less pronounced. These constrictions can have a mechanical effect on the shell during its circulation by squeezing it. Only one of the tubes available is used in this PhD work, but it would be interesting to study all the other tubes. The tube with areas of constriction used here shows constrictions of 4 mm diameter. Since the shells are 2 mm in diameter, they do not undergo mechanical effect caused by the constrictions. So, in this particular tube with areas of constriction, it seems that the shells are

only subject to the gravity and the velocity gradient. As for the straight tube, it was shown that the shells also turn round on themselves.

#### **IV.1.1.3. Circulation of the shells in the short wound tube**

The wound tube is patented by the CEA. The expected role of the wound tube is to avoid the agglomeration of the shells during their circulation. The underlying idea of the utilization of this system by the CEA is the fact that the polymerization occurs during the shells circulation in the wound tube. This fact will be checked during this work. In this system the shells are subject to the gravity and the velocity gradient and turn around themselves as the other two circulation systems. The shells usually travel individually inside the wound tube with space between each other. However, from the first quarter of the wound tube the shells travel sometimes in a close pack of shells, with 1 to 10 shells one after another, forming a sort of shell train.

#### **IV.1.2. Synthesis of shells with three circulation systems and three density gaps**

To study the influence of the circulation process on shells non-concentricity, foam shells were synthesized with the three following circulation systems: the straight tube, the tube with areas of constriction (system used in Chapter III) and the short wound tube. In addition, for each circulation system, three density gaps between the internal water phase and the organic phase have been tested by using the internal water phases W1(3), W1(7) and W1(12). However, for the wound tube, the internal water phase W1(11) was used instead of W1(12). The average non-concentricity results obtained for each experiment are presented in Table IV.1.

Table IV.1: Results of the average non-concentricity (NC) obtained for the three different circulation systems while using three different internal water phases

circulation system	density gap $dW1-dO1$ at 60°C ( $\text{g}\cdot\text{cm}^{-3}$ )	internal water phase used	average NC (%)
straight tube	-0.001	W1(3)	11
	0.029	W1(7)	4.3
	0.078	W1(12)	1.8
tube with areas of constriction	-0.001	W1(3)	9
	0.029	W1(7)	3
	0.078	W1(12)	2
wound tube	-0.001	W1(3)	7.7
	0.029	W1(7)	4
	0.065	W1(11)	2.5

On the one hand, the results obtained in Table IV.1 show that for each circulation system the average non-concentricity decreases when the density gap at 60°C between the internal water phase W1 and the organic phase O1 increases. Thus, whatever circulation system used, better non-concentricity results are obtained when the density gap between the internal water phase and the organic phase is high, which means equal to 0.078 or 0.065  $\text{g}\cdot\text{cm}^{-3}$  at 60°C (W1(12) and W1(11)). On the other hand, the values of the average non-concentricity obtained with each density gap are about the same order for the three circulation systems. This can be considered as a surprising result since the three systems are very different both in their dimension and shape.

In Figure IV.2, the percentages of shells as a function of the shells non-concentricity for the three different circulation systems while using three different internal water phases are plotted. Three different behaviors can be discerned in the evolution of the non-concentricity results. Each behavior corresponds to one of the three internal water phases used. Besides, the results obtained with W1(12) while using the straight tube fit the results obtained for the 11 bottles collected with W1(12) while using the tube with areas of constriction. The same fit is observed for the results obtained with W1(11) while using the wound tube.

So it can be concluded that the straight tube or the wound tube give as good NC results as the tube with areas of constriction while using a density gap of 0.078  $\text{g}\cdot\text{cm}^{-3}$  at 60°C. However, the shell lives are not similar in these three circulation systems.



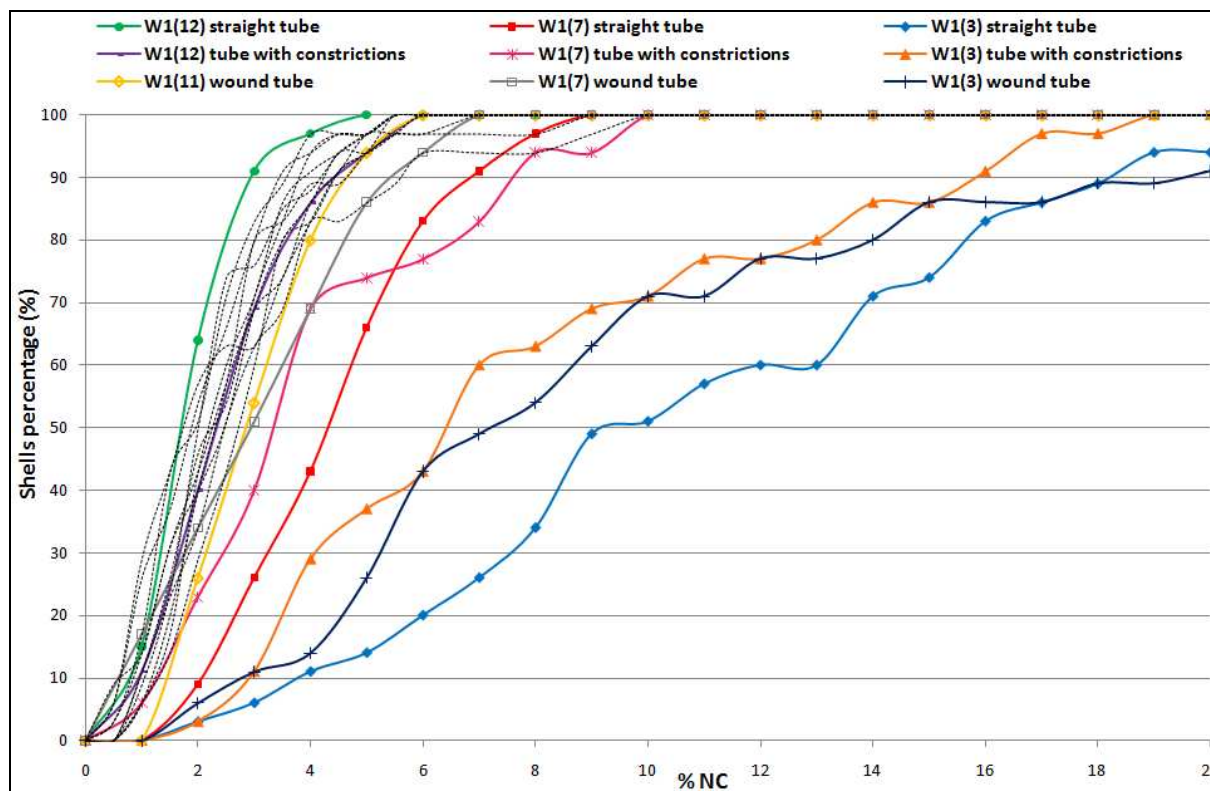


Figure IV.2: Plots of the percentage of shells as a function of the shells non-concentricity for the three different circulation systems while using three different internal water phases. The black dotted lines represent the results obtained for the 11 bottles collected while using W1(12) as the internal water phase with the tube with areas of constriction as presented in Chapter III.

### IV.1.3. Hypothesis to explain the shell's motion in the circulation systems

When the shell is striped off from the droplet generator, its shape appears as illustrated in Figure IV.3. At first, the shell is not spherical and the internal water droplet is not centered inside the oil globule. Then, at the end of the process, the shell has become round and centered. The non-concentricity results obtained with the three circulation systems are equivalent. So, we wondered if the circulation process and/or the agitation of the shells inside the flask had an influence on the shells shape. In that aim, we tried to understand the motion of the shells in the three circulation systems and to evaluate the kinetics of polymerization.

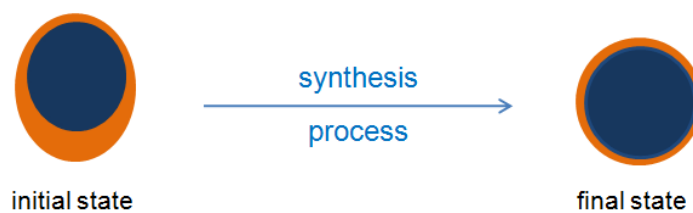


Figure IV.3: Shape of the shell at first and at the end of the whole synthesis process

As explained in Chapter II, the literature, [2], [3], [4], [5], specified that when a W1/O1 emulsion distorts from its originally spherical shape a core-centering force is generated and the W1 droplet moves to the center of the O1 droplet. For a system submitted to acoustic oscillations, with a configuration where the core is a gas and the shell is an inviscid liquid, the core-centering forces come from hydrodynamic forces [6], [7]. Nevertheless, the understanding of the centering of the shells, with a configuration where both the core and the shell are immiscible liquids, is still not completely understood. As yet, no physical model explains the core-centering phenomenon resulting from the shell's deformation. The following explanations of the core-centering phenomenon observed in our systems are only hypothesis.

First, we compared the straight tube and the tube with areas of constriction which are equivalent except for the areas of constriction. For both tubes, the shells turn round on themselves while going down along the tube. However, this phenomenon is not visible to the naked eye during the synthesis. Thus, shells already synthesized were marked accurately with a black dot and introduced with a water flow inside the tubes in order to measure the rotation speed of the shells on themselves. In this aim, movies were made with an ultra fast frame grabber camera. Figure IV.4 illustrates the shells turning around on themselves along the tube from pictures made with the ultra fast frame grabber camera. With the straight tube, the shell's rotation speed is 88.6 rpm, so the shell turns 22.2 times on itself along the tube. With the tube with areas of constriction, the shell's rotation speed is 93.7 rpm, so the shell turns 23.4 times on itself along the tube. The rotation speed is greater with the tube with areas of constriction than with the straight tube, but the difference is really slight.

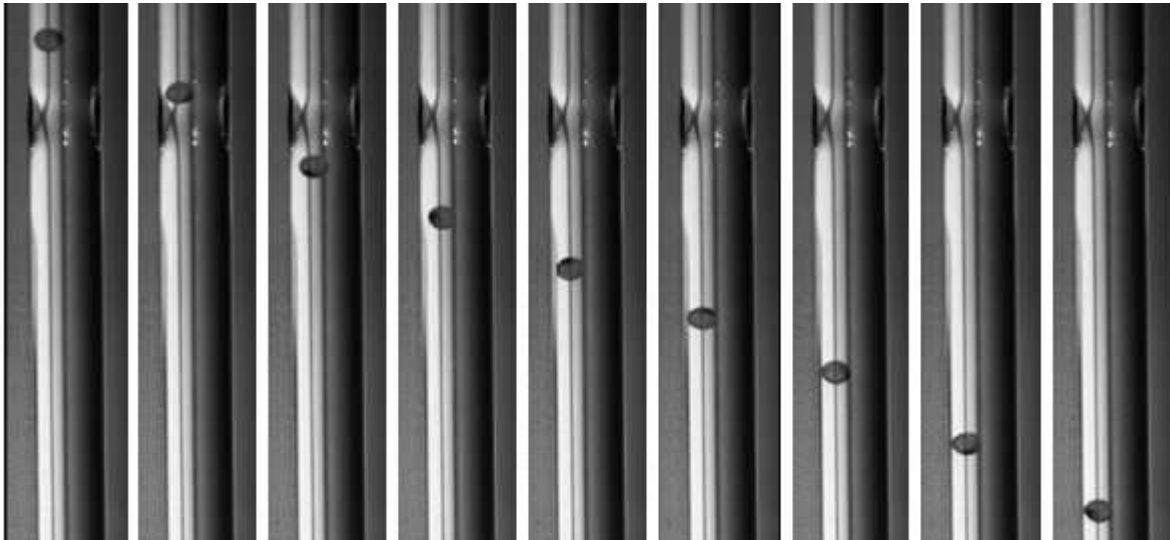


Figure IV.4: Illustration of a shell going down the tube with areas of constriction and turning round on itself. The pictures come from the movie made with an ultra fast frame grabber camera.

Inside the tube with areas of constriction, the shells are not distorted by the inside wall of the glass tube within the constrictions as explained earlier. Indeed, the diameter of the areas of constriction, 4 mm, is wider than the diameter of the shell, 2 mm. Besides, the calculation of the Reynolds number ( $R_e$ ) gives an idea of the nature of the flow regime in the tubes. This dimensionless number can thus be used to determine dynamic similitude between different experimental cases. The Reynolds number is calculated from the following formula:

$$R_e = \frac{V L}{\nu}$$

with:  $R_e$ : reynold's number

$V$ : characteristic velocity

$L$ : characteristic dimension (here the diameter of the tube or the constriction)

$\nu$ : kinematic viscosity

In the domain of fluid mechanics, different flow regimes are established towards  $Re$  values. When  $Re$  is lower than 2300, viscous forces are dominant and a laminar flow takes place in the system. This regime is characterized by a smooth, constant fluid motion. When  $Re$  is higher than 4000, inertial forces are dominant and a turbulent flow occurs. This regime is characterized by the production of various flow instabilities. Since  $Re$  values are close to 40, the flow is laminar through all the tube even within the areas of constriction. The only consequence of the presence of areas of constriction is the increase of the external water phase flow rate inside the constriction. So, the areas of constriction inside the tube only slightly

accelerate the rotation speed of the shells on themselves but do not have any other effect on the shells.

Using W1(12) as the internal water phase, a total of three bottles have been collected with the straight tube and 11 with the tube with areas of constriction (already presented in Chapter III). As illustrated in Figure IV.5, the same NC results are obtained using either a straight tube or a tube with areas of constriction while using W1(12) as the internal water phase. The effects of both tubes on the shells are similar, as for the NC results obtained, therefore these two tubes can be considered as equivalent.

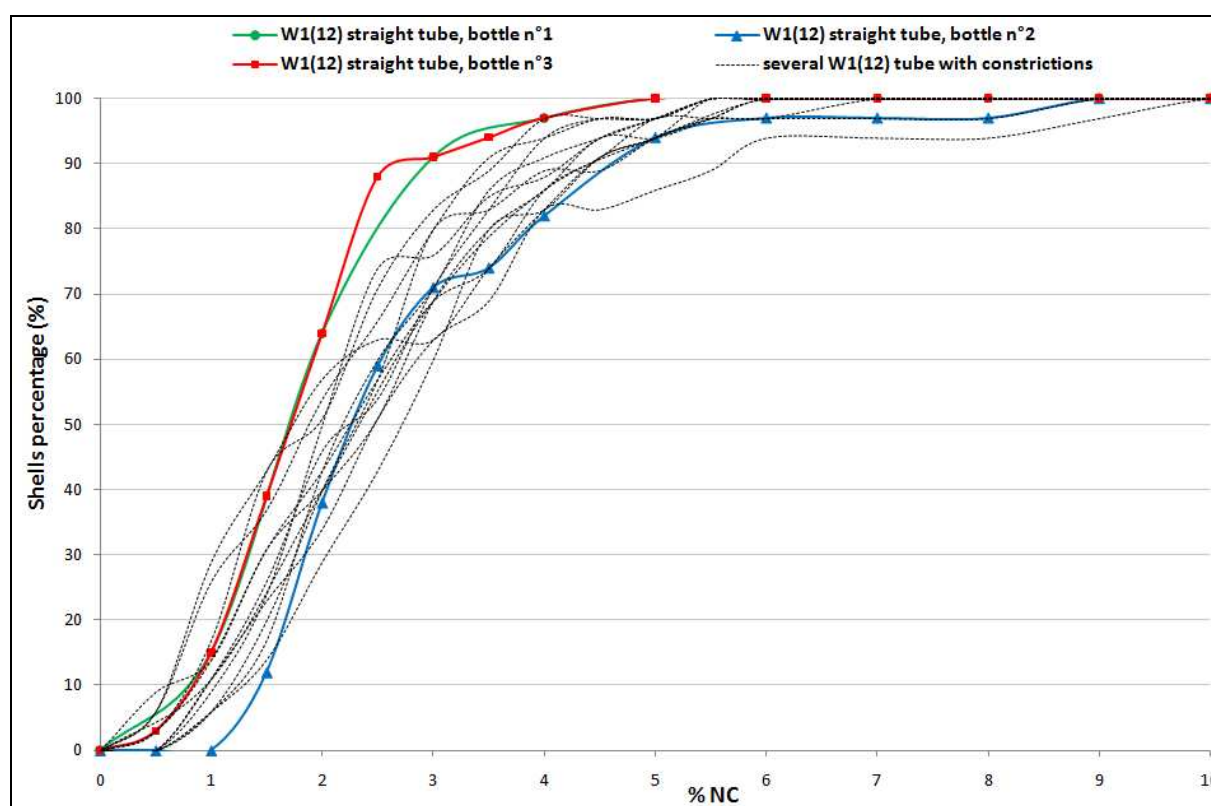


Figure IV.5: Plots of the percentage of shells as a function of the shells non-concentricity for the straight tube (colored curves: green, red and blue) and for the tube with areas of constriction (black dotted curves) while using W1(12) as the internal water phase

In the first part of the wound tube, it can be observed that the shells touch the bottom of the tube (because they are heavier than W2) so they turn round on themselves because of the parabolic velocity gradient inside the tube. An experiment with a shell with a black dot has also been realized inside the wound tube but was not filmed. However, it was visible to the naked eye too that the shells turn around on themselves as stated earlier.

From all these observations, we can say that in the three circulation systems, the shells undergo gravity forces and turn around on themselves. Centering forces due to gravity should be much more efficient with a high density gap between the internal water phase and the organic phase than with the equality. Indeed, when a density mismatch exists between W1 and O1, the internal water phase W1 centers itself to reach an equilibrium position. Thus, a significant density mismatch (as with W1 (12)) will generate a core-centering force. Conversely, a density match (as with W1 (3)) will not generate any force to help center the shell. The shells turning around on themselves allow that the centering does not occur only toward one privileged direction.

Moreover, the time spent by the shells in each of these circulation processes is different. With an external water flow of  $40 \text{ mL}\cdot\text{min}^{-1}$ , the shells go through the straight tube or the tube with areas of constriction (50 cm long with a 5 mm internal diameter) in approximately 15 seconds. Whereas, the shells need around 5 minutes to go through the wound tube (11 meters long with a 5 mm internal diameter).

The shaping of the shell has to occur before the gel point while the polymer is still able to flow. Thus, centering forces can occur inside the shell until the organic phase viscosity is too high. So, it is important to determine the needed time to polymerize completely the organic phase and to measure the evolution of the organic phase viscosity.

## IV.2. INFLUENCE OF THE POLYMERIZATION KINETICS ON THE SHELLS NON-CONCENTRICITY

### IV.2.1. Polymerization process

To be able to compare the three circulation systems, it is necessary to know when the gelification starts, when the shell is completely polymerized and where the shell is located when the gelification occurs. It would be interesting to measure the extent of reaction at the gel point. The extent of reaction ( $p$ ) is defined as:

$$p = \frac{\text{number of reacting groups which reacted}}{\text{number of groups which are liable to react}}$$

However, no absolute method exists to quantify the extent of reaction, especially for highly functionalized monomers such as TMPTMA. At the beginning of this study, we tried by NMR  $^1\text{H}$  to quantify the amount of residual monomers based on the vinyl double bond signals at 5.58 and 6.09 ppm. However, once the polymerization occurs, the spectra obtained reveal the overlaying of the peaks attributed to the residual monomer and the partially reacted monomer incorporated inside the polymeric chains. This method was dropped since no straightforward quantification was possible.

In this work, the reacting monomer has been followed by analyzing its residual amount with gas chromatography along the synthesis. Second, the time to form a crosslinked polymer was measured by rheology measurements. At last, the evolution of the organic phase viscosity during polymerization was determined.

#### **IV.2.1.1. Monomer consumption followed by gas chromatography**

Gas chromatography is used here to measure the quantity of residual monomer for lack of straightforward methods measuring the extent of reaction. Gas chromatography allows us to quantify the residual monomers in solution but it does not quantify the residual monomers trap inside the tri-dimensional network. Besides, gas chromatography does not quantify the functional groups. This means that the functional groups which did not react on a monomer that have already reacted are not quantifiable. So, this method underestimates the quantity of monomer and even more the quantity of double bounds.

The organic phase composition is described in Chapter I. The polymerization reaction was realized inside a balloon flask filled with the organic phase and surmounted by a refrigerant, under a nitrogen atmosphere. The organic phase was polymerized following the time and temperature steps of the synthesis process as described here:

- 2 minutes at room temperature (organic phase within the syringe before the synthesis)
- 2 minutes at 40°C (shell leaving the droplet generator and going through the tubes)
- 25 minutes at 60°C (shell going through the wound tube and/or within the collecting flask)

Samples were taken along the synthesis with a syringe and diluted in a mixture of acetone and hydroquinone to stop the polymerization reaction. The samples were then analyzed by gas chromatography to follow the percentage of residual monomer. Quantitative measurements were realized using the internal standard method with diethyl phthalate as the internal standard. Hence the consumption of the monomer in the organic phase could be followed.

The measures of the percentage of residual monomer in the organic phase as a function of time along the synthesis are presented in Figure IV.6. It seems that only a really slight conversion of the TMPTMA is detected before 15 minutes at 60°C. In the balloon flask, the formation of a gel was identified after 20 minutes at 60°C (area hatched in grey in Figure IV.6). The amount of residual monomer after 20 minutes at 60°C is not necessarily representative since the reaction medium is heterogeneous, some parts being liquid and others being solid. Then, after 25 minutes at 60°C, the organic phase appeared as a swollen gel, without any liquid part, prohibiting any sampling with a syringe. Thus, the fast decrease of the percentage of residual monomer to 65% corresponds to the gel point. So, according to these measurements, the shells present a three-dimensional network after 20 to 25 minutes at 60°C.

The measurements of residual monomer with this process do not lead to accurate results. Indeed, when the percentage of residual monomer stays constant, the measured values oscillate between 96.5 and 104%. Since the measure of the gel point by this gas chromatography technique is not really precise, further measurements were done by rheology.

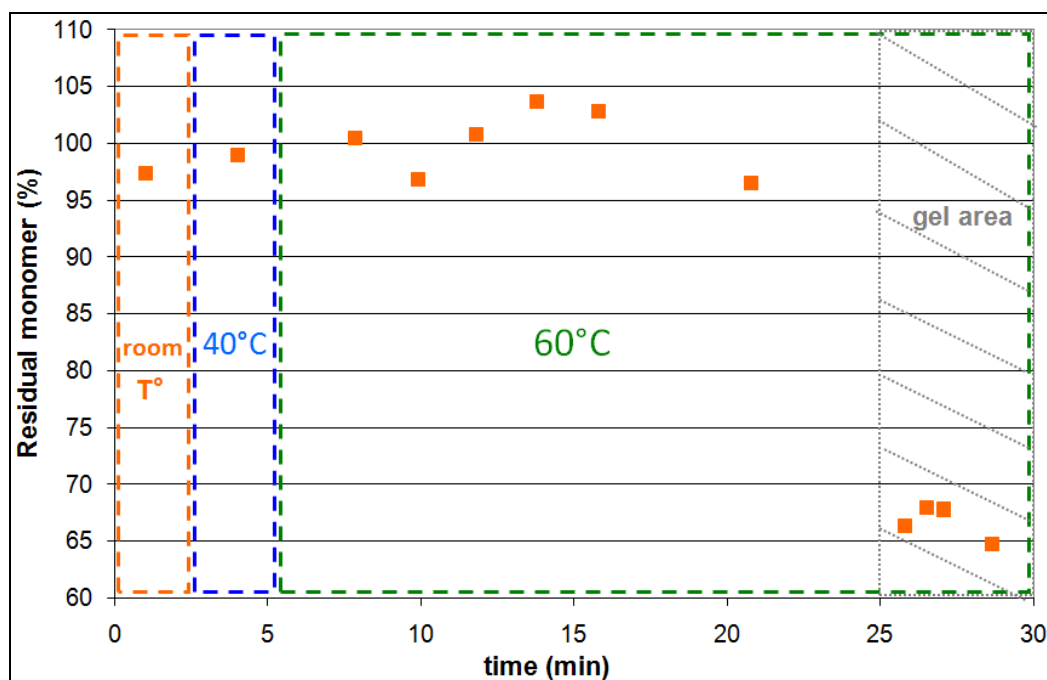


Figure IV.6: Evolution of the percentage of residual monomer as a function of time for the organic phase during the synthesis process

#### IV.2.1.2. Polymerization kinetics followed by rheology

The centering of the internal water phase W1 inside the organic phase O1 droplet is impossible if the organic phase becomes solid or becomes too viscous to be able to flow. Rheology measurements allow the detection of the crossover between the shear storage modulus  $G'$  and the shear loss modulus  $G''$ . The crossover of  $G'$  and  $G''$  means that the sample passes from a liquid viscous behavior to a solid elastic behavior.

A rheometer equipped with a plate/plate measuring system was used to determine the shear storage modulus  $G'$  and the shear loss modulus  $G''$  as the organic solution polymerized. Classically, at the beginning of the experiment, the shear loss modulus  $G''$  is orders of magnitude larger than the shear storage modulus  $G'$ , and at completion of reaction, this order is reversed. The transition from a liquid-like to a solid-like behavior is defined as gelation in non-linear polymerization. The crossover of the storage and loss moduli measured during isothermal curing may be defined as the gel point [8], [9], [10], [11], [12]. The gel point is the transition from a state with chains in solution to a three-dimensional network (chains linked to each others), image (d) and (e) respectively of Figure IV.7 [13].



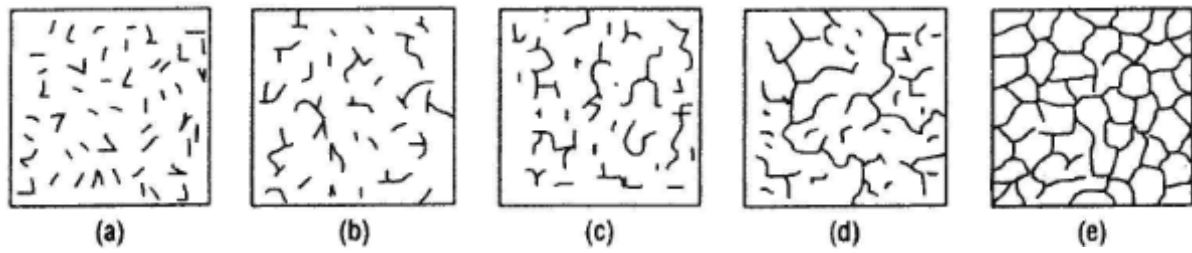


Figure IV.7: Schematization of the successive steps of a crosslinking reaction: (a) mixture of monomers, (b), (c) and (d): intermediary steps, (e) final network [13]

The evolution of the shear loss modulus  $G''$  and the shear storage modulus  $G'$  of the organic phase along the synthesis at  $60^\circ\text{C}$  are illustrated in Figure IV.8. The rheology measurements have been realized three times. The values of  $G'$  from 0 to 20 minutes are noisy since for a liquid sample the signal is really low. The curves for  $G'$  and  $G''$  cross at 23 minutes. The fast increase of  $G''$  values is an indicator of the formation of the network, which corresponds to the transition from state (d) to state (e) in Figure IV.7. Therefore, the structure of a shell is constituted of a tridimensional network after 23 minutes at  $60^\circ\text{C}$ , according to the rheology measurements. After around 26 minutes, due to the loading imposed to the sample by the rheometer during the analysis, the gel is broken and the measurements are not reliable.

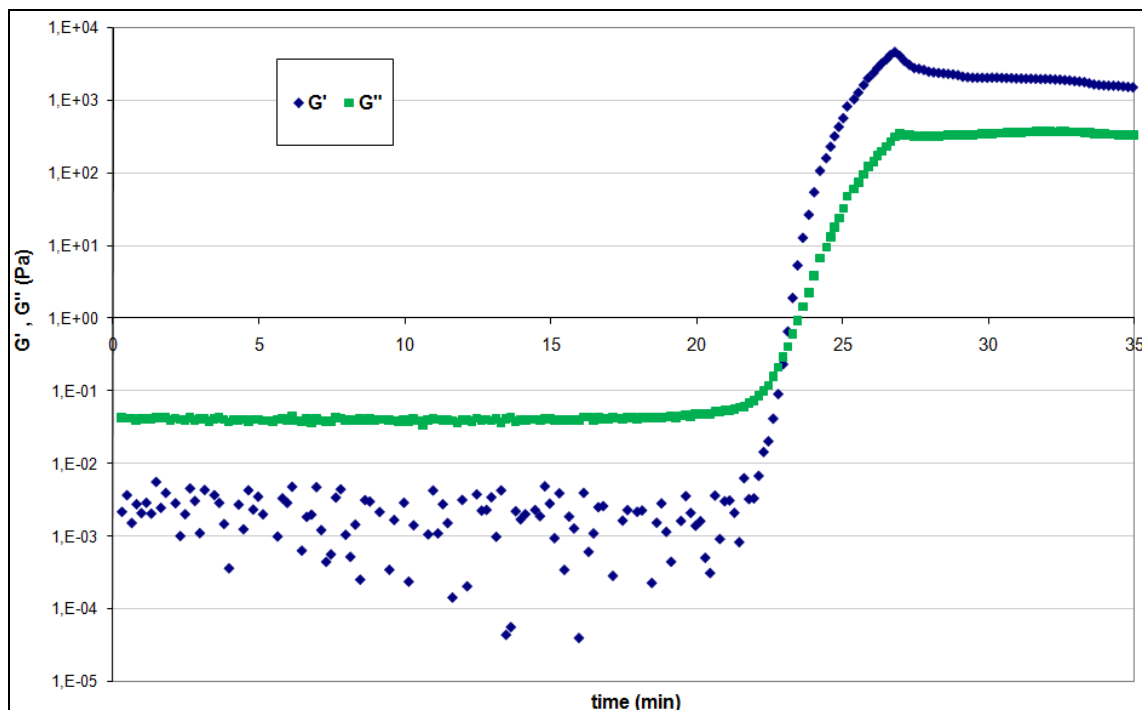


Figure IV.8: Evolution of shear loss modulus  $G''$ , and of shear storage modulus  $G'$ , as a function of reaction time, for the organic phase at  $60^\circ\text{C}$

The polymerization kinetics results obtained by gas chromatography and by rheology are in good agreement. These two methods show that the shells have a three-dimensional network structure around 20-25 minutes. This means that the shells shape is fixed when they are inside the rotating flask, whichever the circulation system used before.

However, both of these methods are not able to show when the viscosity of the organic phase actually starts increasing. Thus, the evolution of the organic phase viscosity during polymerization was measured by kinematic viscosity measurements.

#### **IV.2.1.3. Evolution of the organic phase viscosity during polymerization**

The organic phase was polymerized at 60°C under a nitrogen atmosphere. The polymerization reaction was brutally stopped by, at the same time, adding hydroquinone to the solution, flowing air inside the solution and putting the glass balloon in ice. The solution was then put inside a Hubbelohde tube and its kinematic viscosity was measured at 60°C. The measures of viscosity were done every minute until 7 minutes and 30 seconds. After 7 minutes and 30 seconds the viscosity of the solution was too high to perform any measurement. The results obtained are presented in Figure IV.9. The viscosity of the organic phase is almost constant between 0 and 4 minutes. Then, the viscosity increases really slightly between 4 and 6 minutes, from 4.8 to 9.4 mm<sup>2</sup>.s<sup>-1</sup>. After 6 minutes, the viscosity shoots up from 9.4 to 567 mm<sup>2</sup>.s<sup>-1</sup> in less than 90 seconds. The increase of viscosity can be attributed to the increase of the polymeric chain length in the solution, as illustrated in images (a) to (d) of Figure IV.7.

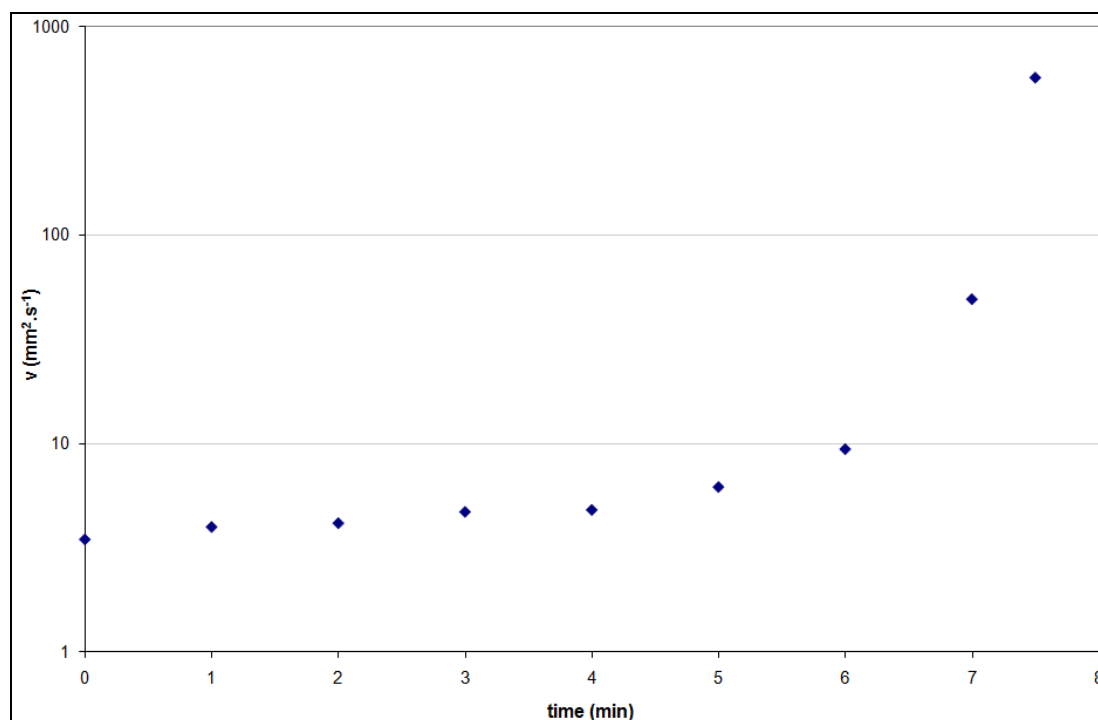


Figure IV.9: Evolution of the kinematic viscosity of the organic phase along the synthesis at 60°C

In conclusion, according to the rheology, gas chromatography and kinematic viscosity measurements, at 60°C, the organic phase O1 of the shell passes through the following states:

- from 0 to 6 min: liquid state, same viscosity as the monomer solution
- from 6 to 7.5 min: liquid state with enhanced viscosity, the polymeric chains start growing
- from 7.5 to 20 min: the polymeric chains are growing, possibly with microgels formation
- from 20 to 25 min: crosslinking of the polymeric chains, the gel point is reached and the shell's structure is fixed
- after 25 min: densification of the three-dimensional network

Therefore, for the three circulation systems, with a circulation time under 5 minutes (straight tube, tube with areas of constriction and short wound tube), the polymeric chains start to grow and crosslink once the shells are collected inside the flask. The time required to fix the shell's shape is thus at least 20 minutes with this polymerization process.

Then, at this stage of the reflection, it seems that both the straight tube and the tube with areas of constriction have no influence over the shells non-concentricity since the shells spend

much more time inside the flask (6 to 7 min) than inside the tubes (15 s) before the polymeric chains start growing. Besides, the shell's shape is set after 20 to 25 minutes inside the rotating flask. Thus, the movements inside the collecting flask seem to be particularly important for the core centering of the shell while using both the straight tube and the tube with areas of constriction.

However, it is still difficult to differentiate the influence of the wound tube from the rotating flask on the shells non-concentricity. Since the time spent inside the wound tube is close to the time when the viscosity of the organic phase increases, we wondered if a longer wound tube would allow us to differentiate the influence of the wound tube versus the agitated flask.

## **IV.2.2. Study of the shells location versus their viscosity**

The challenge was now to test a new circulation system which allows the shells viscosity to increase before the collecting flask. When the shells viscosity is high, none of the forces applied to the shells inside the different tubes or flask will be able to generate a core-centering force, the shells shape is then definitely set. The idea is that if the shells viscosity at the exit of the long wound tube is high enough to set the shells shape, the influence of the long wound tube system on the shells non-concentricity could be thus determined.

### **IV.2.2.1. Synthesis of shells with the long wound tube**

In this aim, we synthesized foam shells using a long wound tube instead of the three previous circulation systems. The long wound tube is 20 meters long, so the shells need around 10 minutes to go through it. Thus, according to the viscosity results in Figure IV.9, the shells viscosity should start increasing inside the long wound tube. Shells were synthesised with the long wound tube while using W1(12) as the internal water phase.

In Figure IV.10, the percentages of shells as a function of the shells non-concentricity for three bottles collected while using the long wound tube are plotted (red, orange and blue curves), as well as for the 11 bottles collected while using the tube with areas of constriction (black dotted lines). The non-concentricity results obtained with the long wound tube are as

good (red and orange curves) or slightly lower (blue curve) than the results obtained with the tube with areas of constrictions.

In conclusion, the non-concentricity results obtained while using W1(12) as the internal water phase, with either the straight tube, the tube with areas of constriction, the short wound tube or the long wound tube, are equivalent. This means that whichever the time spent by the shells in the circulation systems (from 15 seconds to 10 minutes), the non-concentricity results are the same.

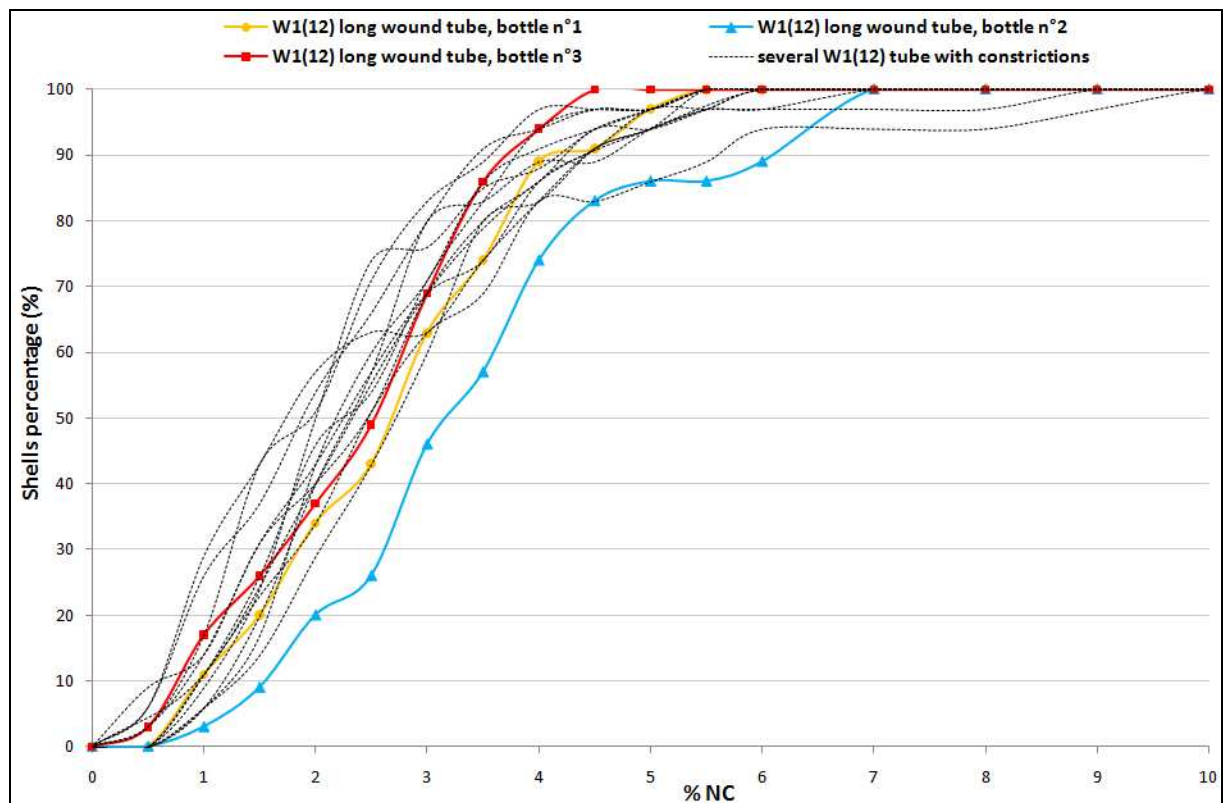


Figure IV.10: Plots of the percentage of shells as a function of the shells non-concentricity for the long wound tube (colored curves: red, orange and blue) and for the tube with areas of constriction (black dotted curves) while using W1(12) as the internal water phase

This result may imply that the non-concentricity is set inside the rotating flask and not inside the long wound tube. As long as the shells are not viscous enough, they do not keep the exact same shape since they are subjected to many deformations. Indeed, we collected shells one by one at the exit of the long wound tube and put them inside haemolyse tubes. The shells underwent phase inversion and became beads in a few seconds after collection. This meant that the shells, at the exit of the long wound tube, were not viscous enough to set their shape definitely and were still inclined to destabilization phenomenon.

When the shells are collected inside the flask, the agitation of the shells is quite energetic. According to the non-concentricity results obtained and to the shell's motions observed along the process, the shells non-concentricity seems to be much more influenced by the rotating flask than by the long wound tube. In order to check this hypothesis, it would be interesting to set the three-dimensional network before collection inside the flask.

#### **IV.2.2.2. Synthesis of shells with the three-dimensional network set before collection inside the flask**

For this purpose, a wound tube of at least 40 meters long should be used but we do not possess such a wound tube. We thought about bounding together the short and the long wound tubes but that would still have not been long enough. The last solution was to extend the time spent by the shells inside the long wound tube from 10 minutes to 20-25 minutes by decreasing the external water phase W2 flow. Hence, the external water phase flow should be decreased from 40 mL.min<sup>-1</sup> to at least 20 mL.min<sup>-1</sup>. A limiting factor was that the pump used for the external water phase could only go down to 15 mL.min<sup>-1</sup>.

If the external water phase W2 flow is decreased, the internal water phase W1 and the organic phase O1 flows have to be lowered proportionally and adjusted to keep shells of the same size and thickness. Indeed, we tried to synthesize shells with an external water phase flow of 20 mL.min<sup>-1</sup> or less, but the diameter of the shells generated was too large, as presented in Table IV.2. Decreasing proportionally all the flows is not sufficient to keep the same shell size because the shell is stripped off by a dynamic system, the W2 flow, which should not be too weak. With a flow of 20 mL.min<sup>-1</sup>, shells with a 2.32 mm diameter are obtained, which gives an error of 16% on the diameter. This error on the diameter is not acceptable. Moreover, to be able to compare the non-concentricity results, the shells diameters have to be of the same order. In addition, if the W2 flow is decreased, the shell's rotation speed on itself will change since it is linked to the velocity gradient inside the tube. Thus, while changing the W2 flow, the influence of the wound tube on the shells non-concentricity could not be compared with the previous results because the shells movements will be different.

Table IV.2: Diameter of the shell at the exit of the droplet generator as a function of the flow of the external water phase W2, the organic phase O1 and the internal water phase W1

W2 flow (mL.min <sup>-1</sup> )	W1 flow (mL.h <sup>-1</sup> )	O1 flow (mL.h <sup>-1</sup> )	diameter of the shell at the exit of the droplet generator (mm)
40	13.2	6.8	2.00
30	9.9	5.1	2.07
20	6.6	3.4	2.32
15	4.9	2.5	2.58

Due to all these dead ends and the lack of time we could not go further on the study of the influence of the deformations on the shells non-concentricity. The next experiments to realize should carry on the influence of the flask rotation speed on the shells non-concentricity. Indeed, according to Nagai *et al.* [5], there should be an optimized rotation speed which gives shells with a uniform wall thickness without destroying the emulsion. These authors optimized vigorous agitation conditions and find that the best non-concentricity results were obtained by following the rotation speed illustrated in Figure IV.11.

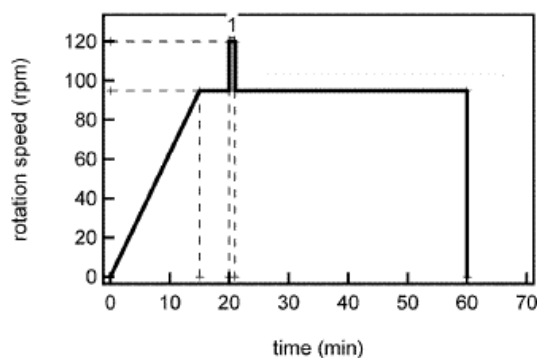


Figure IV.11: Optimized rotation speed versus rotation time

#### IV.2.2.3. Influence of the level of W2 inside the flask on the shells non-concentricity

As stated in Chapter I, when the collection starts, the flask is filled with about ten milliliters of W2, whereas at the end of collection the flask contains around 220 mL of W2. Indeed, a shell collected at the beginning, when the flask is almost empty, does not have the same life that a shell collected at the end of the collection when the flask is one third full. Thus, we wondered if the level of external water phase W2 inside the flask had an effect on the shells non-concentricity.

In this purpose, two bottles of shells were collected while using flasks already filled with 140 mL of external water phase. The non-concentricity results obtained with these two pre-filled bottles are illustrated in Figure IV.12. The curves plotted in Figure IV.12 show that equivalent non-concentricity results are obtained with empty flasks and with pre-filled flasks. Then, the filling level of the external water phase inside the collecting flask has no influence on the shells non-concentricity.

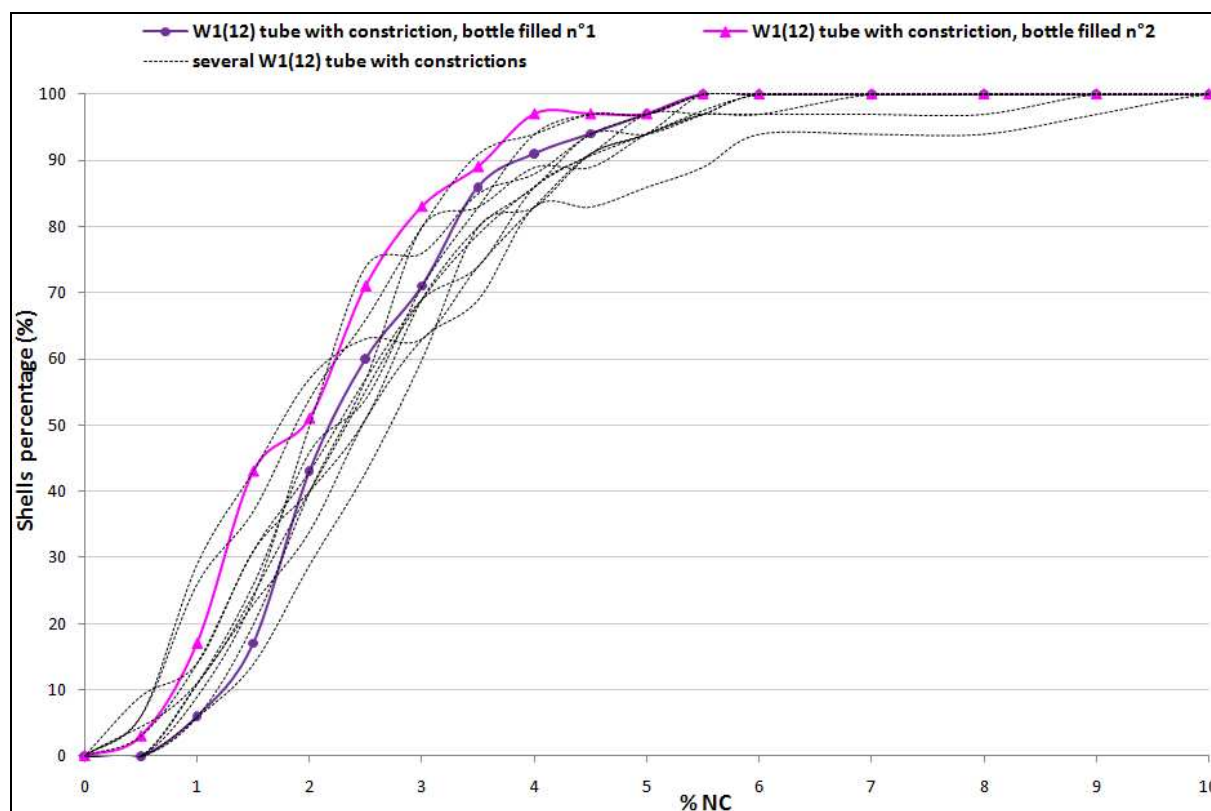


Figure IV.12: Plots of the percentage of shells as a function of the shells non-concentricity for the tube with areas of constriction while using W1(12) as the internal water phase with collecting flasks empty (black dotted curves) and with 2 flasks filled before collection

### IV.3. CONCLUSION

Whichever circulation system used (straight tube, tube with areas of constriction or short wound tube), better non-concentricity results are obtained when the density gap between the internal water phase and the organic phase increases. The straight tube and the wound tube presented in this chapter, lead to non-concentricity results equivalent to those obtained with the tube with areas of constriction while using a density gap of  $0.078 \text{ g.cm}^{-3}$  at  $60^\circ\text{C}$  (W1(12)).



Inside the three circulation systems, the shells undergo gravity forces and turn around on themselves. Centering forces due to gravity should be much more efficient with a high density gap between the internal water phase and the organic phase than with the equality. The shells turning around on themselves allow a multidirectional centering of W1.

The rheology, gas chromatography and kinematic viscosity measurements showed that at 60°C, the polymeric chains of the organic phase start growing after 6 to 7.5 min, then the polymeric chains start crosslinking after 20 to 25 min. So, the polymeric chains start to grow and crosslink once the shells are collected inside the flask for the three circulation systems. The time required to fix the shell's shape is at least 20 minutes.

It seems that both the straight tube and the tube with areas of constriction have no influence over the shells non-concentricity. For both these circulation systems, the time spent by the shells inside the rotating flask allows the centering of the internal water phase inside the organic phase.

Moreover, while using both the short and long wound tubes, the shells non-concentricity seems to be much more influenced by the rotating flask than by the wound tube even if this hypothesis could not be demonstrated by the experiments realized. The filling level of the external water phase inside the collecting flask has no influence on the shells non-concentricity.

The next step of this study of the influence of the deformations on the shells non-concentricity could be to focus on the agitation of the shells via the rotation speed, the flask shape and dimensions.

**Bibliographic references**

1. Guillot, L., P. Vedrenne, and J. Etheve, *Procédé et dispositif de fabrication de billes ou de ballons en mousse polymère*. 2004.
2. Norimatsu, T., et al., *Cryogenic Targets and Related Technologies at ILE Osaka University*. Journal of Vacuum Science and Technology A, 1994. **12**(4): p. 1293-1295.
3. Norimatsu, T., et al., *Modeling of the centering force in a compound emulsion to make uniform plastic shells for laser fusion targets*. Fusion Science and Technology, 1999. **35**: p. 147-156.
4. Streit, J. and D. Schroen. *Foam shells: overcoating progress*. in *High Average Power Laser Program Workshop*. 2005. Lawrence Livermore National Laboratory.
5. Ito, F., et al., *Optimization of gelation to prepare hollow foam shell of resorcinol-formalin using a phase transfer catalyst*. Fusion Science and Technology, 2006. **49**: p. 663-668.
6. Tsamopoulos, J.A. and A.B. Brown, *Dynamic centering of liquid shells*. Physics of Fluids, 1987. **30**: p. 27-35.
7. Pelekasis, N.A., J.A. Tsamopoulos, and G.D. Manolis, *Nonlinear oscillations of liquid shells in zero gravity*. The Journal of Fluid Mechanics, 1991. **230**: p. 541-582.
8. Chambon, F. and H.H. Winter, *Stopping of crosslinking reaction in a PDMS polymer at the gel point*. Polymer Bulletin, 1985. **13**: p. 499-503.
9. Chambon, F., et al., *Rheology of model polyurethanes at the gel point*. Macromolecules, 1986. **19**: p. 2146-2149.
10. Winter, H.H., P. Morganelli, and F. Chambon, *Stoichiometry effects on rheology of model polyurethanes at the gel point*. Macromolecules, 1988. **21**(2): p. 532-535.
11. Muller, R., et al., *Rheological characterization of the gel point: a new interpretation*. Macromolecules, 1991. **24**: p. 1321-1326.
12. Cassagnau, P., et al., *A rheological method for the study of crosslinking of ethylene acetate and ethylene acrylic ester copolymer in a polypropylene matrix*. Polymer Engineering and Science, 1992. **32**(15): p. 998-1003.
13. Trotignon, J.-P., et al., *Matières Plastiques, Structures - Propriétés, Mise en oeuvre, Normalisation*. Précis, ed. AFNOR. 1997: Nathan.

**CHAPTER V. STUDY OF THE INFLUENCE OF  
INCREASED POLYMERIZATION RATES ON  
THE SHELLS CHARACTERISTICS**

In this last chapter, we studied the influence of high polymerization rates on the shells characteristics. The first idea was to increase the polymerization temperature. Then, shells were synthesized either with the wound tube at 90°C or the tube with areas of constriction with the water bath set at different temperatures. The second idea was to induce polymerization by photoinitiation instead of thermal initiation. The influence of UV polymerization on the shells characteristics was studied at last.

## **V.1. STUDY OF THE INFLUENCE OF INCREASED POLYMERIZATION TEMPERATURES ON THE SHELLS CHARACTERISTICS**

### **V.1.1. Behavior of the system with higher temperature**

In the actual process, the polymerization reaction used to synthesize shells takes place at 60°C. The shells structure appears as a starting tridimensional network after 23 minutes at 60°C, according to the rheology measurements presented in Chapter IV. To increase the polymerization rate, the first obvious solution is to increase the temperature of the process. In this aim, kinetics measurements by rheometry were performed to know in which range of time the polymerization rate increases when the temperature increases. The polymerization rate could also have been increased by either increasing the initiator concentration in the organic phase or changing the initiator used. It seemed difficult to have a higher initiator concentration since it is already difficult to completely dissolve the actual quantity of initiator inside the organic phase. Changing the AIBN to an initiator that decomposes near ambient temperature involves that the organic phase will start the polymerization process inside the syringe which is unacceptable.

Thus, a rheometer equipped with a plate/plate measuring system was used to determine the shear storage modulus  $G'$  and the shear loss modulus  $G''$  as the organic phase polymerized at various temperature. The crossover of the storage and loss moduli measured during isothermal curing may be defined as the gel point as explained in Chapter IV.

The evolutions of the shear loss modulus  $G''$  and the shear storage modulus  $G'$  of the organic phase along the synthesis at 60, 70, 80 and 90°C are illustrated in Figure V.1. Then, the times to reach a tridimensional network of the organic phase for temperatures varying from 40 to

90°C are presented in Table V.1. It is easy to see that when the temperature increases from 60°C to 90°C, the time to form a tridimensional network decreases exponentially. The results obtained at 40 and 50°C are not plotted in Figure V.1 because the times of reaction are way too long to fit in the graphic.

The AIBN is used as a thermal initiator here. The time for the thermal initiator to decompose depends on the temperature. Indeed, the decomposition rate constant  $k_d$  of the AIBN in toluene is equal to  $9.15 \cdot 10^{-6} \text{ s}^{-1}$  at 60°C and equal to  $4.86 \cdot 10^{-4} \text{ s}^{-1}$  at 90°C. The half life time  $t_{1/2}$  of the initiator is the time necessary for half of the initiator introduced to be decomposed. The half life time is calculated from the following formula:

$$t_{1/2} = 0.693 / k_d$$

For example, in toluene, the AIBN shows a  $t_{1/2}$  equal to 21 hours at 60°C and 24 min at 90°C. The times to reach a tridimensional network of the organic phase at 50 and 40°C are really long, one hour and a half and eight hours respectively. These long times to reach a tridimensional network are linked to the slow decomposition of the initiator at low temperature. On the opposite, when the temperature is increased up to 90°C, the time to reach a tridimensional network goes down to 80 seconds at 90°C.

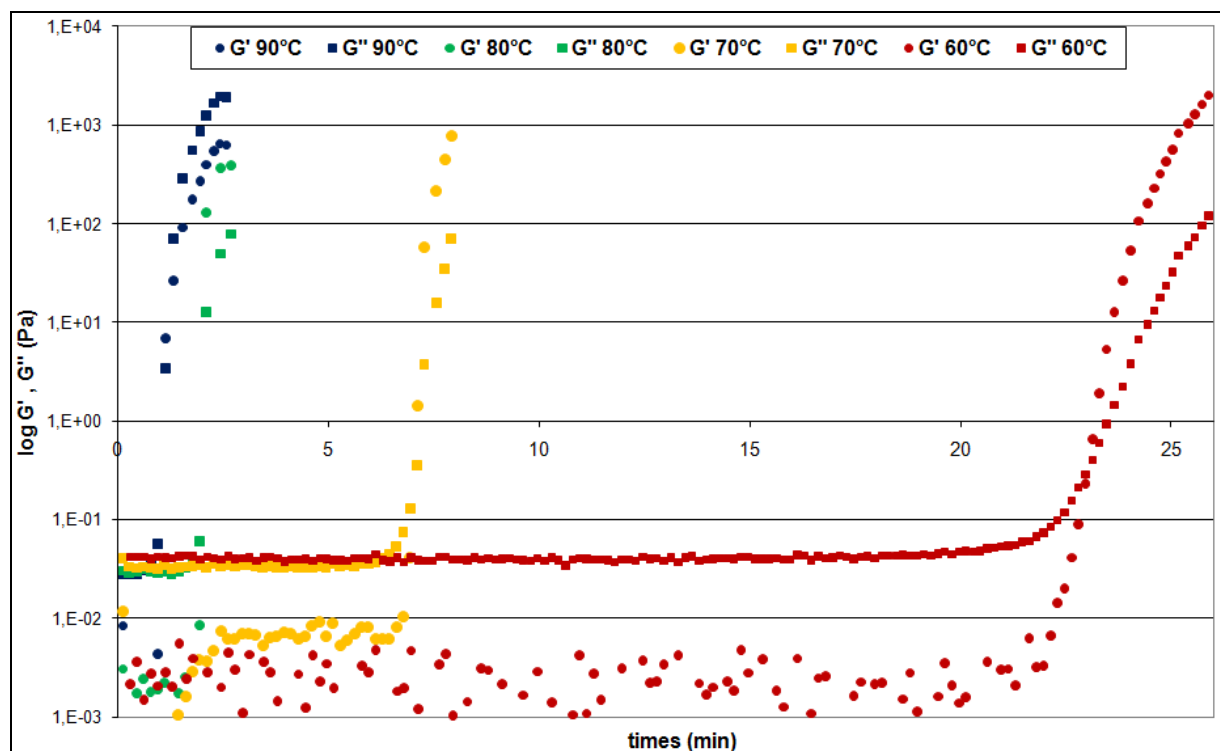


Figure V.1: Evolution of shear loss modulus  $G''$ , and of shear storage modulus  $G'$ , as a function of reaction time, for the organic phase at 60, 70, 80 and 90°C

Table V.1: Times to reach a tridimensional network for the organic phase at various temperatures

Temperature (°C)	Time to reach a tridimensional network
40	8 h
50	1h 26 min
60	23 min
70	7 min
80	2 min 40 s
90	1 min 20 s

The rate constant  $k$  of a chemical reaction can be expressed towards the Arrhenius equation. This relation describes the dependence of the rate constant with the temperature  $T$  and activation energy  $E_a$  as shown below:

$$k = A \exp\left(-\frac{E_a}{RT}\right) \quad (1)$$

with  $A$  as the pre-exponential factor and  $R$  the gas constant. Taking the natural logarithm of the Arrhenius equation (1) yields to the equation (2) below.

$$\ln(k) = \ln(A) - \frac{E_a}{R} \frac{1}{T} \quad (2)$$

So, when a reaction has a rate constant that obeys the Arrhenius equation, the plot of  $\ln(k)$  versus  $1/T$  gives a straight line, whose slope and intercept can be used to determine  $E_a$  and  $A$  respectively.

The rate of polymerization as the equation (8) in Chapter II can be expressed as follow:

$$-\frac{d[M]}{[M]} = k_p \sqrt{\frac{f k_d [I]}{k_t}} dt \quad (3)$$

with:  $[M]$ : monomer concentration

$[I]$ : initiator concentration

$k_p, k_d, k_t$ : propagation, decomposition and termination rate constants

$t$ : time

$f$ : efficiency factor

Then, the equation (3) corresponds to the following equation:

$$\ln \frac{[M]_0}{[M]} = k_p \sqrt{\frac{f k_d [I]}{k_t}} t \quad (4)$$

It is thought that the three-dimensional network always forms for a same extent of reaction whichever polymerization temperature. Then, at the time at which a three-dimensional network is reached, the term  $\frac{[M]_0}{[M]}$  is constant, so  $\ln \frac{[M]_0}{[M]}$  is constant. Besides, the Arrhenius equation of the polymerization reaction can be written as a combination of the three separate Arrhenius-type equations of the propagation, decomposition and termination steps:

$$\ln \left[ k_p \left( \frac{k_d}{k_t} \right)^{\frac{1}{2}} \right] = \ln \left[ A_p \left( \frac{A_d}{A_t} \right)^{\frac{1}{2}} \right] - \frac{\left[ E_{ap} + \frac{E_{ad}}{2} - \frac{E_{at}}{2} \right]}{RT} \quad (5)$$

Then, from the equations (2), (4) and (5), the following equation can be deduced:

$$\ln(t) = \text{cste} + \frac{\left[ E_{ap} + \frac{E_{ad}}{2} - \frac{E_{at}}{2} \right]}{RT} \quad (6)$$

with:  $A_p, A_d, A_t$ : propagation, decomposition and termination pre-exponential factors

$E_{ap}, E_{ad}, E_{at}$ : propagation, decomposition and termination activation energy

So, when a polymerization reaction obeys the Arrhenius equation, the plot of  $\ln(t)$  versus  $1/T$  gives a straight line, whose slope and intercept can be used to determine  $E_a = E_{ap} + \frac{E_{ad}}{2} - \frac{E_{at}}{2}$ .

From the results obtained in Table V.1, we can plot  $\ln(t)$  as a function of  $1/T$  as illustrated in Figure V.2. The linear regression coefficient  $R^2$  of the line obtained is equal to 0.9896. So, we can consider that the polymerization reaction follows the Arrhenius equation. Besides, the activation energy of the polymerization reaction  $E_a$  is equal to 111 kJ.mol<sup>-1</sup>.

According to G. Odian [1], the decomposition activation energy  $E_{ad}$  is in the range of 120-150 kJ.mol<sup>-1</sup> for the most common initiators.  $E_{ap}$  and  $E_{at}$  values for common monomers are in the ranges of 20-40 kJ.mol<sup>-1</sup> and 8-20 kJ.mol<sup>-1</sup>, respectively. Then, the value found for the activation energy of the polymerization reaction  $E_a$  corresponds to the classical value within the literature.

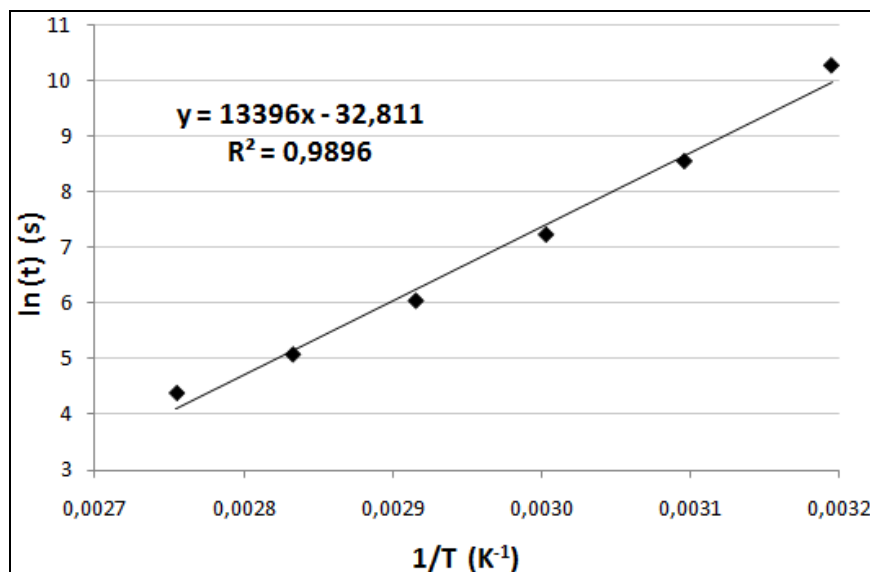


Figure V.2: Plot of  $\ln(t)$  as a function of  $1/T$  for the polymerization reaction of the organic phase

Thus, shells will be synthesized at 90°C to study the influence of high polymerization rate on the shells non-concentricity.

### V.1.2. Shells synthesized at higher polymerization temperature

Shells were synthesized and polymerized at 90°C by using either the wound tube heated at 90°C or the tube with areas of constriction followed by the flask heated at 90°C once the shells are collected. The shells were synthesized using W1(12) as the internal water phase. One major issue that appears with the synthesis taking place at 90°C is that the double emulsion is not stable anymore at 90°C. The double emulsion is quite stable at 60°C even though the phenomenon of phase inversion already occurs leading to the formation of beads instead of shells as illustrated in Chapter III. In fact, when the temperature applied to the double emulsion increases, more and more destabilization phenomena occur.

The contents of a bottle collected with the tube with areas of constriction followed by the flask heated at 90°C once the shells are collected is presented in Figure V.3. The bottle contains only about ten shells, many beads and one agglomerate. The few shells obtained cannot be characterized because of their opacity. So, at 90°C with this process, the inversion phase phenomenon is really significant. The shells at 90°C are supposed to polymerize in 80 seconds but the phase inversion phenomenon is faster than the polymerization.





Figure V.3: Contents of a bottle collected with the tube with areas of constrictions followed by the flask heated at 90°C

When shells are synthesized with the wound tube heated at 90°C, it is visible to the naked eye that the shells inside the wound tube are not concentric. Once the shells are collected inside the flask, they quickly become half shells and then flocculate all together. In that specific case, the flocculation is not reversible because the remaining double bounds of the monomer react to give huge agglomerates as illustrated in Figure V.4.

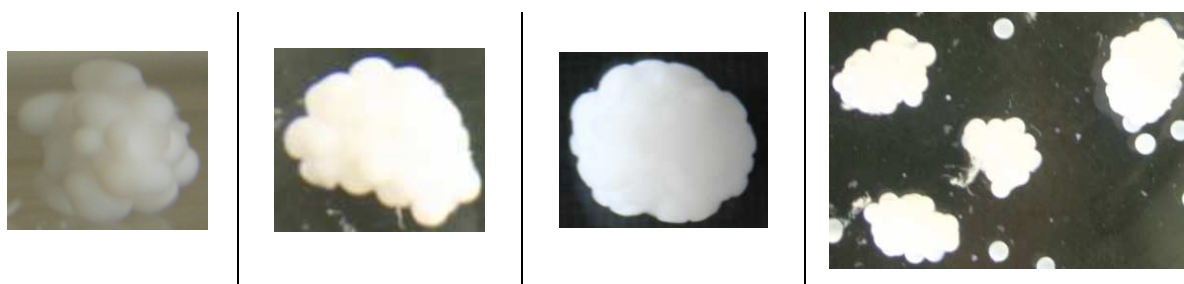




Figure V.4: Bottles collected with the wound tube heated at 90°C

Exploring processes at lower temperature, a trainee at the CEA synthesized shells with the tube with areas of constriction and the flask heated at either 70 or 80°C once the shells are collected. The results obtained by the trainee are presented in Table V.2. At these temperatures, the yield is also really low because phase inversion phenomena already took place at 70°C. Moreover, the non-concentricity of the few shells obtained is severely increased compare to the non-concentricity values obtained at 60°C.

Table V.2: Results of shells synthesis realized at 70 and 80°C

Temperature (°C)	Yield of shells (%)	% of shells with NC < 4%	Photos
70	12	4	
80	5	0	

Therefore, at 70, 80 and 90°C the destabilization phenomena of the double emulsion are quicker than the time required to polymerize the organic phase in order to have stable shells. Indeed, as stated by Chen *et al.* [2], both the destabilization phenomena and the polymerization rate are temperature dependent, then it is necessary to balance these two effects.

However, we wondered if the destabilization of the emulsion was due to the degradation of the surfactant since Cook *et al.* [3] stated that “when the foam is heated to 50°C in the presence of water during the polymerization step, the sorbitan monooleate (Span 80) hydrolyzes to form oleic acid and sorbitol”. Indeed, the degradation of the surfactant would modify the interfacial tension and then lead to the destabilization of the emulsion.

In order to check this hypothesis, we put a mixture of Span 80 and water at 90°C during 30 minutes. Inside water, the Span 80 seems to precipitate and change of color (whitening) and texture. After the thermal aging step, the organic product which appears as a white solid at the surface of water is retrieved by adding dichloromethane to the mixture. The remaining water is eliminated from the organic solution by adding magnesium sulfate. The organic solution is then filtered and the dichloromethane is evaporated using a rotary evaporator. After all these steps, the retrieve product looks like the initial Span 80. However, the retrieved product was analyzed by infrared (IR) spectroscopy.

Pure Span 80 and pure oleic acid IR spectra show a carbonyl absorption at 1739  $\text{cm}^{-1}$  (ester function) and 1710  $\text{cm}^{-1}$  (carboxylic acid function) respectively. We checked that the shift between these two absorptions was enough to split into two peaks. In this goal the IR

spectrum of a mixture of Span 80 and oleic acid was realized. Figure V.5 shows that the two peaks are effectively divided, so it is possible to differentiate the carbonyl function from the Span 80 and from the oleic acid.

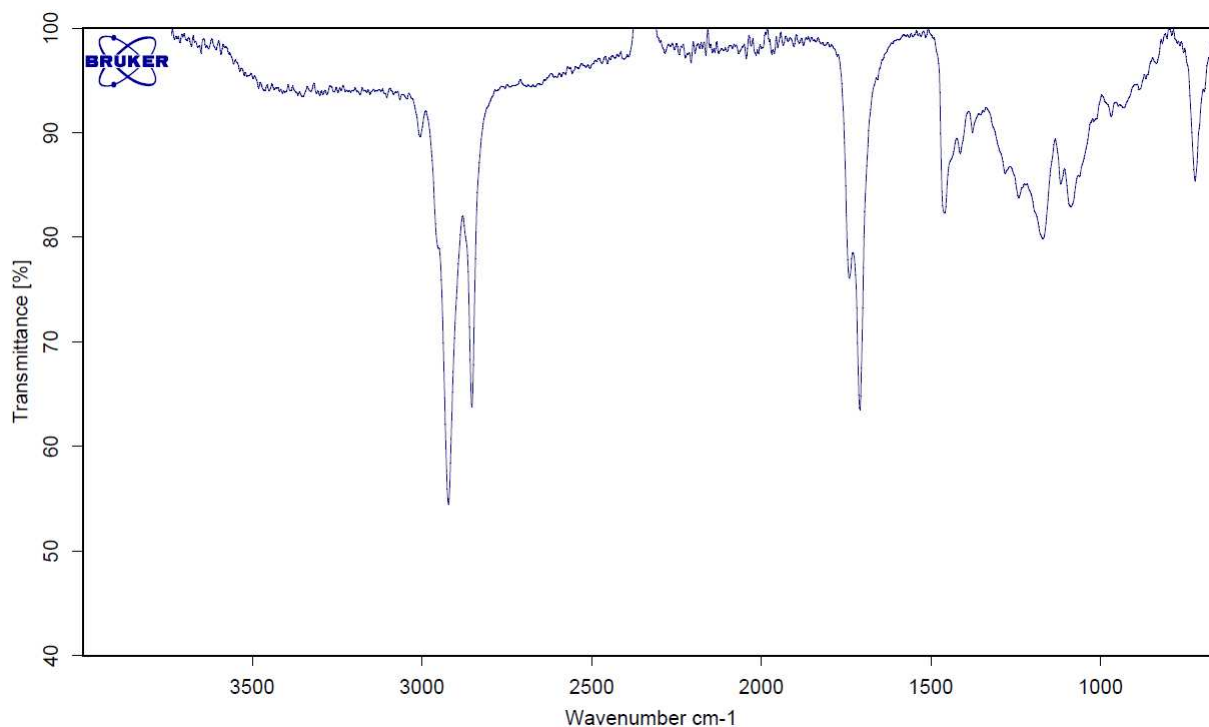


Figure V.5: IR spectrum of a mixture of Span 80 and oleic acid

The IR spectra of the retrieved product, Span 80 mix with water at 90°C during 30 minutes (red spectrum), and the IR spectra of pure Span 80 (blue spectrum), are illustrated in Figure V.6. From the spectra obtained, we can see that there is a unique absorption peak at 1739  $\text{cm}^{-1}$ . Therefore, no hydrolysis of the Span 80 can be shown in our case and the destabilization of the emulsion is not due the degradation of the surfactant.

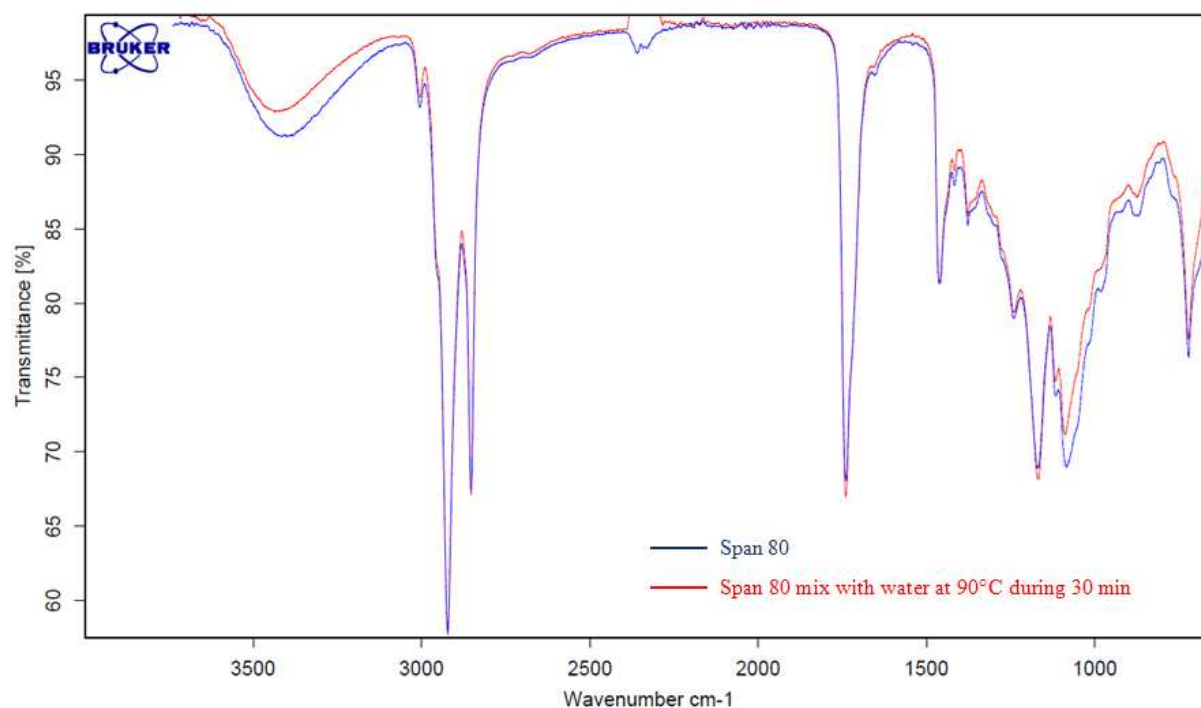


Figure V.6: Spectra of pure Span 80 (blue spectrum) and of Span 80 mix with water at 90°C during 30 minutes (red spectrum)

Then, the influence of high polymerization rate on the shells characteristics could not be studied by increasing the polymerization temperature. This is the reason why we focused our study on the use of UV polymerization in order to get higher polymerization rates.

## V.2. STUDY OF THE INFLUENCE OF POLYMERIZATION BY UV LIGHT ON THE SHELLS CHARACTERISTICS

As stated in Chapter II, UV polymerization is a neat way to reach high level of monomer conversion in a very short time near room temperature. The Americans have never published about the UV polymerization of shells and only one Japanese abstract can be found on this topic [4]. In this abstract, the authors stated that “the yield for uniform hollow foam shells was greatly improved” using polymerization by photoinitiation with a UV light. In 1995, Takagi *et al.* [5], said that “a fabrication technique of foam shells using UV-photo polymerization”, mentioned in reference [4], “showed excellent performance in view point of «shell fabrication»”.

However, the photopolymerization of multifunctional (meth)acrylate monomers is used in various fields such as optical lenses, dental applications [6], surface coating, printed circuit board, information storage system [7] and microfluidic [8], [9], [10], [11]. Xu *et al.* [8]

photopolymerized microspheres made with a microfluidic droplet generator, with diameters ranging from 20 to 200  $\mu\text{m}$ . Nisisako *et al.* [9] photo-polymerized droplets of acrylic monomer prepared in a T-shaped microchannel, with 30-120  $\mu\text{m}$  diameters. Utada *et al.* [10] fabricated a rigid spherical shell by photo-polymerizing a polymer in the middle fluid of a W/O/W double emulsion. Nie *et al.* [11] carried out fast throughput photopolymerization of monomeric shells and obtained spherical polymeric shells. All these successful works in this various fields reinforced our idea to use photopolymerization to synthesize foam shells.

## **V.2.1. Choice of the UV lamp and the photoinitiator**

### **V.2.1.1. Choice of the UV lamp**

To initiate the polymerization by UV light, it is necessary to find a wavelength at which the different phases used in the synthesis process do not absorb, except for the photoinitiator. First, the absorbance of all the phases used was measured using a UV-visible spectrophotometer. The absorbance of the external water phase W2 and the organic phase O1 was measured in the UV wavelength domain, from 190 to 400 nm. The absorbance spectra for O1 and W2 are presented in Figure V.7. The organic and external water phases do not absorb UV light between 350 and 400 nm. Then, a UV lamp emitting at 365 nm can be used to polymerize the acrylic shells.

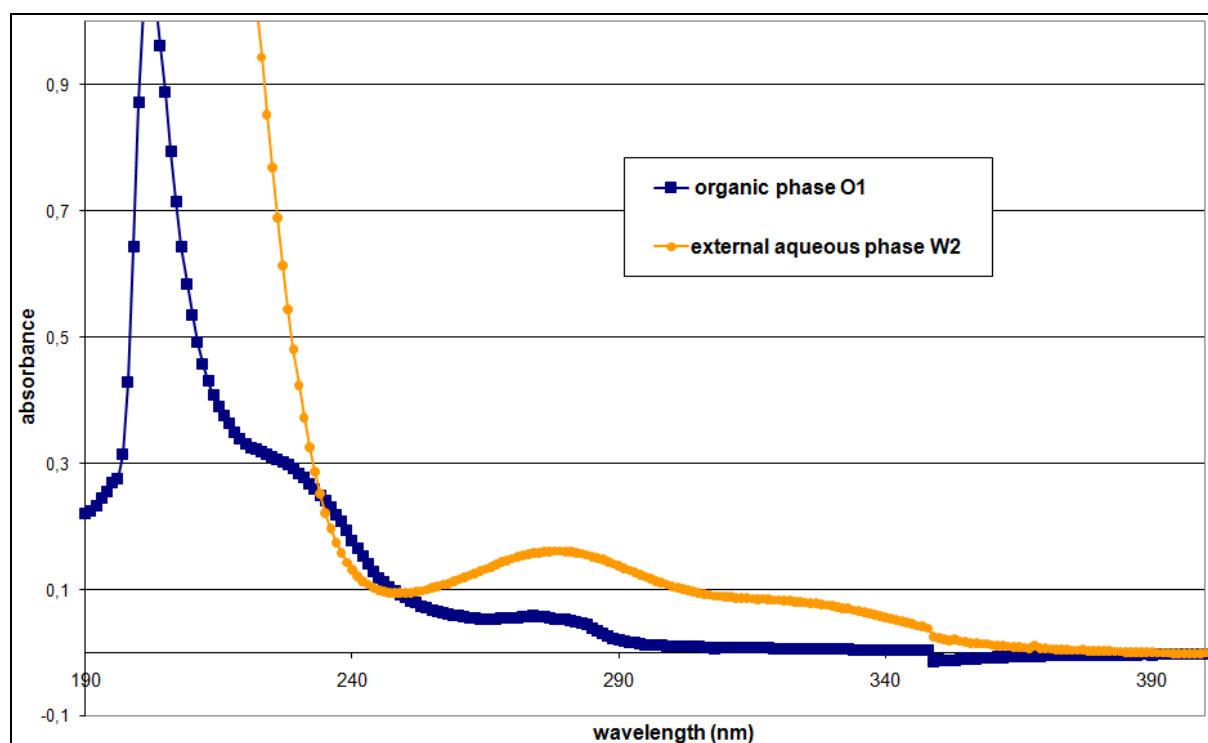


Figure V.7: Absorbance spectrum in the UV domain for the organic phase O1 and the external water phase W2

Two different kinds of UV lamps were available in the laboratory at the CEA. The first one is a UV lamp with two black neons. Its wavelength was 365 nm, with a power of 120 W. The second one is a UV spot emitting at 365 nm with a power of 1000 W. The two different kinds of lamp used are illustrated in Figure V.8.



Figure V.8: Two kinds of UV lamp with a black neon UV lamp on the left and a UV spot on the right

### V.2.1.2. Choice of the photoinitiator

The photoinitiator has to fulfill several requirements. First, the photoinitiator should be composed of only oxygen, carbon and hydrogen, as the organic phase. Second, the photoinitiator should absorb at the same wavelength in which the UV lamp is emitting. Thus,

at this step, we selected four common photoinitiators used in the literature for wavelength ranging between 350 and 380 nm:

- Irgacure 184: 1-hydroxycyclohexylphenyl ketone [8], [11]
- Darocur 1173 : 2-hydroxy-2-methyl-1-phenyl-propan-1-one [9]
- DMPA: 2,2-dimethoxy-2-phenylacetophenone [6], [7], [12]
- BEE: benzoin ethyl ether [12]

Their four absorption spectra are presented below in Figure V.9. The four photoinitiators absorb UV light at 365 nm.

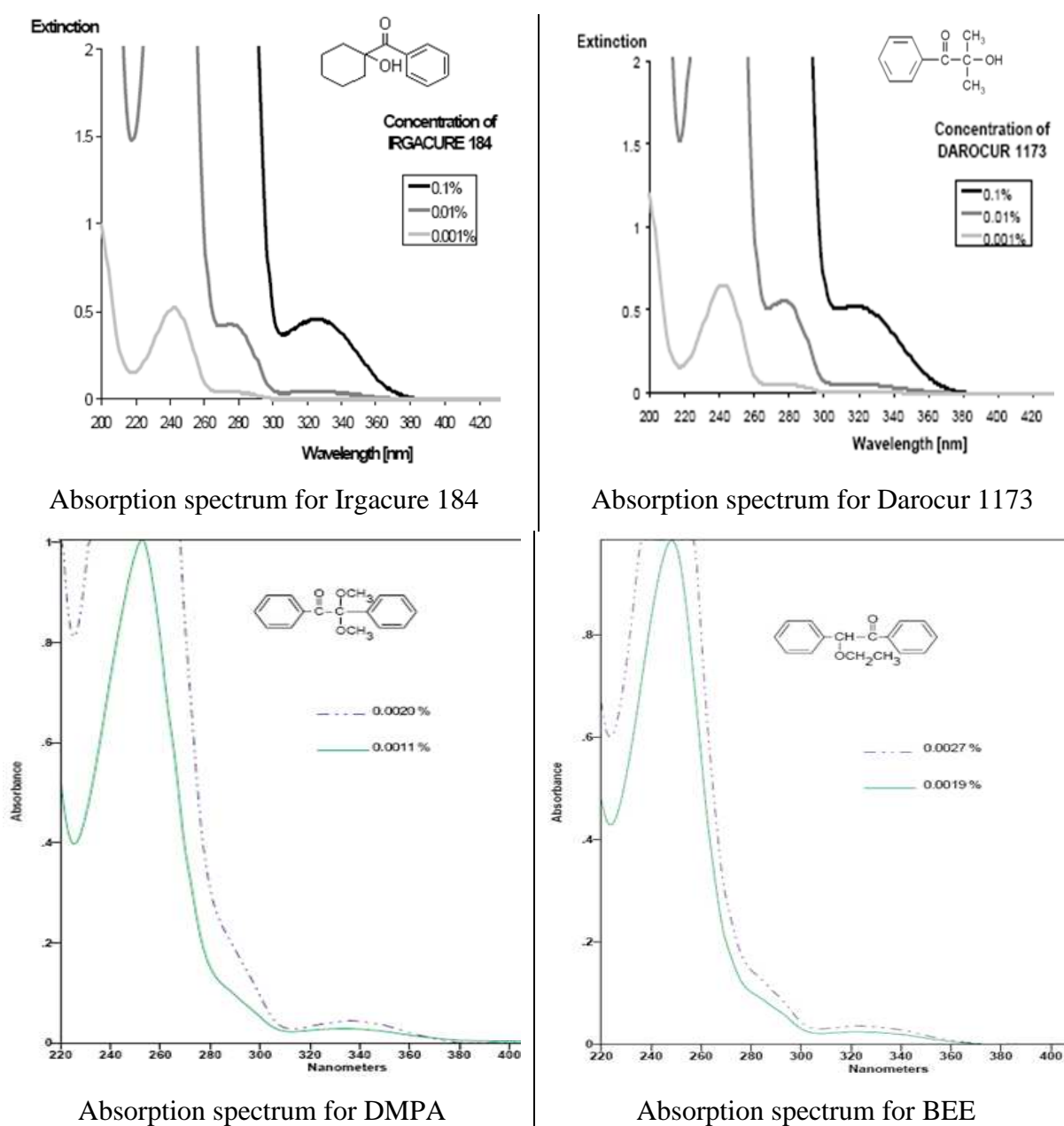


Figure V.9: Absorption spectra of the four selected photoinitiators (Irgacure 184 = 1-hydroxycyclohexylphenylketone, Darocur 1173 = 2-hydroxy-2-methyl-1-phenyl-propan-1-one, DMPA = 2,2-dimethoxy-2-phenylacetophenone, BEE = benzoin ethyl ether)

Third, the photoinitiator should not change the density of the organic phase when it is used instead of the thermal initiator, AIBN. The density difference between the organic phase with the photoinitiator and the organic phase with the thermal initiator lie between 0.1 and 0.3% for the four photoinitiators. The slight density difference observed will be compensated by the quantity of deuterated water added to the internal water phase W1 in order to have the same density mismatch of  $0.078 \text{ g.cm}^{-3}$  at  $60^\circ\text{C}$  between W1(12) and O1.

Even though the polymerization is initiated by UV light, the process temperature will be kept to  $60^\circ\text{C}$  in order for the parameters such as viscosity, density and interfacial tension to remain constant. The fourth requirement for the photoinitiator is then to avoid initiation of the polymerization at  $60^\circ\text{C}$  if the photoinitiator is not exposed to UV light. Thus, the evolutions of the shear loss modulus  $G''$  and the shear storage modulus  $G'$  of the organic phase along the synthesis at  $60^\circ\text{C}$  were measured for the four photoinitiators (Figure V.10). The four photoinitiators do not polymerize TMPTMA at  $60^\circ\text{C}$  without UV light. Indeed, the shear loss modulus and the shear storage modulus remain constant during at least 30 minutes and never cross each other, as illustrated in Figure V.10.

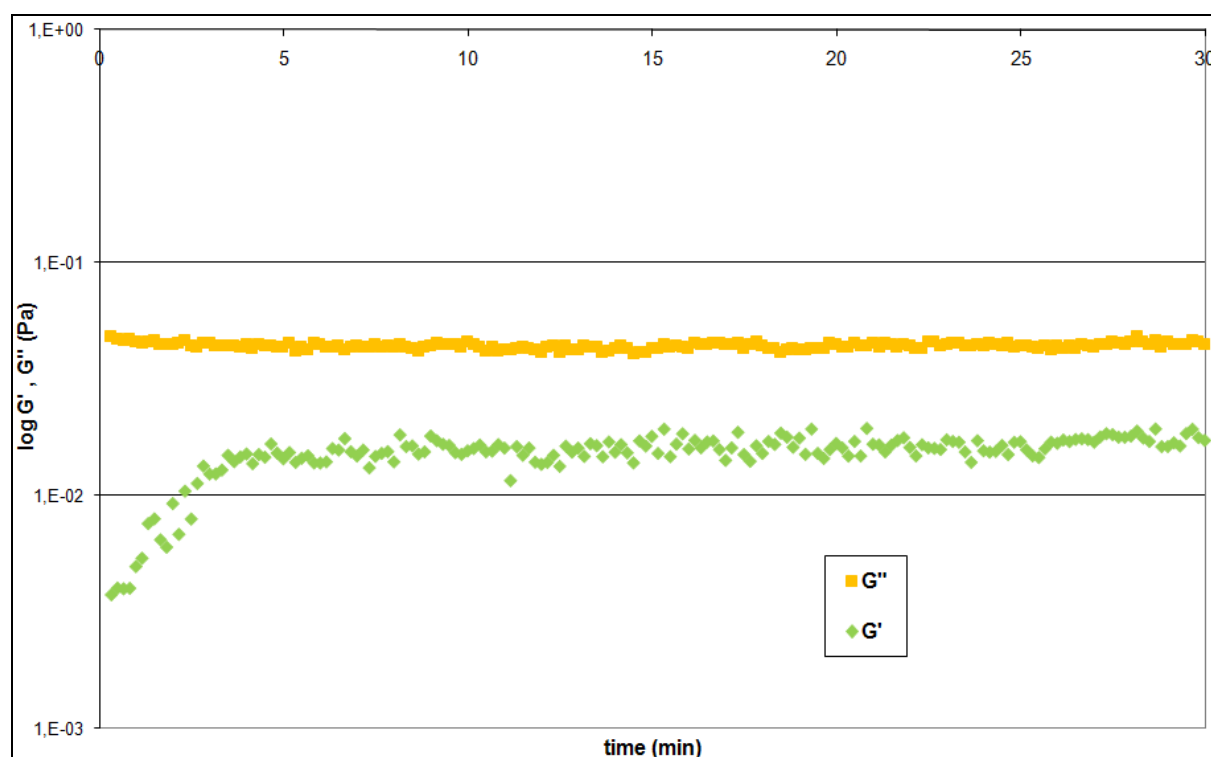


Figure V.10: Evolution of shear loss modulus  $G''$ , and of shear storage modulus  $G'$ , as a function of reaction time for the organic phase and each of the four photoinitiators



As the four photoinitiators answer the four requirements, the most efficient photoinitiator will be selected to synthesize shells. In order to know which photoinitiator is the most efficient, two simple tests were realized. Few drops of the organic phase containing one of the photoinitiator are layed out on a Petri dish. Then, the four Petri dishes are exposed to a UV light intensity of  $3 \text{ mW.cm}^{-2}$  during either 1 minute or 5 minutes. Two photos of the results obtained for these two tests are presented in Figure V.11. The test at 1 minute shows that both Irgacure 184 and Darocur 1173 do not initiate TMPTMA polymerization since the medium stays liquid. The BEE slightly starts the polymerization of TMPTMA on the edge whereas the DMPA seems to be the most efficient. The test at 5 minutes shows that the DMPA completely polymerized the TMPTMA whereas the other three photoinitiators generate partial polymerization of the organic phase. Therefore, the DMPA is the most efficient photoinitiator for our system and will be used to polymerize shells by UV process.

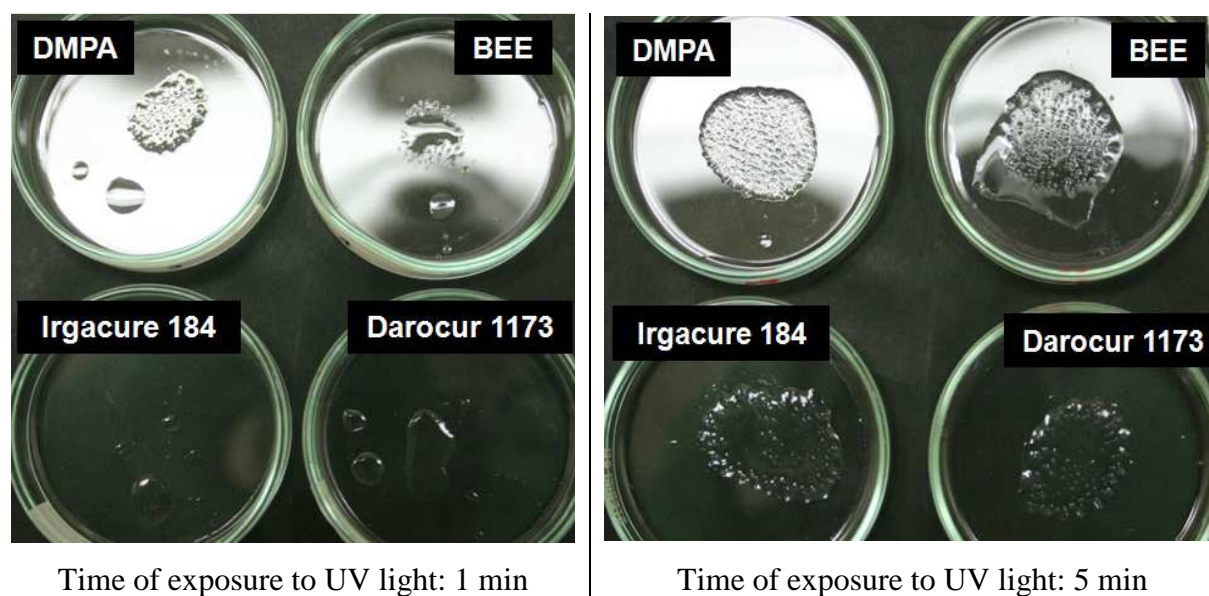


Figure V.11: Organic phases with the four photoinitiators exposed to a UV light intensity of  $3 \text{ mW.cm}^{-2}$  during 1 min (samples on the left) or 5 min (samples on the right)

### V.2.2. Characteristics of shells synthesized using UV polymerization

Shells are synthesized using the tube with areas of constriction. The collected flasks are still heated at  $60^\circ\text{C}$  as before in order to keep constant the densities, the viscosities and the interfacial tensions of the three phases. Shells are synthesized using the same external water phase (W2) as before. The internal water phase used is W1(12) for all the further experiments. The organic phase used is also the same as before except for the initiator used. The 2,2'-azo-

bis-isobutyronitrile (AIBN) is replaced by 2,2-dimethoxy-2-phenylacetophenone (DMPA). The weight percent of AIBN used was 1.3% in O1, as stated in Chapter I, which represents 10% of the weight of monomer introduced in the organic phase. A rapid survey of the literature helped us to choose the judicious scale of the amount of photoinitiator in the organic phase formulation. Only 1 to 5 wt% of photoinitiator is usually used for photopolymerization reaction. Bland *et al.* [6], and Nisiako *et al.* [9] used 1 wt% of DMPA and Darocur 1173 respectively. Nie *et al.* [11], and Xu *et al.* [8] used 4 wt% of Irgacure 184. However, since we used 10% of initiator in thermal polymerization, we will also test higher amount of photoinitiator than in the literature. Thus, the influence of the quantity of DMPA introduced in the organic phase on the shells shape was studied.

Shells are exposed to UV light once the collection is finished (around 5 min) and once that the collected flask has been moved to another agitation motor under another extractor wood. For safety issues with UV radiations, it is not possible for now to put the UV lamp in the extractor wood containing the injection system. First, the results obtained with the UV black neon will be presented. Then, the results obtained with the UV spot will be exposed.

### V.2.2.1. Characteristics of shells synthesized with a UV black neon lamp

The UV lamp is placed on the top of the rotating flask as illustrated in Figure V.12. The UV lamp is 15.5 cm far from the bottom of the flask and 12.5 cm far from the level of W2 solution in the bottle. The UV light intensity measured with a photometer inside the flask is equal to  $2 \text{ mW.cm}^{-2}$ . The shells are exposed to UV light during 5 minutes. A UV protector film is stick to the window of the extractor wood to protect the operator from UV radiations.

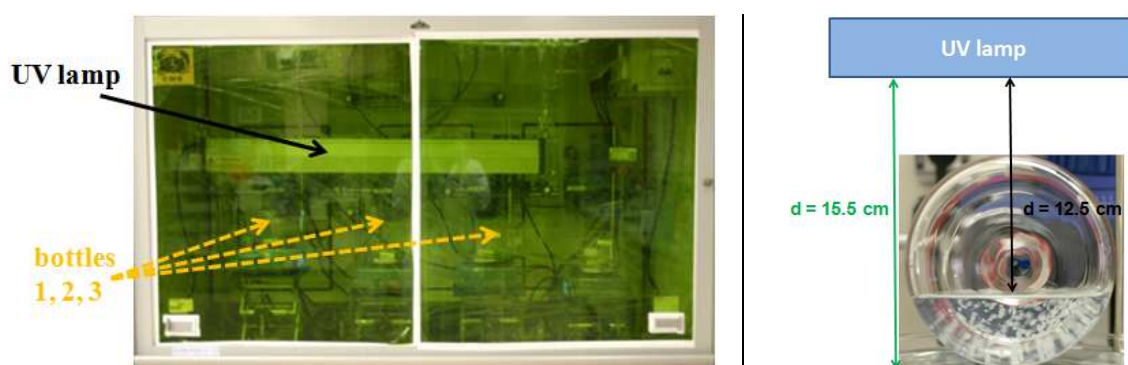


Figure V.12: On the left, picture of the extractor wood with the UV black neon lamp placed on top of the rotating flasks. On the right, illustration of the distance between the UV lamp and the flask filled with shells

Shells were synthesized with four different organic phases containing 1, 5, 10 or 15% of DMPA. The yield, thickness and average non-concentricity results obtained are presented in Table V.3.

Table V.3: Yield, thickness and average non-concentricity results obtained for the synthesis of shells with 1, 5, 10 and 15% of DMPA and UV black neon lamp

% DMPA	yield of shells (%)	average thickness ( $\mu\text{m}$ )	average NC (%)
1	3	68	-
5	23	96	23
10	39	108	19
15	55	113	22

For the synthesis with 1% of DMPA, less than ten shells are obtained at the end of the process. The few shells obtained present a lower thickness than the shells obtained by thermal polymerization, as illustrated in Figure V.13. Figure V.14 presents pictures of shells synthesized by thermal polymerization to be able to compare with the shells obtained by photopolymerization. Their average thickness is around 68  $\mu\text{m}$  whereas the usual thickness of the shells synthesized in Chapter III and IV is around 120  $\mu\text{m}$ . Thus, the shell's thickness with 1% DMPA is very low, which means that the shells polymerization is not complete. In addition, we tried to increase the time of exposure to UV light with 1% DMPA, but the exact same results of yield and thickness were obtained. So, a quantity of 1% DMPA as photoinitiator is not enough to polymerize the shell in all its thickness. A diffusion of free TMPTMA from one shell to another can easily occur once the shells flocculate. Then, the polymerization reaction occurs between shells and around them to give irreversible agglomerates. This explained why such agglomerates, as illustrated in Figure V.13, are obtained after the UV radiation.



Figure V.13: Picture of a shell, on the left, and pictures of shells agglomerates, obtained during the synthesis of shells with 1% DMPA

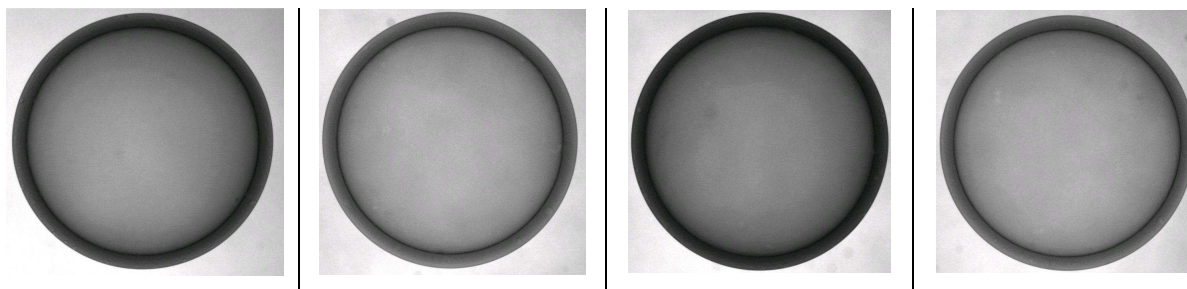


Figure V.14: Pictures of shells synthesized by thermal polymerization

For the synthesis with 5% of DMPA as photoinitiator the yield of shells obtained is still low since it is situated around 23%. The shells flocculate in big packs when they are in the external water phase but once they are exchanged in ethanol, the shells separate from each other. The average thickness of the shells is around 96  $\mu\text{m}$  which is low compared to the thickness obtained in thermal polymerization. The shells are covered with thin layers of polymerized organic phase linked to the wall of the shell, as it is illustrated in Figure V.15.

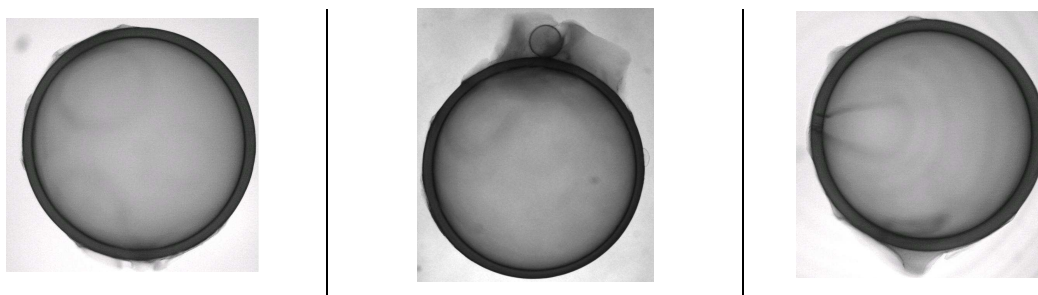


Figure V.15: Pictures of three shells obtained with 5% of DMPA

For the synthesis with 10 and 15% of DMPA, the yield of shells obtained is higher than for 1 and 5% of DMPA. However, the average non-concentricity remains high whichever the quantity of photoinitiator used. The high non-concentricity of the shells obtained can easily be seen with the naked eye (the two pictures on the left) as illustrated in Figure V.16. The average thickness of the shells lays between 108 and 113  $\mu\text{m}$  which comes closer to the thickness obtained in thermal polymerization. This means that with 10 or 15% of DMPA, the shells almost polymerized in all their thickness.

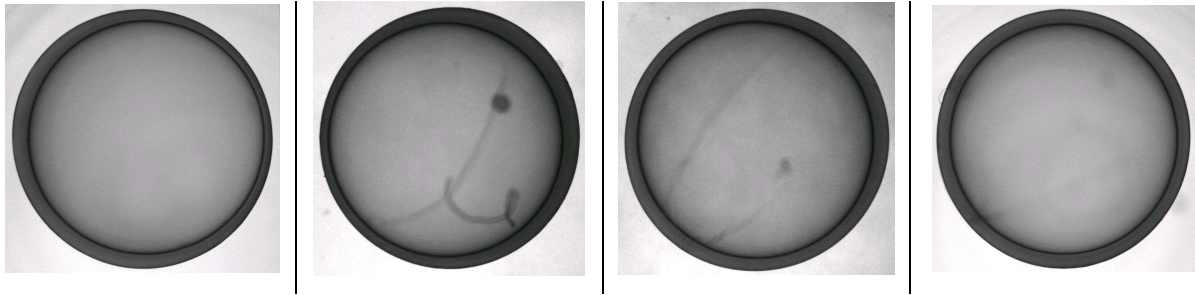


Figure V.16: Pictures of shells obtained with 10 and 15% of DMPA

Moreover, some of the shells synthesized by this UV process have been dried and characterized by scanning electron microscopy (SEM). The SEM images of the internal wall surface obtained for the four quantity of photoinitiator are presented in Figure V.17.

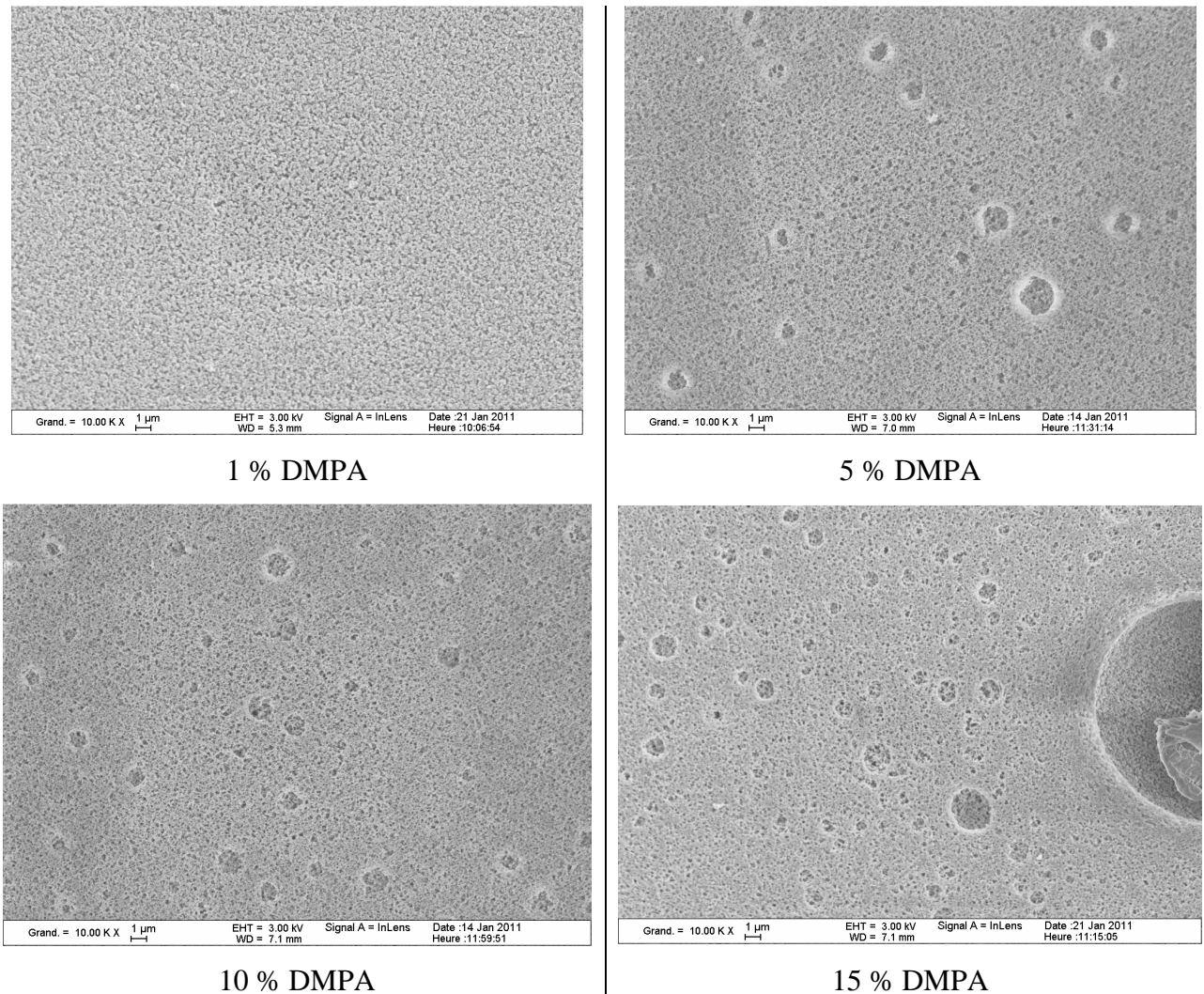


Figure V.17: SEM images of the internal wall surface of dry shells synthesized with either 1, 5, 10 or 15% of DMPA. The magnification for the four SEM images is 10000.

The images obtained show that when the amount of photoinitiator increases, the internal wall surface shows a more aerated structure and an increased density of holes with a wide size

distribution. This behavior occurring at the internal interface is not explained. This could be due to instabilities occurring at the interface during the UV process performed with the black neon UV lamp. The same phenomenon may occur at the external interface but the structure is so rough that the holes are not as visible as for the internal interface (Figure V.18).

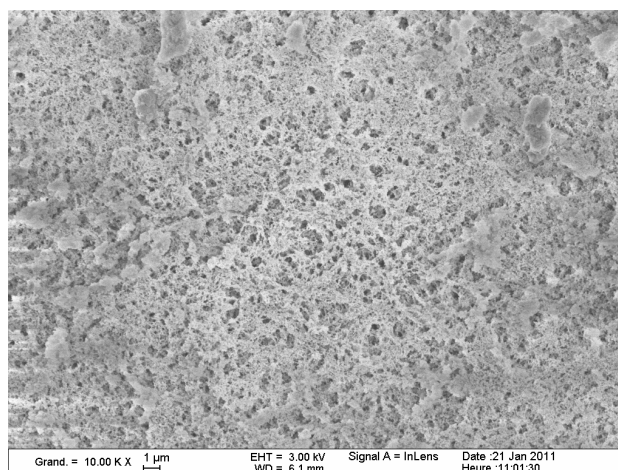


Figure V.18: SEM images of the external wall surface of dry shells synthesized with 15% of DMPA. The magnification for the SEM image is 10000.

To summarize, shells synthesized while expose to the UV black neon lamp after 5 minutes, give really poor results of non-concentricity and the thickness of the shells is lower than the thickness obtained with the usual thermal process. The light intensity supplied by this lamp is equal to  $2 \text{ mW.cm}^{-2}$ , which is too low to be able to polymerize the shells in all their thickness. Thus, syntheses of shells with a higher light intensity, using a UV spot, have been realized afterwards.

#### V.2.2.2. Characteristics of shells synthesized with a UV spot

The UV lamp is placed on the top of the rotating flask as illustrated in Figure V.19. The UV lamp is 11 cm far from the bottom of the flask and 7.5 cm far from the level of W2 solution in the bottle. The UV light intensity measured with a photometer inside the flask is equal to  $70 \text{ mW.cm}^{-2}$ . With this light intensity, all the objects and fluids under the spot heat really fast. The shells will not be exposed to UV light during 5 minutes as with the previous lamp since it is important that the water bath remains at  $60^\circ\text{C}$  and does not warm up. So, once the collected flask has been moved to another agitation motor under the UV spot, the shells are exposed to UV light during 2 minutes. However, during the first minute the UV light intensity increases from 0 to  $70 \text{ mW.cm}^{-2}$  and during the second minute, the UV light intensity remains at

$70 \text{ mW.cm}^{-2}$ . The temperature of the water bath remains at  $60^\circ\text{C}$  during this two minutes of UV irradiation.



Figure V.19: On the left, picture of the UV spot placed on top of the rotating flask. On the right, illustration of the distance between the UV spot and the flask filled with shells

As previously, shells were synthesized with four different organic phases containing 1, 5, 10 or 15% of DMPA. The yield, thickness and average non-concentricity results obtained with the UV spot are presented in Table V.4.

Table V.4: Yield, thickness and average non-concentricity results obtained for the synthesis of shells with 1, 5, 10 and 15% of DMPA and the UV spot

% DMPA	yield of shells (%)	average thickness ( $\mu\text{m}$ )	average NC (%)
1	54	115	18
5	90	125	17
10	80	129	24
15	80	127	27

The yield of shells obtained greatly improves when the UV light intensity increases from 2 to  $70 \text{ mW.cm}^{-2}$ . Indeed, the same yield of shells is obtained for 1% of DMPA with the UV spot than for 15% of DMPA with the UV black neon lamp. The yield of shells for 5, 10 and 15% of DMPA with the UV spot lay between 80 and 90%. This is really higher than the yield obtained with thermal polymerization which was around 58%.

The average thickness for 5, 10 and 15% of DMPA with the UV spot lay between 125 and  $129 \mu\text{m}$ , which is slightly higher than the  $120 \mu\text{m}$  average thickness obtained with thermal polymerization. This means that with the UV spot, the shells are quickly polymerized in all

their thickness. Indeed, the shells neither flocculate nor agglomerate after being exposed to UV radiation.

However, even with a higher UV light intensity, the average non-concentricity remains around 20% as previously. Pictures of the shells obtained with the UV spot are presented in Figure V.20.

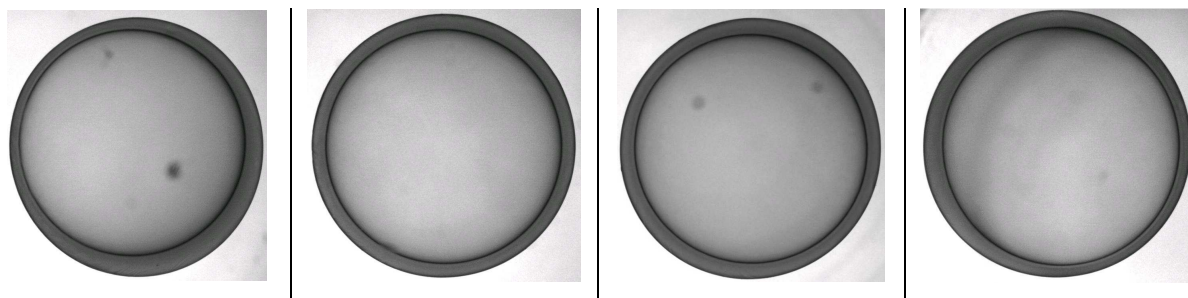


Figure V.20: Pictures of shells obtained with the UV spot with either 1, 5, 10 or 15 % of DMPA

Moreover, some of the shells synthesized have been dried and characterized by scanning electron microscopy (SEM) as previously. The SEM images of the internal and external wall surfaces obtained with 10% of photoinitiator are presented in Figure V.21. For the shells synthesized with the UV spot, there are no holes detected as previously. However, the external interface shows a rougher surface with cracks than the internal interface.

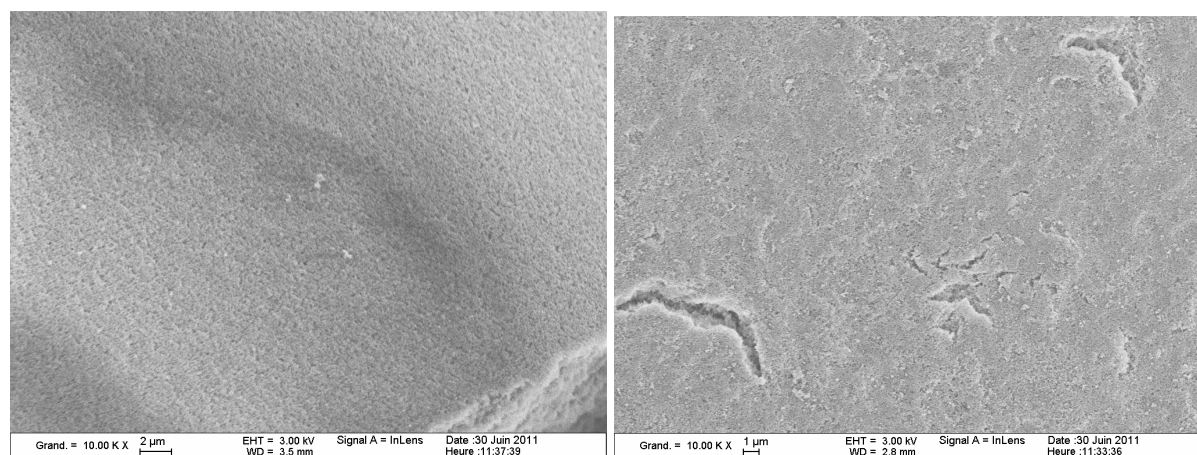


Figure V.21: SEM images of the internal wall surface (picture on the left) and of external wall surface (picture on the right) of dry shells synthesized with 10% of DMPA. The magnification for the SEM images is 10000.

For comparison, two SEM images of the internal and external wall surfaces obtained with thermal polymerization are presented below in Figure V.22. On the image of the internal wall



(on the left) the defect on the surface is due to a brush stroke since the dry shells are manipulated with a paintbrush and are very fragile. For both interfaces, there are no holes detected at the surface. Besides, the external interface does not show a rough surface as for both UV polymerization processes.

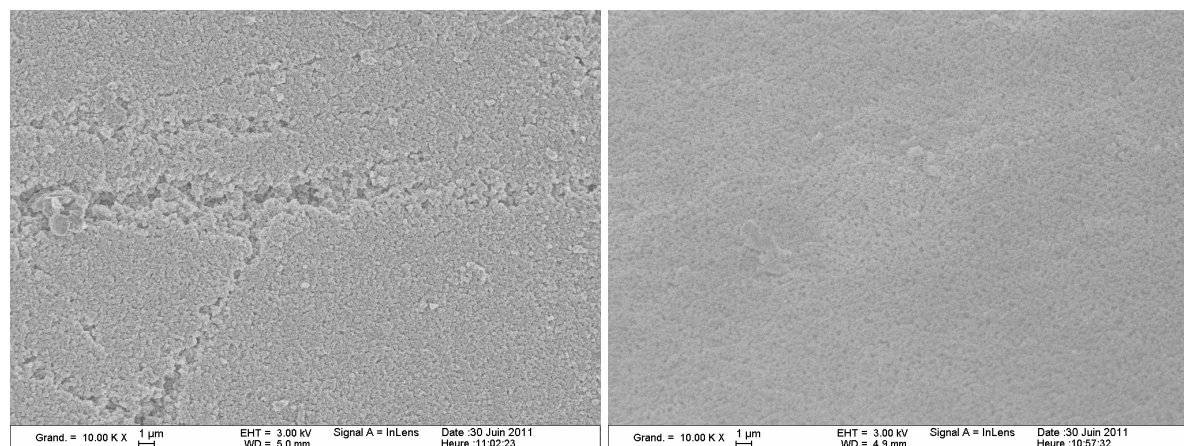


Figure V.22: SEM images of the internal wall surface (picture on the left) and of external wall surface (picture on the right) of dry shells synthesized by thermal polymerization. The magnification for the SEM images is 10000.

### V.2.2.3. Discussion about the shells NC obtained by thermal or photo polymerization

As shown in Chapter IV, with the thermal polymerization process, the polymeric chains of the organic phase start growing after 6 to 7.5 min, then the polymeric chains start crosslinking after 20 to 25 min. The thermal polymerization process leads to an optimized average NC of 2.4%. The time required to fix the shell's shape is at least 20 minutes with this process.

In this chapter, we have shown that the UV polymerization process is very fast and efficient. Indeed, while using the UV spot, the polymeric chains start crosslinking within the exposure time, i.e. 2 minutes. The UV polymerization process leads to an average NC of around 20%. With the UV polymerization process, really higher non-concentricity results are obtained than those obtained with the thermal polymerization process.

As explained in Chapter IV, while using a tube with areas of constriction, the movements inside the collecting flask seem to be particularly important for the core centering of the shell. With the thermal polymerization process, the shells spent at least 20 to 25 minutes inside the flask before the shell's shape is fixed. This time spent inside the flask allows the centering of the internal water phase inside the organic phase. With the UV process, the shells spent less than 5 minutes inside the flask before the UV exposure. Then, the bad non-concentricity

results obtained with the UV process may be linked to the short time spent by the shells inside the flask. Indeed, 5 minutes of rotation inside the flask during the collection might be not enough time for the shells to center. Thus, an idea could be to expose the shells to UV light after different periods of time spent inside the flask in order to study the influence of this parameter on the shells non-concentricity.

### V.3. CONCLUSION

The aim of this chapter was to study the influence of high polymerization rates on the shells characteristics by either increasing the polymerization temperature or by using UV polymerization. The times to reach a tridimensional network at 60°C and 90°C are 23 min and 80 seconds respectively. However, at 70, 80 and 90°C, the destabilization phenomena of the double emulsion are faster than the time required to polymerize the organic phase in order to have stable shells. Thus, the influence of high polymerization rate on the shells characteristics could not be studied by increasing the polymerization temperature.

We then focused our study on the use of UV polymerization at 60°C in order to get higher polymerization rates and to avoid destabilization phenomena. With a UV light intensity of 2 mW.cm<sup>-2</sup>, delivered by the UV black neon lamp, the synthesized shells have a lower thickness and a higher non-concentricity than with the thermal process. Moreover, the yields of shells increases when the amount of photoinitiator increases. Nevertheless, the UV light intensity is too low to polymerize the shells in all their thickness.

With a UV light intensity of 70 mW.cm<sup>-2</sup>, delivered by the UV spot, the shells synthesized have a slightly higher thickness and a really higher yield (80-90%) than the shells synthesized by thermal polymerization (58%). However, for both light intensities, the average non-concentricity of the shells remains around 20%, which is really high compared to the 2.4% average non-concentricity obtained with thermal polymerization. The bad non-concentricity results obtained with the UV process may be due to the short time spent by the shells inside the flask before the UV radiations.

So, for further studies of shells syntheses with UV polymerization, the UV spot should be used. The study of the influence of UV polymerization on the shells non-concentricity presented here is just the beginning of the research. An interesting idea could be to expose the

shells to UV light at different times after their collection to study the influence of the agitation time in the rotating flask on the shells non-concentricity.

**Bibliographic references**

1. Odian, G., *Radical chain polymerization*, in *Principles of Polymerization*. 2004, John Wiley & Sons, Inc. p. 198-349.
2. Chen, C., et al., *Low density hydrocarbon foams for laser fusion target*. Progress report - 1986, 1987. **UCID-21080-86**: p. 1-23.
3. Cook, R.C., et al., *Low density foam materials from styrene-divinylbenzene inverse emulsions: final report*. Final Report - Lawrence Livermore National Laboratory, 1992. **UCRL-LR-109207**: p. 1-15.
4. Takagi, M., et al. *High yield fabrication of uniform, large diameter foam shells for laser fusion targets using polymerization by photo initiation with UV light*. in *41st National Symposium*. 1994. Denver, Colorado.
5. Takagi, M., et al., *Development of low density, low atomic number foam shell with gas barrier for laser fusion target*. Material Research Society Symposium Proceedings, 1995. **372**: p. 199-202.
6. Bland, M.H. and N.A. Peppas, *Photopolymerized multifunctional (meth)acrylates as model polymers for dental applications*. Biomaterials, 1996. **17**: p. 1109-1114.
7. Dietz, J.E. and N.A. Peppas, *Reaction kinetics and chemical changes during polymerization of multifunctional (meth)acrylates for the production of highly crosslinked polymers used in information storage systems*. Polymer, 1997. **38**: p. 3767-3781.
8. Xu, S., et al., *Generation of monodisperse particles by using microfluidics: control over size, shape, and composition*. Angewandte Chemie International Edition, 2005. **44**: p. 724-728.
9. Nisisako, T., T. Torii, and T. Higuchi, *Novel microreactors for functional polymer beads*. Chemical Engineering Journal, 2004. **101**: p. 23-29.
10. Utada, A.S., et al., *Monodisperse double emulsions generated from a microcapillary device*. Science, 2005. **308**: p. 537-541.
11. Nie, Z., et al., *Polymer particles with various shapes and morphologies produced in continuous microfluidic reactors*. Journal of the American Chemical Society, 2005. **127**: p. 8058-8063.
12. Apen, P.G., *Polymeric foam by photoinitiated polymerization of trimethylolpropanetriacrylate: initiator and solvent effect*. Journal of Cellular Plastics, 1995. **31**: p. 74-92.

## **CONCLUSION**

In order to achieve ignition on the French high power laser LMJ (Laser Mega Joule), different target designs are being developed. Low gain targets made of low density organic foam shells can be used to study fusion. This work deals with the fabrication process of low density foam shells and the sharp control of their shape. The aimed criteria for the shells, i.e. diameter, thickness, density, sphericity and non-concentricity, are influenced by several parameters during the synthesis process. Three of the aimed criteria, the diameter, thickness and density, are relatively easy to fulfill. During this PhD, we focused on the non-concentricity which is the most difficult specification to meet.

The shells are synthesized using a droplet generator which gives a W/O/W double emulsion. The organic phase is then polymerized by thermal polymerization at 60°C. Once the shells are polymerized, they undergo several water washes and alcohol exchanges. Finally, they can be characterized using a telecentric optical microscope which gives the diameter, thickness, sphericity and non-concentricity of the shells. The whole process to synthesize shells and perform their characterization is very specific and quite complicated. It takes at least ten days to go through the whole process.

According to the literature, three major parameters, the density of the three phases, the deformations of the shells along the process and the kinetics of the polymerization have a direct influence on the shells non-concentricity. An overview of the state of the art revealed that three nations are involved in the foam shells synthesis i.e the United States, Japan and France. The US and Japan started researches on the topic in the 80's whereas France started only since 2002. Besides, China just started recently researches on foam shells.

The influence of a density gap between the internal water phase W1 and the organic phase O1 on the shells NC was carefully studied during this PhD. The results obtained showed that when the density gap increases, the TMPTMA shells non-concentricity improves. Since the curve of the yield of shells as a function of the density gap shows a bell-shaped profile, a compromise has to be made between good non-concentricity results and a high yield of shells. Thus, we chose for further experiments to work with the internal water phase W1(12) which gives a density gap  $dW1 - dO1 = 0.078 \text{ g.cm}^{-3}$  at 60°C and a yield of shells of 58%. Until now, these NC results are the best results obtained with foam shells, by the CEA Valduc.

From the results obtained during this PhD, the synthesis process can be considered as reproducible. The slight variation in the reproducibility results obtained may be due to the fact

that this synthesis is a complicated and heavy process where the least little dust or air bubble can destabilize the whole injection process.

Moreover, the interfacial tension at the interface of the internal water phase and the organic phase may partly explain the better non-concentricity results obtained with an important density mismatch. However, the interfacial tension measurements are not entirely trustworthy and should be done again. In addition, it would be interesting to study the synthesis process from a physical point of view in order to understand the physical phenomena leading to the centering of the shells when using a high density gap between dW1 and dO1.

Another point discussed in this work was the movements underwent by the shells when circulating in the different tubes of the system. While using the same internal water phase, equivalent non-concentricity results are obtained using either a straight tube, a tube with areas of constriction or a short wound tube. Inside these three circulation systems, the shells undergo gravity forces and turn around on themselves. Centering forces due to gravity should be much more efficient with a high density gap between the internal water phase W1 and the organic phase O1 than with the equality. The shells turning around on themselves allow a multidirectional centering of W1.

Concerning the kinetic aspects of the reaction, for the three circulation systems, the polymeric chains start to grow and crosslink once the shells are collected inside the flask. The time required to fix the shell's shape is at least 20 minutes with thermal polymerization.

It seems that the time spent by the shells inside the rotating flask allows the centering of the internal water phase inside the organic phase, whatever the circulation process used. Moreover, the filling level of the external water phase inside the collecting flask has no influence on the shells non-concentricity. A perspective to this work could be the study of the agitation of the shells via the rotation speed, the flask shape and dimensions.

For polymerization temperature higher than 60°C, the destabilization phenomena of the double emulsion are faster than the time required to polymerize the organic phase in order to have stable shells. Thus, the influence of high polymerization rate on the shells characteristics could not be studied by increasing the polymerization temperature.

In order to get higher polymerization rates and to avoid destabilization phenomena, we then focused our study on photopolymerization. When the synthesis is performed using a UV lamp with an efficient light intensity, the shells have a slightly higher thickness than the shells synthesized by thermal polymerization. Moreover, a really higher yield, around 80%, is

achieved with UV polymerization. However, the average non-concentricity of the shells synthesized lays around 20%, which is really high compared to the 2.4% average non-concentricity obtained with thermal polymerization. The bad non-concentricity results obtained with the UV process may be due to the short time spent by the shells inside the flask before UV radiations. It would be interesting to expose the shells to UV light at different times after collection in order to study the influence of the agitation time on the shells non-concentricity.

To conclude, the thermal polymerization process allows the synthesis of foam shells with low NC results and with a medium yield of shells. However, the thermal polymerization process is long. If we knew when the shells present a good NC inside the flask, we could UV polymerized them a this right moment and obtain better yield of shells. Besides, to simplify the circulation process, a simple straight tube should be used.



# **APPENDIX**

## A.1. Gas chromatography

The gas chromatography used is the GC 9000 series from Fisons Instruments, equipped with a flame ionization detector (FID) as illustrated in Figure A.1. The GC separation is carried out using a non-polar column HP-5 (30 m x 0.32 mm I.D. x 0.25  $\mu\text{m}$ , Agilent Technologies). The column temperature program is an isotherm at 220°C. The temperature of the injector is 200°C and the temperature of the detector is 290°C. Helium is the carrier gas with a constant flow of 110 kPa. Quantitative measurements are realized using the internal standard method with diethyl phthalate as the internal standard.



Figure A.1: Gas chromatography GC 9000 series from Fisons Instruments

## A.2. Rheology

The rheometer used is the ARES rheometer from Rheometric Scientific, equipped with a 5 cm diameter plate/plate measuring system as illustrated in Figure A.2. The shear storage modulus  $G'$  and the shear loss modulus  $G''$  are measured with a small amplitude oscillatory shear set to 0.5. The measurement method used is a dynamic sweep as a function of time with the rotation frequency set to 10  $\text{rad}\cdot\text{s}^{-1}$ . The gap between the plates lies between 0.6 and 0.7 mm. The temperature is set to 60°C and the solution is degassed before the measurements.

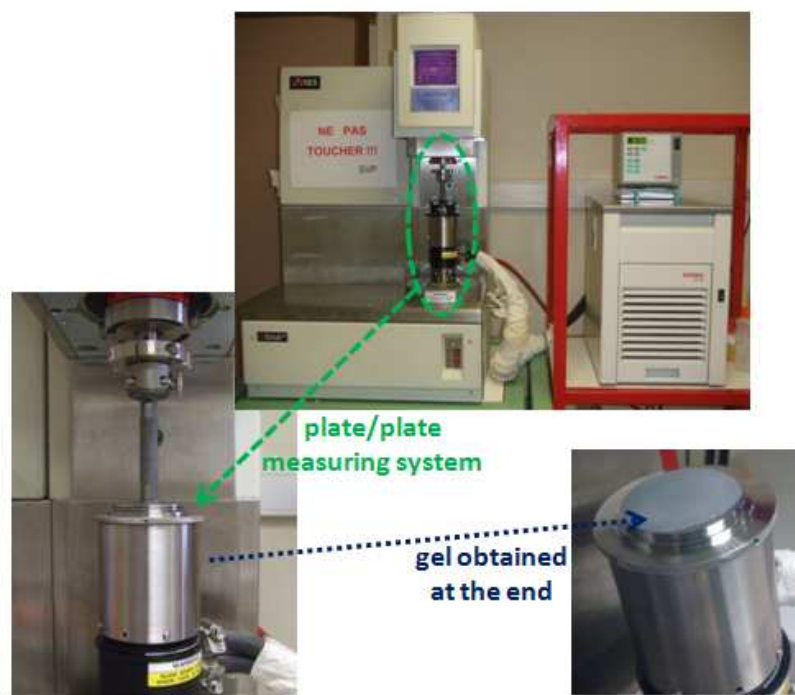


Figure A.2: ARES rheometer from Rheometric Scientific

### A.3. Density

The densitometer used is the DMA 5000 from Anton Paar<sup>®</sup> as illustrated in Figure A.3. This specific densitometer uses the oscillating U-tube technique. The density of the liquid is calculated from the electronic measurements of the oscillation frequency of the U-tube filled with the liquid. The characteristic frequency of an oscillating U-tube depends directly on the density of the sample that it contains. The U-tube has to be filled without any gas bubble and less than 1 mL of solution is necessary for the measurements. The densitometer accuracy is  $10^{-6}$  g.cm<sup>-3</sup> for density measurement and 0.001°C for temperature measurement.



Figure A.3: Densitometer DMA 5000

## A.4. Viscosity

The kinematic viscosity is determined by capillary viscometry using micro-Ubbelohde viscometers. The kinematic viscosity is calculated from the time taken for a fluid to flow through a capillary with a known diameter and known length. The measuring range of viscosity is determined by the capillary diameter of the micro-Ubbelohde viscometer. Each capillary diameter corresponds to a capillary number as illustrated in Table A.1. The capillary number Ic, II, IIc and III are used for the measurements. Less than 4 mL of solution is necessary for the viscosity measurements with a micro-Ubbelohde viscometer. A measuring stand is used to measure automatically the time for the fluid to flow through the capillary. Besides, the viscometer is introduced inside a water bath with a thermostat which maintained a constant temperature during the experiment as illustrated in Figure A.4.

Table A.1: Measurements and device constants for the micro-Ubbelohde viscometers

Ref. No.	Capillary No.	Capillary $\varnothing_i$ (mm)	Constant K (approx.)	Measuring range $\text{mm}^2/\text{s}$ (cSt) (approx.)	
... 10	I	0.40	0.01	0.4	to 6
... 13	Ic	0.53	0.03	1.2	to 18
... 20	II	0.70	0.1	4	to 60
... 23	IIc	0.95	0.3	12	to 180
... 30	III	1.26	1	40	to 800

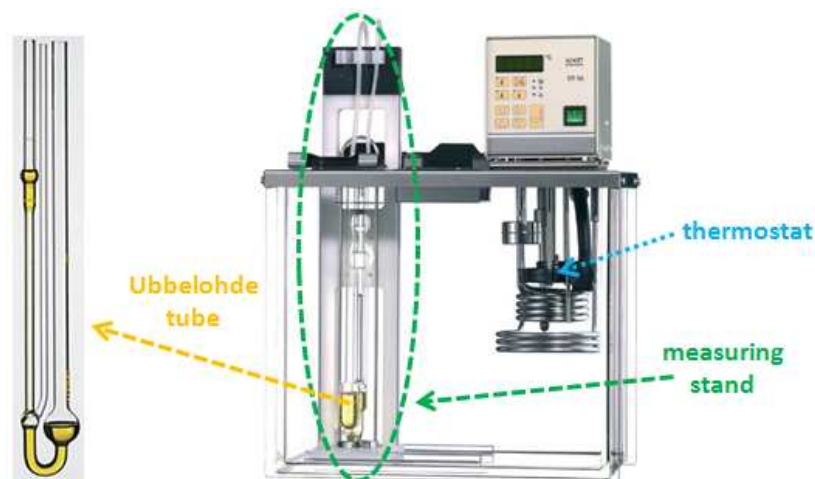


Figure A.4: Capillary viscometry with a micro-Ubbelohde viscometer

## A.5. Interfacial tension

The interfacial tension between the two phases is measured using a pendant drop apparatus. The pendant drop apparatus used is the Digidrop DGD Fast/600 Contact Angle Meter from GBX as illustrated in Figure A.5. The liquid with the lowest density is used to fill a glass container of approximately 15 mL. The glass container is thermostated to work at constant temperature. The liquid with the higher density is sucked in a syringe and placed on top of the glass container. The drop volume is controlled by a micrometer screw gauge. The interfacial tension is determined from the drop shape and the density difference between the two components at relevant temperature as explained in Chapter III.

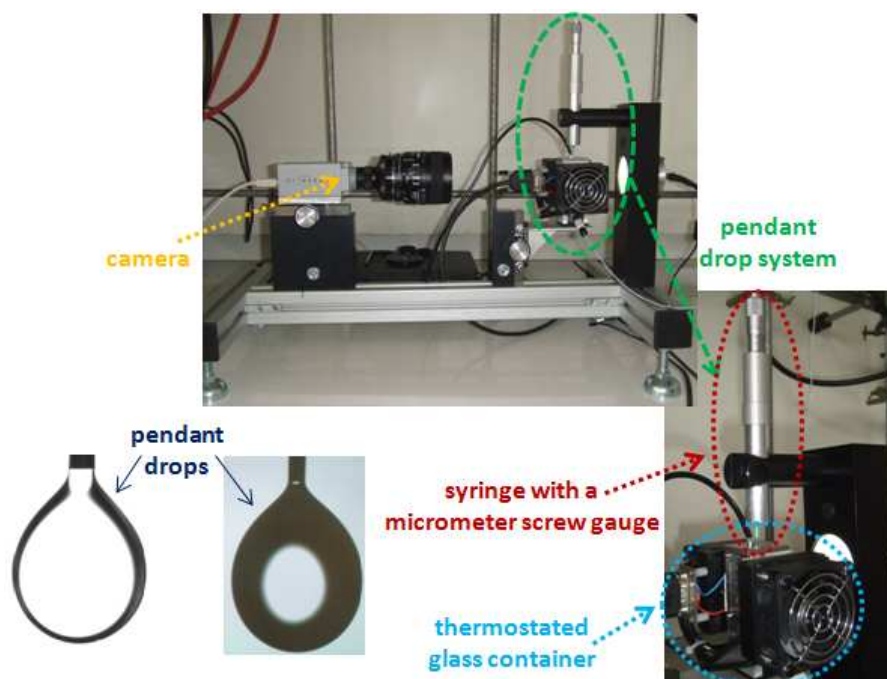


Figure A.5: pendant drop apparatus from GBX

## A.6. Infrared spectroscopy

The FT-IR spectrometer used is the IFS 28 from Bruker. The attenuated total reflectance (ATR) sampling technique is used in conjunction with the IR spectroscopy. With the ATR, the sample can be directly analyzed without further preparation. Then, the sample to be analyzed is directly deposited on the ATR crystal and examined from 600 to 4000  $\text{cm}^{-1}$  at room temperature.

## A.7. UV-visible spectroscopy

The UV-Visible spectrophotometer used is the Cary 1E from Varian. The absorbance is measured in the UV wavelength domain, from 190 to 400 nm. Samples to analyze are diluted with ethanol and place inside a 3 mL cell.

## A.8. Telecentric optical microscope

Shells in alcohol were characterized using a telecentric optical microscope, Optique Peter® from Melles Griot. Since the foam shells are transparent while they are in alcohol, the inside and outside edges of the shells can be determined. However, with this technique only one equator of the shell is observed. Several parameters can be measured with this telecentric optical microscope: the inner and outer diameter, the sphericity and the wall uniformity. The software used with the telecentric optical microscope is home made by the CEA. Figure A.6 illustrates the computer screen given by the software.

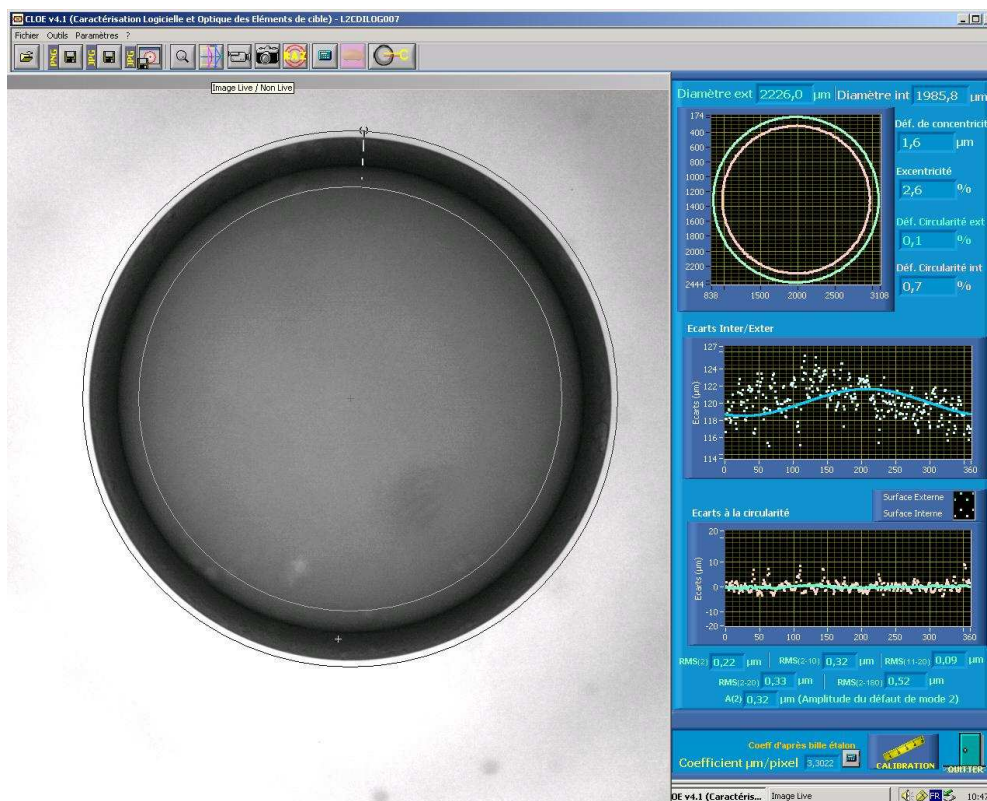


Figure A.6: Illustration of the software used to analyze a shell

- **Fitted thickness:**

When a shell is analyzed, the software detects the contour points of the external and internal walls of the shell. Then, the software draws two fitted circles of the external and internal walls and also gives a graphic of the thickness variation between the fitted internal and external circle (blue curve in Figure A.7). The fitted thickness at a detection angle  $\alpha$  is calculated with the following formula:

$$fitted\ thickness(\alpha) = \sqrt{(Xfit_{ext}(\alpha) - Xfit_{int}(\alpha))^2 + (Yfit_{ext}(\alpha) - Yfit_{int}(\alpha))^2}$$

With  $Xfit_{ext}(\alpha)$  and  $Yfit_{ext}(\alpha)$  the Cartesian coordinates of the external fitted circle at the detection angle  $\alpha$  and  $Xfit_{int}(\alpha)$  and  $Yfit_{int}(\alpha)$  the Cartesian coordinates of the internal fitted circle at the detection angle  $\alpha$ .

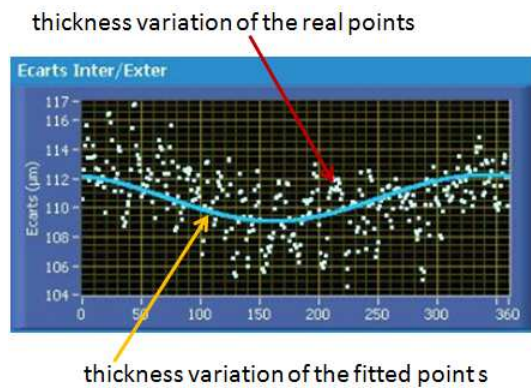


Figure A.7: Curves of the thickness variation of the real points (white dots) and of the fitted points (blue curve)

- **Real thickness:**

The software also gives a graphic of the thickness variation between the real internal and external circle (white dots in Figure A.7). The real thickness at a detection angle  $\alpha$  is calculated with the following formula:

$$real\ thickness(\alpha) = \sqrt{(X_{ext}(\alpha) - X_{int}(\alpha))^2 + (Y_{ext}(\alpha) - Y_{int}(\alpha))^2}$$

With  $X_{ext}(\alpha)$  and  $Y_{ext}(\alpha)$  the Cartesian coordinates of the detected external wall of the shell at the detection angle  $\alpha$  and  $X_{int}(\alpha)$  and  $Y_{int}(\alpha)$  the Cartesian coordinates of the detected internal wall of the shell at the detection angle  $\alpha$ .

- Non-concentricity:

The non-concentricity calculated by the software is the peak to peak amplitude of the curve of the thickness variation between the fitted internal and external circle (blue curve in Figure A.7), divided by the average wall thickness:

$$NC = \frac{\Delta \text{ fitted wall thickness}}{\text{average thickness}}$$

- Sphericity:

A graphic of the variation of the sphericity deviation for the internal (pink dots in Figure A.8) and external (green line in Figure A.8) walls is also presented. The sphericity deviation at a detection angle  $\alpha$  is the difference between the detected wall and the fitted circle at this angle. The external and internal sphericity deviations are calculated with the following formulas:

$$\text{external sphericity deviation } (\alpha) = \sqrt{(X_{fit_{ext}}(\alpha) - X_{ext}(\alpha))^2 + (Y_{fit_{ext}}(\alpha) - Y_{ext}(\alpha))^2}$$

$$\text{internal sphericity deviation } (\alpha) = \sqrt{(X_{fit_{int}}(\alpha) - X_{int}(\alpha))^2 + (Y_{fit_{int}}(\alpha) - Y_{int}(\alpha))^2}$$

Thus, the sphericity calculated by the software is the peak to peak amplitude of the curve of the external sphericity deviation (green line in Figure A.8), divided by the external diameter:

$$\text{sphericity} = 100 - \frac{\Delta \text{ external sphericity deviation}}{\text{external diameter}}$$

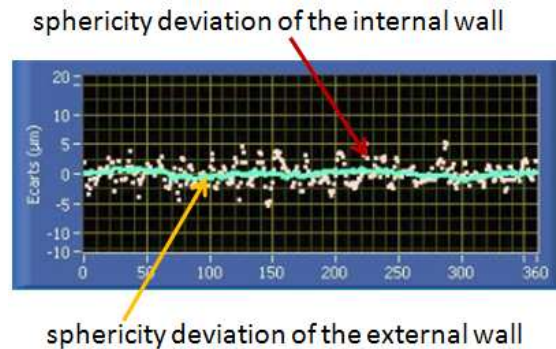


Figure A.8: Curves of the sphericity deviation for the internal wall (pink dots) and for the external wall (green curve)



## **A. 9. Scanning electron microscope**

The scanning electron microscope (SEM) used is the Leo 1225 from Gemini. Shells to analyze are cut in half and the pieces are stuck to specimen stubs with argent glue. The samples are coated with an ultrathin coating of gold before use by low vacuum sputter coating. Images are realized with the detection of secondary electron at 3kV.